Aus dem Institut für Neurophysiologie

der Medizinischen Fakultät Charité – Universitätsmedizin Berlin

DISSERTATION

Dichotomy of Subicular Principal Cells in the Involvement in Sharp Waves and Gamma Frequency Oscillations

Zur Erlangung des akademischen Grades

Doctor medicinae (Dr. med.)

vorgelegt der Medizinischen Fakultät

Charité – Universitätsmedizin Berlin

von Joanna Maria Eller

aus Oppeln, Polen

Datum der Promotion: 05.06.2016

To my grandmother Maria Soltysiewicz.
Thank you for your love, support,
and your infinite believe in me.

Table of Contents

Zusammenfassung

Als efferentes Organ der hippocampalen Formation entsendet das Subiculum prozessierte mnemonische und räumliche Information zu verschiedenen kortikalen und subkortikalen Gehirnregionen. Außerdem ist das Subiculum an der Pathophysiologie neurologischer Erkrankungen wie der Epilepsie und Schizophrenie beteiligt. Netzwerkoszillationen im Gamma-Frequenzbereich (30-100 Hz) und Sharp Wave Ripple Oszillationen (100-250 Hz) spielen eine besondere Rolle in der hippocampalen Formation. Beide Rhythmen sind funktionell vergesellschaftet und an der Speicherung und dem Abruf von Gedächtnisinhalten beteiligt. Im Subiculum gibt es zwei Arten von Prinzipalzellen, die anhand ihrer Reaktion auf die Applikation depolarisierender Strominjektionen unterschieden werden: intrinsically bursting (IB) und regular spiking (RS) Zellen. Bisher ist es allerdings unklar, wie die beiden Zelltypen an der subicularen Netzwerkaktivität beteiligt sind. Anhand eines *in vitro* Modells, das sowohl die Untersuchung von Sharp Waves als auch von Gamma Oszillationen erlaubt, wurden in 400 µm dicken murinen hippocampalen Schnitten simultan Aufnahmen lokaler Feldpotentiale und mithilfe der sharp microelectrode Technik intrazelluläre Aufnahmen durchgeführt. Die intrinsischen und synaptischen Eigenschaften subicularer Prinzipalzellen und ihre funktionelle Bedeutung während beider Netzwerkrhythmen wurden untersucht. Biocytin diente der morphologischen Identifizierung. Die elektrophysiologisch identifizierten Zellen zeigen die typische Form von Pyramidalzellen. Dye Coupling, das dem morphologischen Korrelat elektrischer Synapsen entsprechen soll, kann in einem IB Zellpaar aber nicht in RS Zellen nachgewiesen werden. In Ergänzung zu der elektrophysiologischen Dichotomie und dem individuellen Feuerverhalten, wird zudem eine funktionelle und zelltyp-spezifische Trennung der Netzwerkbeteiligung im Subiculum deutlich. Die Mehrheit der IB Zellen zeigen aktives und am Netzwerk beteiligtes Verhalten, während die RS Zellen im Großteil unbeteiligt und „still“ sind. RS Zellen scheinen eine stärkere Netzwerkerregung zu benötigen, um an den Netzoszillationen teilzunehmen. Werden die RS Zellen jedoch über das Schwellenpotential hinaus depolarisiert, zeigen sie ein zelltyp-spezifisches und unabhängiges Aktivitätsmuster in strikter Korrelation zum Netzwerk. Folglich kann ein bimodales Arbeitsmodell im Subiculum angenommen werden, das abhängig von dem Level subicularer Netzwerkerregung ist. Des Weiteren unterscheiden sich die synaptischen Potentiale subicularer IB und RS Zellen deutlich voneinander. Das deutet darauf hin, dass sowohl die zelluläre Verschaltung als auch die afferenten Strukturen subicularer Prinzipalzellen unterschiedlich sein müssen. Zusammenfassend erlauben die Ergebnisse den Rückschluss, dass eine funktionelle und zelltyp-spezifische Separation subicularer IB und RS Zellen existiert, die zwei voneinander unabhängige und parallele Kanäle der Informationsverarbeitung repräsentieren.

Abstract

As the hippocampal output structure, the subiculum's purpose is to integrate and distribute mnemonic and spatial information to various cortical and subcortical brain regions. The subiculum is also involved in the pathophysiology of neurological conditions such as epilepsy and schizophrenia. Network oscillations in the gamma (30-100 Hz) frequency range as well as sharp wave ripple oscillations (100-250 Hz) are most prominent within the hippocampal formation. Both rhythms appear to be functionally connected and are involved in memory storage and retrieval. Within the subiculum, there are two types of principal cells (PC) that can be discriminated based on their firing properties following a depolarizing current injection: intrinsically bursting (IB) and regular spiking (RS) neurons. So far, it remains uninvestigated how these two distinct subicular PC classes participate in oscillatory network activity. Using an *in vitro* model that allows the investigation of sharp wave and gamma frequency oscillations in the subiculum, simultaneous local field potential and sharp microelectrode recordings were made in 400 µm thick murine hippocampal slices. The intrinsic and synaptic properties of subicular PCs as well as their functional involvement in the two major oscillatory rhythms were investigated. Biocytin was used for the morphological identification of recorded neurons. Morphologically, the electrically identified neurons display the typical shape of pyramidal cells. Interestingly, one pair of IB, but not RS cells, shows dye coupling which has been suggested to be the morphological correlate of electric synapses. The results reveal furthermore, that in addition to the electrophysiological dichotomy and distinct firing properties of the subicular PC classes, there exists a strict functional segregation of the active, participating IB cells and mostly silent RS cells during both network states. The silent RS PCs appear to require a higher network activation than IB PCs in order to participate in the oscillatory activity. When depolarized above threshold, they show a cell-type specific and independent firing pattern in correlation to the local field. This suggests a bimodal working model within the subiculum dependent on the level of network excitation. Additionally, the subicular IB and RS cells reveal divergent synaptic properties in the active network which suggest distinct synaptic connectivity and possibly input structures. These results altogether indicate a functional cell-type-specific segregation of subicular PCs representing two independent and parallel streams of information processing within the subiculum resulting in two distinct processing channels within the hippocampal formation.

List of Abbreviations

τ	time constant
ACSF	artificial cerebrospinal fluid
AMPA	α-amino-3-hydroxy-5-methyl-4-isoxazolepropionic acid
AP	action potential
°C	degree Celsius
CA	cornu ammonis
Ca^{2+}	calcium ion
$CaCl_2$	calcium chloride dihydrate
$C_2H_3KO_2$	potassium acetate
CO_2	carbon dioxide
DAB	diaminobenzidine
DG	dentate gyrus
EC	entorhinal cortex
EEG	electroencephalogram
EPSP	excitatory postsynaptic potential
FEM	Forschungseinrichtung für Experimentelle Medizin
FFT	fast Fourier transformation
GABA	gamma-aminobutyric acid
hf	hippocampal fissure
Hz	hertz
IB	intrinsically bursting
I_h	hyperpolarization activated current
IPSP	inhibitory postsynaptic potential
ISI	interspike interval
K^+	potassium ion
KA	kainic acid (kainate)
KCl	potassium chloride

KHz	kilohertz
LEC	lateral entorhinal cortex
LFP	local field potential
M	molar
MΩ	mega-ohm
MEC	medical entorhinal cortex
$MgSO_4$	magnesium sulphate
min	minute
ms	millisecond
mV	millivolt
Na^+	sodium ion
NaCl	sodium chloride
NADPH	nicotinamide adenine dinucleotide phosphate
NaH_2PO_4	sodium di-hydrogen phosphate
$NaHCO_3$	sodium hydrogen carbonate
µm	micrometer
nM	nanomolar
ns	not significant
nuc.	nucleus
nV	nanovolt
O_2	oxygen
OsO_4	osmium tetroxide
pA	picoampere
PaS	parasubiculum
PB	phosphate buffer
PC	principal cell
PER	perirhinal cortex
PrS	presubiculum
PSD	power spectral density

PSP	postsynaptic potential
R_{in}	input resistance
RMP	resting membrane potential
RS	regular spiking
s	second
SEM	standard error of the mean
str.	stratum
SWR	sharp wave ripple
V	volt
V_{peak}	maximum voltage deflection
V_{ss}	steady-state voltage deflection

List of Tables

List of Figures

1. Introduction

1.1 The Subiculum

The hippocampus has been subject to intensive neurophysiological research for the past decades. This can be attributed to its functional relations with higher brain functions such as memory formation and learning as well as to its relatively plain three-layered histological structure (Andersen 2007; Lynch and Schubert 1980; Naber et al. 2000; O'Mara et al. 2001; Scoville and Milner 1957). The hippocampal formation consists of the dentate gyrus (DG), the hippocampus proper with the cornu ammonis 3 (CA 3), CA2, and CA1 areas, the entorhinal cortex (EC), and the subiculum (Figure 1). The subiculum is its major output structure and acts as the final relay in the polysynaptic loop between the EC and the hippocampal areas (Swanson and Cowan 1975). With its strategic position, its purpose is to integrate and distribute processed mnemonic and spatial information to a series of cortical and subcortical brain regions (Finch et al. 1983; O'Mara et al. 2001). In 1983, Finch et al. showed in a morphological study that the axons of subicular principal cells (PCs) reach beyond the border of the subiculum classifying them as projection neurons. The first electrophysiological studies were performed *in vivo* by Ranck in 1973 and Finch and colleagues in 1988. Subsequent *in vitro* studies segregated the glutamatergic PCs into intrinsically bursting (IB) and regular spiking (RS) cells based on the firing behavior (Mason 1993; Mattia et al. 1993; Stewart and Wong 1993; Taube 1993). Functionally, the two types of subicular PC, IB and RS cells, appear to be 'place cells' and are involved in spatial navigation similar to the PCs of the hippocampal CA1 area (Graves et al. 2012; Sharp and Green 1994).

1.1.1 Subicular Morphology

Anatomically, the subiculum borders the CA1 region of the hippocampus at one end and the presubiculum (PrS) at the other (Figure 1). As part of the phylogenetically old allocortex, the subiculum consists of three cell layers (Andersen 2007; O'Mara et al. 2001). The stratum (str.) moleculare is the most superficial one. It is continuous with strata lacunosum-moleculare and radiatum of the hippocampal CA1 field. Adjacent to this relatively cell free layer lies the subicular principal cell layer containing the somas of the IB and RS cells. The CA1/subiculum border is marked by a widening of the tightly packed str. pyramidale of the CA1 region to a more diffuse pyramidal cell layer of the subiculum (Figure 1). Finally, there is the polymorphic layer. Below the polymorphic layer lies the alveus. It contains hippocampal axons as well as projections from the adjacent parahippocampal regions. A change of laminar architecture marks the border to the PrS (Witter et al.

2000). Adding a superficial layer, the three-layered allocortex of the hippocampal formation is replaced by the four-layered construction of the perisubicular cortex.

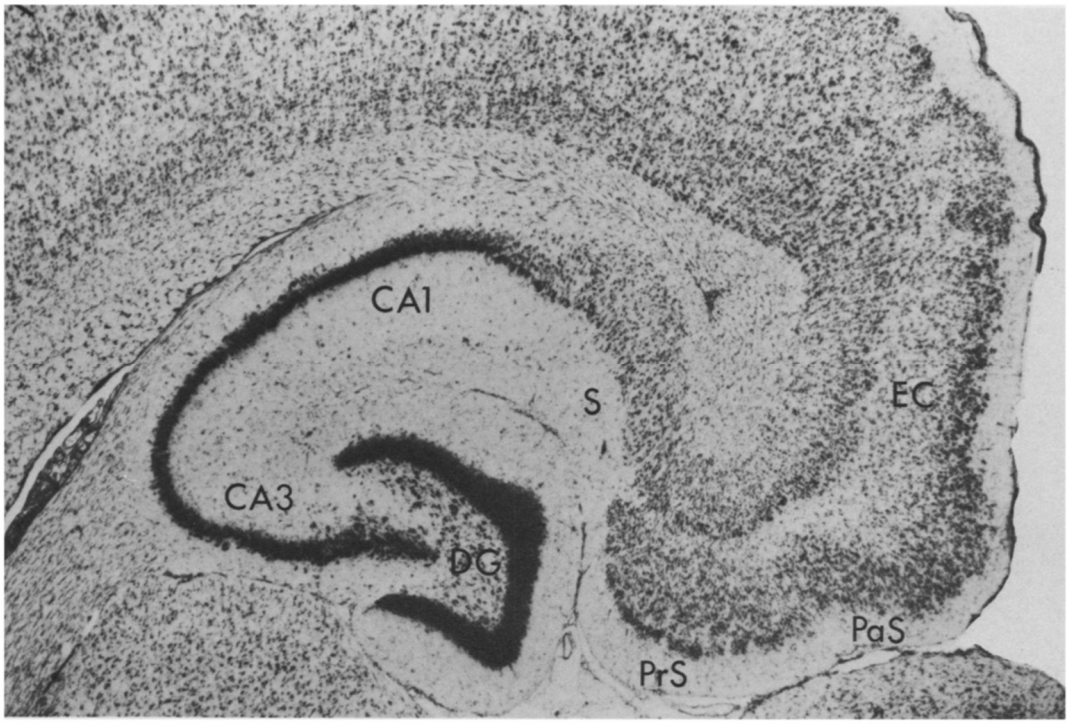

Figure 1. The hippocampal formation and the adjacent parahippocampal region.

The photomicrograph of Thionin-stained horizontal section of a rodent hippocampus adapted from Amaral and Witter (1989) demonstrates the various components of the hippocampal formation (dentate gyrus, DG; CA3 and CA1 area of the hippocampus; subiculum, S; entorhinal cortex, EC) and adjacent parahippocampal cortices (presubiculum, PrS; parasubiculum, PaS). The border of the hippocampal CA1 region to the subiculum is marked by the widening of the str. pyramidale. A change of laminar organization occurs at the border of the subiculum to the PrS and PaS when an additional superficial layer is added.

1.1.2 Subicular Connections

The hippocampal formation is one of only a few brain regions that receives multimodal sensory information from a variety of neocortical areas (Naber et al. 2000; O'Mara et al. 2001). As the hippocampus's main gateway, the subiculum holds a key position by filtering or amplifying the passing information which results in an input-specific modulation of hippocampal output. The most prominent glutamatergic input to the subiculum arises from the EC and the hippocampal CA1 region (Andersen et al. 1973; Behr et al. 1998; Finch and Babb 1980; Stewart 1997; Swanson and Cowan 1977; Swanson et al. 1978; Taube 1993; Witter et al. 1989). The entorhinal projections, the perforant path, pass through the subiculum on their way to the DG with some of the traversing fibers terminating within the subiculum (Witter and Amaral 1991). The projection originates mainly from entorhinal layer III cells forming excitatory synapses on the distal part of the apical dendrites within the molecular layer of the subiculum (Behr et al. 1998; Dugladze et al. 2001; Steward and Scoville 1976; Witter and Amaral 1991). Thus, the EC constitutes both a significant input structure as well as a modulator of hippocampal output. The axons of CA1 projection neurons ramify intensively within the subicular pyramidal cell layer, forming a columnar arborization and terminating on the basal dendrites and the proximal part of the apical dendrites (Amaral et al. 1991; Tamamaki et al. 1987; Tamamaki and Nojyo 1990). The excitatory projection is arranged in a topographical manner: proximal CA1 PCs, located closest to the CA2 border, project to the distal subiculum, which is closest to the border to the PrS (Amaral et al. 1991). Distal CA1 cells, located adjacent to the subiculum, give rise to axons that terminate in the proximal subiculum just across the CA1-subiculum border (Figure 2).

The subiculum projects to numerous cortical and subcortical brain regions, some of which are the entorhinal, perirhinal, and postrhinal cortices, the retrosplenial, infralimbic, and prelimbic cortices, and the septal nuclei, the nucleus accumbens, the ventral striatum, the amygdale, and several thalamic and hypothalamic nuclei (Andersen 2007; Naber and Witter 1998; O'Mara et al. 2001; Witter et al. 1989; Witter et al. 2000). Furthermore, the subiculum projects back to the hippocampal CA1 region (Finch et al. 1983; Harris and Stewart 2001b; Knopp et al. 2005; Köhler 1985). The subicular output, corresponding to its input, is organized in a topographical manner (O'Reilly et al. 2013): The distal subiculum projects to the medial entorhinal cortex (MEC), whereas the proximal portion of the subiculum targets the lateral entorhinal cortex (LEC).

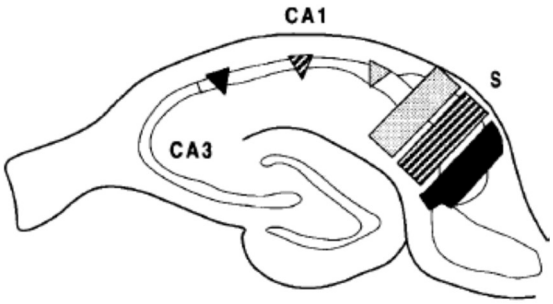

Figure 2. Organization of CA1 projection to the subiculum.

Schematic overview of hippocampal CA1 projection to the subiculum adapted from Amaral et al. (1991). The three differently shaded triangles indicate the place of origin of cellular projection within the proximal, middle, and distal CA1 fields. The shading pattern is reflected in the corresponding projection areas within the subiculum (S).

1.2 Subicular Principal Cells

1.2.1 Cellular Morphology

The comparably large subicular PCs have so far received less attention than the PCs of the neighboring CA1 and CA3 areas. Most authors agree that IB cells outnumber the RS neurons within the subiculum (Knopp et al. 2005; Mason 1993; Stewart and Wong 1993; Taube 1993; Wu et al. 2006). IB as well as RS cells show the typical shape of pyramidal neurons (Graves et al. 2012; Greene and Totterdell 1997; Taube 1993). The triangular shaped soma gives rise to long apical dendrites that extend into the molecular layer with some of the branches reaching the hippocampal fissure (Greene and Totterdell 1997; Harris et al. 2001; Taube 1993). The shorter basal dendrites spread within the deeper portions of the str. pyramidale (Taube 1993). Both apical and basal dendrites have spines (Greene and Totterdell 1997; Harris et al. 2001). The axon leaves the subiculum via the alveus traveling towards the EC, the PrS, and the hippocampal CA1 area (Finch et al. 1983; Harris et al. 2001; Ranck 1973). Both cell types display extensive axonal collateralization within the cellular layer (Harris et al. 2001). In terms of morphological discrimination, some authors claim that there are no obvious morphological differences between the two types of subicular PCs (Greene and Totterdell 1997; Knopp et al. 2005; Menendez de la Prida and Gal 2004; Staff et al.

2000; Taube 1993). However, IB neurons were found to display a longer unbranched apical dendrite than RS cells (Graves et al. 2012; Greene and Totterdell 1997). This could be attributed to the distinct localization of the cell body within the str. pyramidale (Harris et al. 2001). RS cells, on the other hand, display more extensive basal dendrites (Graves et al. 2012).

There is a variable number of small, gamma-aminobutyric acid (GABA)-ergic nonpyramidal neurons with diversely shaped cell bodies located mainly in the str. radiatum (Greene and Totterdell 1997; Soriano et al. 1993). Regarding their morphology as well as their connectivity, the subicular interneurons remain poorly studied. It has been suggested that the majority of subicular interneurons show fast-spiking activity (Fidzinski et al. 2011; Menendez de la Prida 2006; Menendez de la Prida et al. 2003).

The phenomena of dye coupling has been observed within the subiculum (Finch et al. 1988; Harris et al. 2001). Interestingly, it has been noted exclusively in electrophysiologically identified IB cells. Dye coupling has been associated with the electrophysiological correlate of electrical synapses between single cells (Baimbridge et al. 1991; Schmitz et al. 2001).

1.2.2 Location within the Cell Layer

The two classes of subicular PCs differ with regard to their location within the subicular cell layer. RS PCs are found more frequently at the CA1-subicular border whereas the percentage of IB neurons increases along the proximo-distal axis with their highest density at the distal end of the subiculum (Jarsky et al. 2008; Staff et al. 2000). RS cells are encountered more often in the superficial part of the subicular cell layer, which is nearest to the hippocampal fissure. IB PCs are more common in the deep cell layer furthest from the hippocampal fissure (Greene and Mason 1996; Greene and Totterdell 1997; Harris et al. 2001; Mason 1993). However, the distribution is not exclusive and the cell types overlap. Interestingly, the electrophysiological properties of subicular RS cells recorded in the superficial layer were found to be very similar to the ones recorded deeper within the subiculum (Greene and Mason 1996). Furthermore, the local distribution of axon collateralization differs between subicular PC types (Harris et al. 2001). Deep cells, mostly IB neurons, display a columnar organization of axonal arborization, with their axons ascending and circumscribing their own apical dendrites. More superficial cells, most often RS PCs, give rise to axonal collaterals with a more widespread range along the transverse axis, resulting in a laminar arrangement (Harris et al. 2001). In this way, RS neurons can integrate cellular activity across multiple columns and along the transverse subicular axis. It has been observed that the dendritic

as well as axonal pattern correlate better with the position of the cell body than with the electrophysiological properties of a cell group (Harris et al. 2001). The distinct arrangement of the two types of subicular PCs appears to provide optimal circumstances for different connectivity and parallel information processing channels (Greene and Totterdell 1997; Harris et al. 2001).

1.2.3 Cellular Connectivity

The subicular position within the polysynaptic hippocampal information loop as well as the electrophysiological dichotomy of subicular PCs suggests a complex functional processing system within the subiculum.

So far, there has been no indication that the afferences of IB and RS PCs differ from each other (Norimoto et al. 2013; Stewart 1997; Taube 1993). It has rather been demonstrated that the inputs from the LEC and the hippocampal CA1 region converge onto single subicular PCs *in vivo* (Gigg et al. 2000) and *in vitro* (Norimoto et al. 2013). Subicular interneurons, on the other hand, have been demonstrated to receive excitatory input from the hippocampal CA1 area but not the EC (Gigg et al. 2000). Given the arrangement of subicular PCs along the superficial-deep and proximo-distal axis of the subiculum, the two distinct subicular PC classes might receive input from different cell groups of the CA1 area and the EC (Amaral et al. 1991; Greene and Totterdell 1997). The distribution of dendrites and axons within the subicular pyramidal cell layer adds to the segregation of inputs reaching different subicular subfields or even cell classes (Harris et al. 2001).

In contrast to the input, the two subicular PC classes were found to differ with regard to their target areas, IB PCs project to the PrS but not to the EC, whereas RS neurons project to the MEC but not the PrS (Naber and Witter 1998; Stewart 1997). The subicular efferent connections were further found to be subdivided into four areas along the dorso-ventral and proximo-distal axis with distinct target regions (Figure 3). Cells within these areas send their axons exclusively to one specific region of the many possible destinations and it has been demonstrated that one single subicular cell projects to only one extrahippocampal target (Naber and Witter 1998; Witter et al. 1989). The output connections of subicular PCs were found to be organized in a laminar fashion, resulting in a sublamination of the str. pyramidale. Interestingly, the target region was associated with a specific size of cell body (Ishizuka 2001; Naber and Witter 1998). Regarding the separate output, IB and RS PCs are likely to serve distinct tasks of information processing within the subiculum (Greene and Totterdell 1997; Staff et al. 2000).

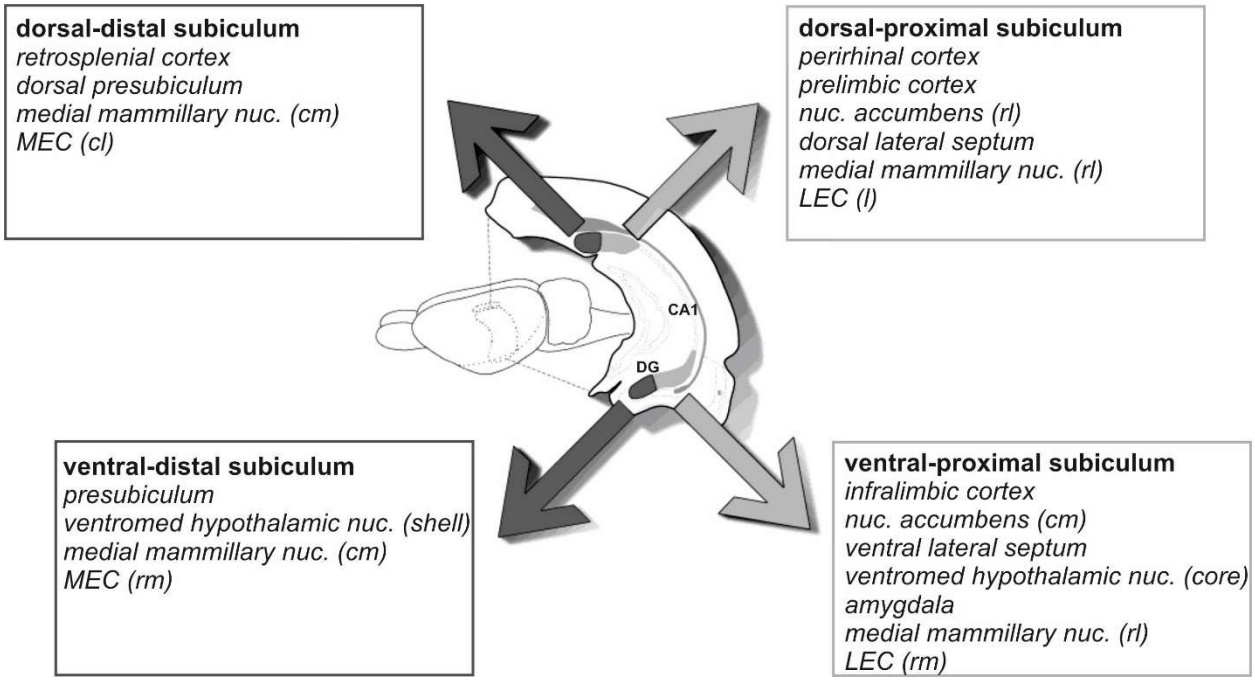

Figure 3. Target regions of the subiculum.

The schematic drawing of a coronal hippocampal slice, adapted from Naber and Witter (1998), shows the four distinct projection regions of the subiculum, with the distinct target structures listed in the corresponding boxes. Nuc., nucleus; cm, caudomedial; cl, caudolateral; rl, rostrolateral; rm, rostormedial; l, lateral; ventromed, ventromedial.

There exists very limited information concerning the local connectivity of IB and RS PCs and interneurons among each other. There has been morphological (Harris et al. 2001) and electrophysiological (Harris and Stewart 2001a) evidence of synaptic contacts between subicular PCs within the subiculum. On both subicular PC classes, autapse-like contacts have been observed, indicating a high intrinsic connectivity (Knopp et al. 2005). The generation and spread of epileptic activity within the isolated subiculum supports this theory (Behr et al. 1996). On the other hand, some authors have argued that the different firing pattern of the two subicular PCs indicate a lack of connectivity between subicular IB and RS cells (Sharp and Green 1994; Stewart and Wong 1993). In contrast to the divergent opinions regarding PCs, subicular interneurons are suggested to be strongly interconnected, forming a local inhibitory network (Gigg et al. 2000; Menendez de la Prida 2006).

1.2.4 Electrophysiological Properties

To date, there exists considerable disagreement regarding the distinct electrophysiological properties of the two types of subicular PCs (O'Mara et al. 2001).

1.2.4.1 Firing Behavior

The subicular IB and RS cells differ with regard to their electrophysiological response to an intrasomatic depolarizing current injection. At threshold, IB cells fire an action potential (AP) burst which consists of a small number of APs riding on top of a slow depolarizing potential followed by a hyperpolarizing afterpotential (Behr et al. 1996; Greene and Mason 1996; Mason 1993; Mattia et al. 1997a; Staff et al. 2000; Stewart 1997; Taube 1993). The APs vary in number and reach frequencies >200 Hz depending only slightly on the strength of the applied current injection (Mattia et al. 1997a; Staff et al. 2000). The interspike interval (ISI) within a burst averages around 5 ms (Gigg et al. 2000; Mattia et al. 1997a; Staff et al. 2000; Stewart 1997; Wu et al. 2006). During a burst, a progressive increase in AP duration and a reduction in amplitude with an elevation of firing threshold is evident, so that the bursting behavior is self-limiting (Staff et al. 2000; Stewart 1997). If the depolarization is maintained, single APs follow the initial burst for the remainder of the stimulus with a frequency proportional to the strength of the current pulse (Behr et al. 1996; Greene and Mason 1996; Mason 1993; Mattia et al. 1997a; Stewart and Wong 1993). The train of APs does not display distinct accommodation behavior (Behr et al. 1996; Kim and Spruston 2012; Mattia et al. 1997a). Single APs show a prominent afterdepolarization (ADP) which decreases with membrane depolarization (Stewart and Wong 1993; Taube 1993). A further depolarization of membrane potential leads to a change of spiking mode resulting in the termination of burst firing and the induction of a tonic firing mode mediated by a prolonged inactivation of sodium ion (Na^+) channels (Cooper et al. 2005; Mason 1993; Mattia et al. 1993; Mattia et al. 1997b; Stewart and Wong 1993). The IB cell was found to be the most robustly bursting cell type in the hippocampal formation with a stereotypical bursting pattern. Various subtypes of voltage-activated Ca^{2+} channels near the soma appear to be involved in the generation of burst firing (Jung et al. 2001). The calcium ion (Ca^{2+}) tail current is activated by the preceding AP and induces an ADP that triggers consecutive APs when reaching threshold. A balance between inward Na^+ currents, which activate the Ca^{2+} conductance, and outward potassium ion (K^+) currents, which terminate the bursting, is essential for burst generation (Jung et al. 2001). Functionally, bursting has been attributed to an amplification and strengthening of information transfer by increasing the probability of synaptic transmitter release and, in this way, inducing long-term potentiation and long-term depression

when propagating into the dendrites (Hablitz and Johnston 1981; Lisman 1997; Miles and Wong 1986). The burst answer at the beginning of the signal indicates the arrival of new information activating the receiving cellular structures, whereas the following tonic AP firing serves to preserve the unregulated network state (Cooper et al. 2005).

Subicular RS neurons do not burst but fire a train of single APs when depolarized above threshold (Greene and Totterdell 1997; Mason 1993; Stewart 1997; Stewart and Wong 1993; Taube 1993). The frequency of AP discharge depends on the strength of the applied pulse reaching ISIs similar to those recorded during burst firing in IB cells (Stewart 1997; Stewart and Wong 1993). RS neurons cannot be converted into burst firing neurons by a change of membrane potential. Instead, the increase of depolarizing power leads to a higher frequency of AP firing (Stewart and Wong 1993; Taube 1993). RS PCs show an adaptation of spiking behavior over the course of a stimulus (Behr et al. 1996; Wu et al. 2006).

1.2.4.2 Action Potentials

Comparing the properties of single APs, IB cells were found to display a more hyperpolarized AP threshold, a higher amplitude, and a longer AP duration compared to RS cells (Kim and Spruston 2012). Furthermore, the spike rise times have been observed to differ significantly (Kim and Spruston 2012). However, other authors did not observe these differences (Behr et al. 1996; Staff et al. 2000; Taube 1993).

1.2.4.3 Intrinsic Membrane Properties

There remains much controversy regarding the membrane properties of the two classes of subicular PCs. Some authors agree that with respect to membrane features and cable properties, IB and RS neurons constitute a homogenous cell group (Traub1993, Staff 2000), whereas others argue that subicular IB cells displayed a more negative resting membrane potential (RMP) (Behr et al. 1996; Greene and Mason 1996; Kim and Spruston 2012), a lower input resistance (R_{in}) (Greene and Mason 1996; Greene and Totterdell 1997; Kim and Spruston 2012; Menendez de la Prida et al. 2003; Panuccio et al. 2012), and a shorter time constant (τ) (Greene and Mason 1996; Mason 1993; Stewart and Wong 1993) compared to RS cells. A recent study performed by Panuccio and colleagues in 2012, on the other hand, came to the conclusion that the τ of IB PCs is not shorter but significantly longer compared to RS cells. Given the lack of unity, a discrimination based on passive membrane properties seems unreliable.

1.2.4.4 Active Membrane Properties

In contrast to the passive membrane properties, there exists more unity concerning the active membrane features of subicular PCs. IB cells display a significantly greater sag potential compared to RS cells, which is mediated by a hyperpolarization-activated cation conductance (I_h) (Greene and Mason 1996; Greene and Totterdell 1997; Kim and Spruston 2012; Mason 1993;

Stewart and Wong 1993; Taube 1993; van Welie et al. 2006). A hyperpolarizing current injection causes a shift of membrane potential towards a more hyperpolarized potential followed by a rebound depolarization mediated by Na^+ and K^+ conduction through the I_h channel (Pape 1996; Robinson and Siegelbaum 2003). Upon the termination of a hyperpolarizing pulse, IB cells respond with a depolarization of membrane potential caused by Na^+ influx, namely anodal break potential, which can induce burst firing at depolarized membrane potentials that would otherwise prevent bursting (Stanford et al. 1998; Stewart and Wong 1993; van Welie et al. 2006). The anodal break potential is more prominent in IB than in RS cells (van Welie et al. 2006). There is no difference of voltage-dependency and kinetic properties of I_h in the two types of subicular PCs suggesting a similar composition of subunits (van Welie et al. 2006).

1.2.5 Neurochemical Discrimination

A neurochemical discrimination of subicular PCs can be observed due to their distinct reactions to the application of chemical agents. In IB cells, the application of the neurotransmitter somatostatin leads to a greater hyperpolarization of membrane potential and reduction of R_{in} than in RS cells (Greene and Mason 1996). Furthermore, it has a greater influence on GABAergic inhibition in IB compared to RS PCs. Neurons that are immunoreactive for somatostatin are located within the ventral subiculum projecting to the nucleus accumbens (Aylward and Totterdell 1993), suggesting that IB but not RS neurons are involved in the subiculum-nucleus accumbens pathway. A loss of activity in this pathway has been associated with some symptoms of schizophrenia (Gray et al. 1991). In addition, synaptic transmission in the subiculum is influenced in a cell-specific manner. The glutamatergic transmission at CA1-subicular synapses is depressed by group II metabotropic glutamate receptors (Kintscher et al. 2012). The reduction of excitatory currents is higher in IB than in RS cells. In contrast to this, the nicotinamide adenine dinucleotide phosphate (NADPH)-diaphorase activity and the neuronal isoform of nitric oxide synthase has been discovered exclusively in RS but not IB PCs (Greene et al. 1997). Nitric oxide is involved in the induction of long-term potentiation acting as an intracellular messenger (Garthwaite et al. 1988) and is involved in the protection from toxic cell damage as well as apoptosis (Behrens et al. 1996).

1.3 Network Oscillations

Rhythmic synaptic activity of neuronal assemblies leads to a fluctuation of network potential which can be measured in an electroencephalogram (EEG) or extracellularly as local field potential (LFP) (Buzsáki and Draguhn 2004). Neuronal rhythmic activity has been categorized into frequency bands and distinct frequencies have been associated with specific behavior and became the subject of extensive research (Buzsáki and Draguhn 2004). An insight into the complex neuronal structure of the brain is aspired by exploring the cellular structures underlying the behavior-specific oscillatory pattern. Cellular synchrony plays an essential role in the generation of network oscillations and serves to coordinate and create associations among distant cellular groups (Singer 1993). The exact timing of neuronal discharge is crucial for the process of information coding and binding (O'Keefe and Recce 1993). The hippocampal formation is capable of generating rhythmic cellular activity in various frequency bands (Buzsáki et al. 2003; Klausberger and Somogyi 2008). Network oscillations in the theta (5-10 Hz) and gamma (30-100 Hz) frequency ranges and high frequency oscillations associated with slower potential fluctuations, so called SWR oscillations, are the most prominent. Recent research indicates a functional connection between the two major network states of gamma and SWR oscillations (Zylla et al. 2013). Gamma oscillations promote activity-dependent plasticity in neuronal assemblies, whereas the SWR rhythm acts to stabilize preformed neuronal groups. There exists very little information regarding the involvement of the subicular IB and RS PCs in the generation of network oscillations within the subiculum.

1.3.1 Sharp Wave Ripple Oscillations

SWR oscillations are composed of high frequency oscillations (200 Hz) superimposed on slower sharp waves (Buzsáki et al. 1992). This form of oscillatory activity has received a variety of different names, some of which are spontaneous population rhythmic activity (Wu et al. 2006), population bursts (Ellender et al. 2010) and SWR (Buzsáki et al. 1992; Kubota et al. 2003; Maier et al. 2002; Maier et al. 2003; Wu et al. 2002). Within the intact brain, sharp waves are present during slow-wave sleep and awake immobility (Buzsáki 1986; Buzsáki et al. 1992). Functionally slow waves have been associated with memory consolidation regulating synaptic plasticity (Axmacher et al. 2008; Buzsáki 1998; Colgin et al. 2004) and facilitating the transfer of memory traces to extrahippocampal regions for long-term storage (Buzsáki 1989; Sadowski et al. 2011). Within the hippocampal formation, SWR oscillations exist *in vitro* independent of pharmacological or electrical stimulation (Maier et al. 2003; Wu et al. 2005a; Wu et al. 2006).

1.3.1.1 Generation of Sharp Wave Ripple Oscillations

The most extensive research concerning the generation of SWR oscillations has been performed in the hippocampal CA1 area under both *in vitro* (Bähner et al. 2011; Maier et al. 2003; Wu et al. 2002) and *in vivo* experimental conditions (Buzsáki 1986; Buzsáki et al. 1992; Csicsvari et al. 1999; Maier et al. 2011; Ylinen et al. 1995) and across several rodent species (Wu et al. 2002). On a cellular level, the generation of SWR oscillations depends on the balance of excitatory synaptic transmission mediated by glutamatergic α-amino-3-hydroxy-5-methyl-4-isoxazolepropionic acid (AMPA) receptors and a $GABA_A$ receptor-mediated inhibition (Draguhn et al. 1998; Ellender et al. 2010; Maier et al. 2003; Wu et al. 2002). Sharp waves are blocked by serotonergic as well as cholinergic activation, thus sharp waves are present in the hippocampus when this input is reduced (Buzsáki 1986; Buzsáki et al. 1989; Kubota et al. 2003). Within the hippocampal formation, SWR oscillations originate in the CA3 region triggered by spontaneous population bursts of hippocampal PCs (Buzsáki et al. 1983; Kubota et al. 2003; Schlingloff et al. 2014; Wu et al. 2005a). The network activity is generated and maintained by the extensive intrinsic recurrent connectivity of the CA3 region (Amaral and Witter 1989; Buzsáki et al. 1983; Maier et al. 2003; Miles and Wong 1986; 1987). The rhythmic excitation propagates to the CA1 region, reaching both the PCs and GABAergic interneurons via feedforward activation (Csicsvari et al. 1999; Wu et al. 2002). Within the CA1 and CA3 region, the majority of PCs remain silent and the active cells fire only sporadically (Buzsáki et al. 1992; Bähner et al. 2011; Ellender et al. 2010; Wu et al. 2005a). As a group, however, the PCs impose a sufficient excitatory drive onto GABAergic neurons. Single interneurons are interconnected synaptically (Hájos and Mody 1997) and electrically (Hormuzdi et al. 2001) forming a network. The activated interneuron network discharges rhythmically imposing phasic inhibitory postsynaptic potentials (IPSPs) onto the hippocampal PC assembly, thus synchronizing and timing the PC firing (Buzsáki et al. 1992). Additionally, it has been demonstrated that single perisomatic targeting interneurons can suppress and consequently facilitate sharp wave generation via rebound depolarization and in this way synchronize PC firing (Cobb et al. 1995; Ellender et al. 2010). These interneurons have been identified as parvalbumin-positive somatically targeting basket cells (Csicsvari et al. 1999; Klausberger et al. 2003; Klausberger and Somogyi 2008; Schlingloff et al. 2014; Ylinen et al. 1995). Sharp waves, therefore, represent the summation of interneuron-mediated IPSPs in a large synchronized PC assembly (Wu et al. 2002; Ylinen et al. 1995). The pronounced synchronous discharge of active cells during the SWR rhythm facilitated by synaptic inhibition strengthens the hippocampal connections to the neocortex and subcortical projection areas, creating windows of low and high neuronal excitability in target cells (Buzsáki

et al. 1992; Chrobak and Buzsáki 1996; Csicsvari et al. 1999; Ylinen et al. 1995), while strict segregation of participating and silent PCs improves the signal-to-noise ratio (Buzsáki et al. 1992; Bähner et al. 2011; Maier et al. 2003).

The fast ripple component has been suggested to result from electrical coupling via gap junctions between the axons of PCs (Draguhn et al. 1998; Maier et al. 2002; Maier et al. 2003; Schmitz et al. 2001; Traub and Bibbig 2000; Traub et al. 1999; Ylinen et al. 1995). More recent publications, however, indicate that the generation of fast ripple oscillations dependents on the precise interaction between excitatory and inhibitory neuronal networks (English et al. 2014; Stark et al. 2014).

1.3.1.2 Sharp Wave Activity in the Subiculum

The sharp wave rhythm spreads from the hippocampal CA3 and CA1 region to the subiculum and then further to the EC (Chrobak and Buzsáki 1996; Maier et al. 2003; Wu et al. 2006). The sparse discharge of CA1 PCs sufficiently activates the subicular network (Norimoto et al. 2013; Wu et al. 2002; Wu et al. 2006). However, in isolation, the subiculum is also capable of intrinsically generating sharp waves even though the frequency and amplitude are reduced (Wu et al. 2006). So far, there has been one single study examining the intracellular correlates of sharp waves within the subiculum (Wu et al. 2006). Subicular PCs show sharp wave-correlated mixed inhibitory and excitatory synaptic potentials mediated by $GABA_A$ and AMPA receptors, respectively (Wu et al. 2006). Neurons that tend to be active are mostly IB neurons (Norimoto et al. 2013; Wu et al. 2006). The active neurons display correlated intracellular inwards currents while the silent cells show prominent IPSPs (Wu et al. 2006). There has been no explicit identification of firing pattern within the subiculum showing the involvement of the two distinct subicular PC classes during spontaneous sharp wave activity.

1.3.2 Gamma Frequency Oscillations

Network oscillations in the gamma frequency range (30-100 Hz) have been documented in many different brain regions including the hippocampal formation (Bragin et al. 1995; Buzsáki and Draguhn 2004; Csicsvari et al. 2003; Fries et al. 2007) and throughout various species, including rodents and humans (Fries et al. 2007). Within the hippocampal formation, gamma oscillations can be recorded in *in vivo* (Bragin et al. 1995; Buzsáki et al. 2003; Csicsvari et al. 2003) and *in vitro* experimental settings (Buhl et al. 1998; Dugladze et al. 2012; Fisahn et al. 1998; Gloveli et al. 2005a; Gloveli et al. 2005b). Gamma frequency oscillations express their largest amplitude when nested within the slower theta rhythm (Bragin et al. 1995; Colgin and Moser 2010), but they also

occur separately. An orthogonal arrangement of gamma and theta rhythm-generating microcircuits has been observed within the hippocampal area CA3 (Gloveli et al. 2005a). In the freely moving animal, gamma and theta waves are present during spatial exploration and the REM phase of sleep (Bragin et al. 1995). The gamma rhythm is essential for the processing of spatial and episodic memory and is involved in higher mental tasks including sensory stimulation as well as memory storage and retrieval (Bartos et al. 2007; Colgin and Moser 2010; Fries et al. 2007). Oscillations in the gamma frequency range provide a temporal framework that assists in encoding and retrieval of memory traces binding neurons to coherently working assemblies by promoting cellular synchrony over a wide distance (Bragin et al. 1995; Csicsvari et al. 2003).

Gamma frequency oscillations *in vitro* can be induced mainly in two different ways: (1) electrical tetanic stimulation, which generates transient phases of gamma oscillations (Traub et al. 1996; Whittington et al. 1997) and (2) chemical activation of receptors, which results in sustained gamma waves: the muscarinic acetylcholine receptor activated through the pharmacological agent carbachol (Fisahn et al. 1998), the kainite receptor (Buhl et al. 1998; Fisahn 2005; Fisahn et al. 2004; Gloveli et al. 2005b), and metabotropic glutamate receptor (Whittington et al. 1995). These different manners, in which gamma oscillations can be initiated *in vitro*, have deviant electrophysiological features. This concerns especially the excitatory drive that is triggered by the various agonists of excitatory receptor families, whereas the gamma generation crucially relies on an intact inhibition mediated through $GABA_A$ receptor transmission (Buhl et al. 1998; Buzsáki and Wang 2012; Fisahn 2005). Since the *in vitro* observations are comparable to the *in vivo* situation with some variation, it has been suggested that the different mechanisms of gamma oscillation represent a region- and state-dependency of network oscillation and thus, are all crucial within the intact brain to some extent (Bartos et al. 2007).

1.3.2.1 Generation of Gamma Oscillations

Within the hippocampal formation, there exist two established independent gamma generators: one in the DG and another in the CA3-CA1 region. The gamma generator in the DG requires an extrahippocampal drive. Following the removal of the EC, the gamma power decreases significantly, suggesting that the entorhinal input to the DG acts as an external initiator (Bragin et al. 1995). The CA3 region of the hippocampal formation generates gamma frequency oscillations independently, which then propagate to the CA1 region (Csicsvari et al. 2003; Fisahn et al. 1998). On a cellular level, the hippocampal gamma activity results from the feedback process of glu-

tamatergic PC and GABAergic interneurons, the balance between synaptic excitation and inhibition playing a crucial role (Bartos et al. 2007; Buzsáki and Wang 2012; Csicsvari et al. 2003; Fisahn et al. 1998; Fries et al. 2007; Mann and Paulsen 2007; Traub et al. 1996). Based on the information available from the CA3-CA1 gamma generator, the necessary cellular mechanisms involved in the generation of gamma oscillations are a mutually interconnected interneuron network with $GABA_A$ mediated inhibition and a sufficient excitatory drive (Buzsáki and Wang 2012; Traub et al. 1996). The gamma frequency depends on the strength of excitatory input and on the properties of the kinetics of interneuronal coupling (Buzsáki and Wang 2012; Traub et al. 1996; Whittington et al. 1995). The hippocampal PCs give rise to an excitatory drive activating the interconnected interneuron network. This synchronized inhibitory network terminates the pyramidal cell firing and arranges it into single time frames. In this context, the perisomatic targeting basket cells appear to be the most promising interneuron type (Bartos et al. 2007; Buzsáki and Wang 2012). The firing frequency of PCs is very low and only a fraction of PCs is recruited for a given gamma cycle, whereas the fraction of interneurons that fire phase-locked to the field is much higher (Csicsvari et al. 2003; Gloveli et al. 2005b). The PCs' firing is synchronized and timed by the interneuron network which can be measured as LFP in the gamma frequency range.

1.3.2.2 Gamma Oscillations in the Subiculum

Early studies show that oscillatory activity in the gamma frequency range can be induced in the subiculum by tetanic stimulation of the CA1 area or the subiculum itself (Colling et al. 1998; Stanford et al. 1998) and gamma oscillations in the presubicular cortex can be triggered tetanically after stimulation of the subiculum (Funahashi and Stewart 1998). A more recent study has investigated the generation of spontaneous slow (25-50 Hz) and fast (100-150 Hz) gamma oscillation in the whole hippocampal preparation (Jackson et al. 2011). It has been shown that the isolated subiculum can generate gamma frequency oscillation independent of intra- or extrahippocampal input, suggesting that the subiculum is the third spontaneous gamma generator in the hippocampal formation. Curiously, Jackson and colleagues explicitly excluded the IB cell type from their investigations, which appears to be the most promising cell class with regard to the generation of network oscillations (Colling et al. 1998; Menendez de la Prida 2003; Taube 1993; van Welie et al. 2006; Wu et al. 2006). Very recently, our team, examining different slice orientations and subicular subregions, could demonstrate in an *in vitro* study that the subiculum can generate gamma frequency oscillations in isolation (Eller et al. 2015). Thus, the subiculum constitutes the third independent gamma generator of the hippocampal formation.

1.4 Aim of the Thesis

The subiculum, as the hippocampal relay and output structure, holds a strategic position in the information processing circuit of the hippocampal formation. Surprisingly, the participation of the two distinct classes of subicular PCs, IB and RS cells, in the two major hippocampal network rhythms, sharp waves and gamma frequency oscillations, remains poorly studied. This study focuses on the investigation of the involvement of the subicular PC classes in the oscillatory network activity in the subiculum. Furthermore, this study aims at examining whether the two electrophysiologically distinct subicular cell classes are suited to carry out different functional tasks within the subicular network which could then result in two separate and parallel streams of information flow through the subiculum and further on to the hippocampal target areas. For this purpose, the intrinsic and synaptic properties of subicular PCs during sharp waves and subsequent gamma frequency oscillations are evaluated. On a single cell level, the participation within the network oscillations is identified, which leads to characterizing differences between subicular IB and RS cells.

The hippocampal formation represents the origin of epileptic activity and neuropathological conditions such as schizophrenia. In the light of a general medical approach, the investigation of the underlying cellular structures within the subiculum might aid in comprehending fundamental pathophysiological structures and thus reveal future targets for the development of medical therapeutic approaches.

2. Methods

2.1 Ethical Approval

All procedures were approved by the Regional Berlin Animal Ethics Committee, T 0124/05, and are in full compliance with national regulations.

2.2 Experimental Animals

Experiments were performed on 26 adult (>6 weeks of age) C57/Bl6 mice of both sexes. The animals were obtained from the Forschungseinrichtungen für Experimentelle Medizin (FEM) of the Charité – Universitätsmedizin Berlin.

2.3 Slice Preparation

The slice preparation was performed as published previously (Eller et al. 2015; Kehrer et al. 2007; Winkelmann et al. 2014). The animals were anesthetized with inhaled isoflurane (Forene®, Abbott, B506) and decapitated. After removing the brain from the skull, the cerebellum was dissected. The brain was then placed on a cooled tile and the apical pole was cut and then glued (UHU® Sekundenkleber) to the holding device of a microtome slicer (Leica VT1200 Microtom, Leica Mikrosysteme Vertrieb GmbH, Wetzler, Germany) with the frontal side up. The artificial cerebro-spinal fluid (ACSF) used during preparation, incubation, and recording was made with deionized distilled water and contained (in mM): NaCl, 129; KCl, 3; NaH_2PO_4, 1.25; $CaCl_2$, 1.6; $MgSO_4$, 1.8; $NaHCO_3$, 21; glucose, 10 at a pH of 7.4 and an osmolarity of 300 ± 5 mOsm/kg; saturated with 95 % O_2 and 5 % CO_2. The holding chamber was filled with oxygenated ACSF. It was then integrated into a second chamber that was padded with ice to secure a cool environment. The hemispheres were separated and horizontal slices of 400 µm thickness were obtained. The slices contained the hippocampus proper, the subiculum, the EC, and some adjacent cortices. On average, five to six slices per hemisphere were gained from one experimental animal. The slices were transferred to an in-house-built 'interface chamber' lined with lens cleaning paper (Kodak, USA). The slices were placed on small fragments of the same paper. The chamber was continuously perfused with ACSF at a rate of 1.8 to 2.0 ml/min with a Minipuls3 pump (Gilson Inc., WI, USA). The temperature of the chamber was maintained at 34 ± 1°C. The fluid level was adjusted so that the superficial surface of the slice was perfused by a thin ACSF fluid layer. Pieces of nylon stockings, which were sterilized prior to every experiment, controlled the level of fluid within the chamber ensuring rapid drainage. The holding chambers were covered with small plastic plates laminated with tissue paper to maintain the moist environment. The interface chamber was situated on a

vibration-cushioned table (Newport, USA). The table was topped with a Faraday cage to shield the recordings from 50 Hz noise (Figure 4). After preparation, the slices were allowed to rest for at least 1 hour for recovery prior to the recordings.

2.4 Extracellular Field Recordings

Extracellular recording electrodes were drawn on a horizontal micropipette puller (ModelP-97, Sutter Instruments Co., CA, USA) from borosilicate glass (GB150F-8P with filament, Science Products GmbH, Hofheim, Germany). The tip resistance varied from 4 to 5 MΩ. For recording purposes the electrodes were filled with ACSF before they were placed over a chlorinated silver wire. The silver wire was chlorinated prior to the recordings with a 1 M KCl solution and a 9 V block battery. The reaction was allowed to take place until the wire was covered with a translucent white coating. All electrodes were placed under direct visual guidance with the Askania Stereomikroskop (Askania Mikroskop Technik, Rathenow, Germany). Extracellular recordings were obtained from the middle of the subicular str. pyramidale. An *in vitro* model was used that permits the reproduction of the two major network states, spontaneous SWR and gamma frequency oscillations (Eller et al. 2015; Gloveli et al. 2005a; Maier et al. 2003; Winkelmann et al. 2014). 400 nM of kainic acid (KA, Ascent Pharmaceuticals Inc., NY, USA) was applied to the bath to induce gamma network oscillations. Sharp waves and gamma frequency oscillations were recorded extracellularly within the subiculum. The LFP was amplified with a custom-made amplifier, digitalized with a sampling rate of 2 kHz (Digidata 1322A, Axon Instruments Inc., CA, USA), and analyzed with the pClamp software package (notch filter 50 Hz; Axon Instruments Inc., CA, USA). Oscillatory peak power and frequency were determined by fast Fourier transforms (FFT) with a 1 Hz spectral resolution. Only slices with a gamma frequency oscillation $>9x10^{-6}$ mV^2/Hz were included into the sample or analyzed further.

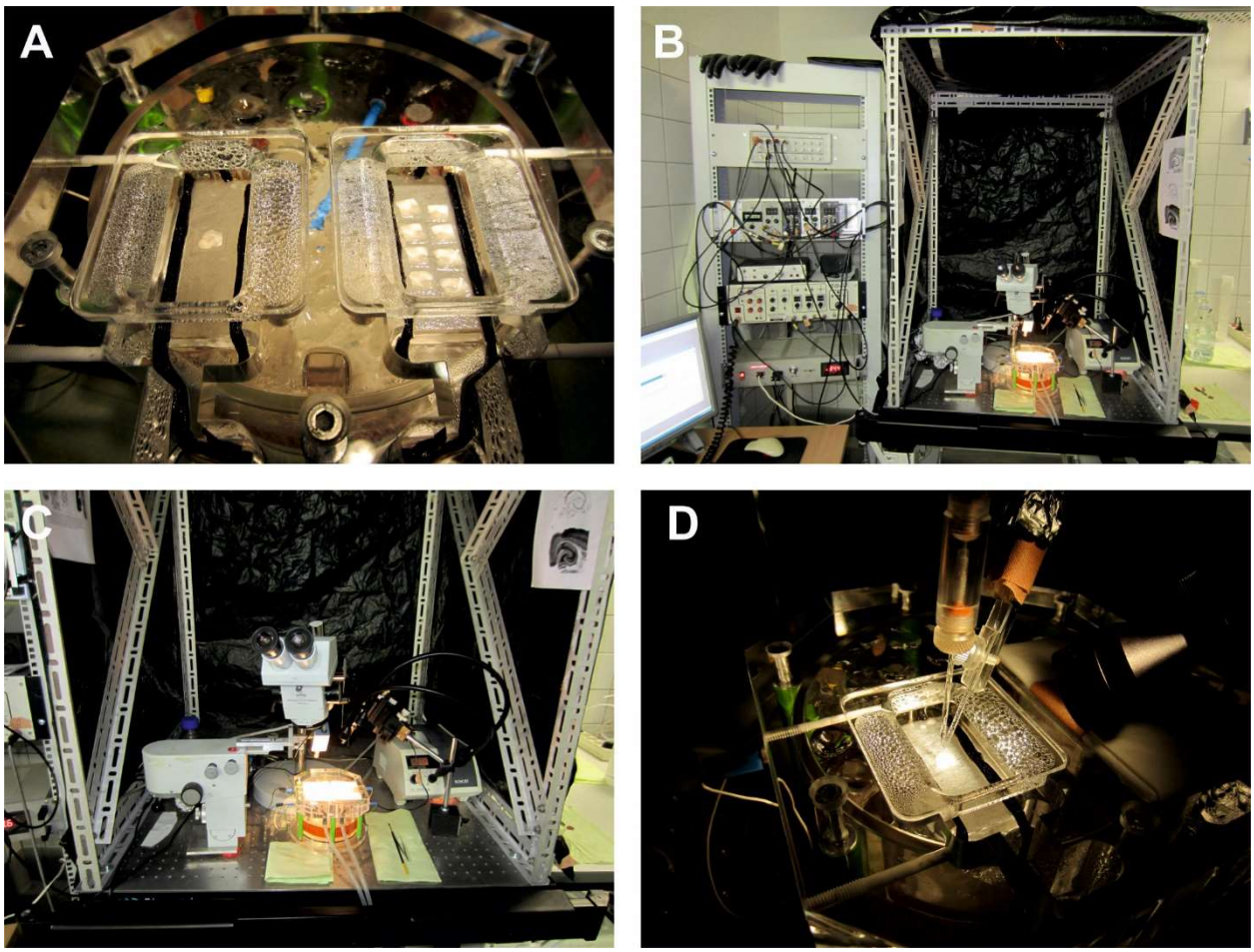

Figure 4. Experimental set-up.

(A) 'Interface chamber' with the recording (left) and the storage chamber (right). The slices rest on pieces of lens cleaning paper while pieces of nylon stocking ensure the necessary fluid level. The chamber is heated and the plastic covers ensure a moist environment.

(B) Experimental set-up with the rack containing the electrophysiological equipment for extracellular and intracellular recordings and the radiator (left) as well as the Faraday cage containing the 'interface chamber' lined with electro foil to shield from 50 Hz noise (right).

(C) The experimental setting contains the 'interface chamber', a light source, the microscope, and the electrodes for extracellular (left) and intracellular recordings (right) resting on a vibration-cushioned table.

(D) Enlarged view of the recording chamber. The intracellular recordings electrode (left) penetrates the tissue vertically. The extracellular electrode (right) targets the middle of the subicular str. pyramidale.

2.5 Intracellular Recordings

Intracellular microelectrodes were made of borosilicate glass and filled with intracellular solution containing 2 M potassium acetate ($C_2H_3KO_2$) and 2% biocytin administered through a 0.22 µm filter unit (Millex-GV, Carrigtwohill, Co. Cork, Ireland) to prevent the electrode from occluding. The tip of the electrode was back filled with the filtered solution for about one minute (min). The same chlorinated silver wire was used for this as that used for extracellular recordings. The tip resistance ranged from 60 to 110 MΩ. Electrodes not falling within this range or displaying an instable tip resistance were rejected. Sharp microelectrode recordings were obtained from subicular PCs. The electrodes were placed in the str. pyramidale of the subiculum under visual guidance. Cells were impaled and then allowed to rest for ten min. A negative current injection was applied in order to hyperpolarize the membrane potential and assist the cell in recovering from impalement. Only cells with a RMP ≤ −50 mV, an AP half-width of ≤ 1.2 ms, and stable electrophysiological properties throughout the experimental protocol were accepted for further analysis. Signals were amplified with an IR-183 Intracellular Recording Amplifier (Neuro Data Instruments Corp, PA, USA) with an active bridge circuit and digitalized using a 16 Bit Data Acquisition system (Digi Data 1322A, Axon Instruments Inc., CA, USA). The bridge balance was monitored continuously throughout the experiment. It was adjusted as needed by optimizing the cell's response to a small negative current injection. Transient suppression was used to remove the capacitance artifacts in some of the recordings. Excitatory postsynaptic potentials (EPSP) and IPSP were recorded at about −80 mV and 0 mV, respectively (Jackson et al. 2011; Taube 1993).

2.6 Data Analysis

The RMP was measured from the voltage baseline without current injection after the initial impalement-induced depolarization had subsided. During gamma frequency oscillations, the membrane potential was determined in the same way given that a sufficient gamma power was detected extracellularly. The membrane potential during gamma frequency oscillations without current injection will be referred to as membrane potential in contrast to the RMP during sharp wave activity. The detected value was corrected for an offset which was determined when the microelectrode was withdrawn from the cell. For the offset correction, the tip potential within the cell was subtracted from the voltage potential measured in the extracellular space at the end of the experiment. AP were analyzed for all cells. If the cell was not spontaneously active, it was depolarized just above threshold by a positive current injection and the first induced AP was used for analysis. If the cell fired spontaneously, any of the uniform APs was taken into account for measurement. The

amplitude of AP was measured from the level of RMP to the maximum peak of AP. The half-width was calculated as the time difference between half of the maximal amplitude on the ascending and descending slope of the AP. For the purpose of AP threshold determination, recordings with small steps of depolarizing or hyperpolarizing current injections were performed during the experiment. For inactive cells, the membrane potential that caused the cell to initiate AP firing was considered as AP threshold. Cells that fired spontaneous AP at RMP were hyperpolarized and the last membrane potential at which the cell was still active was accepted as threshold. The measured potential was again corrected for the offset value recorded extracellularly. The ISI was determined as the time difference between the maximum amplitude of APs. The ISI between the first and the consecutive AP within a burst was calculated. The afterdepolarization (ADP) and afterhyperpolarization (AHP) were measured when present. The maximum or minimum deflection was determined in relation to the RMP in order to calculate the ADP or AHP, respectively. If the cell was not spontaneously active, the ADP or AHP was measured at the membrane potential just above threshold. The accommodation of AP firing was determined by depolarizing current injection with a progressive increase of 40 pA per step, a step duration of 1 s, and a maximum current injection of 500 pA. Due to the fact that high current injections can result in distorted AP waveforms accommodation was measured at the last current step displaying normal AP shapes which would differ between individual recordings. The ISI between the first (t_1) and the last (t_2) pair of APs was measured and the accommodation was calculated as the time difference between the first pair of APs divided by the time difference of the last pair of APs at the end of the stimulus, ($100x\ \Delta t_1/\Delta t_2$). At the slope of increasing membrane potential, burst firing or a salve of APs could be recorded in subicular PCs. The ISIs within a burst and salve were similar and were thus unreliable as discrimination tools. The burst firing differed from the salve of fast AP, displaying an underlying depolarizing envelope followed by a hyperpolarizing afterpotential, both of which a salve lacked. Initial AP bursts or salvos were discarded for accommodation analysis. Current-voltage relations (IV-curve) were constructed from the changes in membrane voltage response during both positive and negative current steps. Steps of 20 pA, starting at −320 pA and increasing up to 200 pA, with a step duration of 500 ms were applied. The R_{in} was determined from the cell's response to a −100 pA current pulse calculated after any sag potential had subsided. The τ represents the time needed to reach 63% of the steady-state voltage deflection during the same current pulse. During negative current injection, the degree of hyperpolarization-activated sag potential was measured when present. The sag was determined as the maximum voltage deflection (V_{peak}) from a baseline of steady-

state voltage deflection (V_{ss}) in response to a −100 pA, −200 pA and −300 pA hyperpolarizing current injection (100x (V_{peak} –V_{ss})/V_{peak}; Greene and Mason, 1996).

2.7 Matlab Analysis

The recorded data was further processed in Matlab (The Mathworks®, Inc.) with customized routines. The LFP was bandpass-filtered 3-100 Hz with a Butterworth filter. The 50 Hz noise was filtered with a second-order IIR notch filter. In order to remove membrane potential fluctuations during gamma oscillations, the intracellular recordings of EPSPs and IPSPs were high-pass-filtered at 2 Hz with the pClamp software prior to the Matlab import. LFP oscillatory peaks as well as APs and EPSPs/IPSPs were identified as maximal deflections above a manually set threshold. The maximum of sharp wave or gamma frequency peak deflections were defined as time 0 and the averaged time difference of the corresponding AP, EPSP, or IPSP triggered peaks in the simultaneous intracellular recording trace was determined. For sharp waves with a maximal negative LFP polarity, the minimum was defined as time 0. In this context, the subicular PCs displayed a comparable general phase-locked behavior for both sharp wave polarities, so that the data for all sharp wave analysis were pooled together. The illustrated mean sharp wave signal is solely based on the positive waveform deflections in summarizing illustrations, however. For the determination of the mean sharp wave amplitude, the absolute value was considered. The analyzed time window was set to 150 ms before and after the triggered LFP for sharp wave and 60 ms for gamma frequency oscillations. A mean peak EPSP and IPSP value was calculated separately for each recording of sharp wave and gamma frequency oscillations. The mean peak EPSP and IPSP amplitude distribution of all analyzed recordings was further displayed as box plots and aggregated to a grand mean population value for each oscillatory network pattern. Furthermore, the aggregated APs were displayed as spike time points per triggered LFP peak within a rast dot plot and as a cumulative spike time histogram with a temporal resolution of 1 ms. In order to evaluate the phase-coupling of APs with respect to sharp wave and gamma frequency oscillations, the cumulative spike-time histogram was analyzed. PCs were considered to be phase-locked if the LFP triggered AP histogram displayed a clear peak of AP generation. For some subicular PCs, a prominent inhibition correlated with the peak of triggered LFP deflection resulted in a pause of AP generation. These cells were considered to be inhibited during the peak LFP deflection. Cells that did not display a clear arrangement of AP firing with reference to the field potential were considered unclassified and were not taken into account for further analysis of firing behavior. For the purpose of spectral analysis of SWR and gamma frequency oscillations, the recordings were divided into consecutive

1 s time bins. An FFT was calculated for each time bin and the frequency of the peak spectral amplitude was detected within each power spectrum. The FFT-based spectrogram (1 s time bins, Hamming window, 50 % overlap) was computed to illustrate gamma frequency oscillations and a complex Morlet wavelet transform (cmor2-1) was used to display SWR (bandpass filter 100-300 Hz). The sharp-wave associated high frequency ripple component was not investigated systematically. For exemplary illustration of the ripple component, a complex Morlet wavelet transform (cmor2-1) was used (bandpass filter 100-300 Hz). The mean frequency component of each ripple episode was defined as the spectral frequency analog with the maximal peak power of the wavelet transform (Figure 5). Furthermore, a phase distribution of the AP and IPSP mean values was calculated for each cell type and oscillatory network state based on normalized oscillatory cycle length (24 ms for gamma frequency oscillations, 80 ms for SPWs, with the peak assigned to 180° each) and displayed as polar diagrams (Figure 27).

For the purpose of illustrations, the graphic design software CorelDRAW (Version 12 and X7, Corel Cooperation, Ontario, Canada) was utilized. The extracellular traces were bandpass-filtered at 2-100 Hz and 50 Hz notch-filtered with the pClamp software in all figures displayed unless indicated otherwise.

2.7.1 Statistics

Statistical calculations were performed in Microsoft Excel or Matlab. The assumption of normal distribution was justified by the Lilliefors test. The paired student's t-test was used for statistical analysis and differences were considered statistically significant if $p<0.05$. Significance levels are marked with an asterisk: * = $p<0.05$; ** = $p<0.01$; *** = $p<0.001$. Average values are expressed as the mean ± standard error of the mean (SEM).

2.8 Classification of Intrinsically Bursting and Regular Spiking Cells

Intracellular recordings were made exclusively from subicular PCs. The cells were categorized as intrinsically bursting (IB) or regular spiking (RS) based on their firing properties. IB cells fired a burst of APs in response to a depolarizing current injection. A burst consisted of two to six APs riding on top of a depolarizing wave followed by a depolarizing afterpotential. The consecutive APs within a burst characteristically decreased in amplitude and gained in width. The ISI within a burst was considered ≤ 8 ms (Wu et al. 2006). In some cells, bursting could also be elicited at the break of hyperpolarizing current injection (anodal break potential). RS cells fired a train of single APs with ISIs similar to those during bursting. No burst firing could be induced in these cells.

Once the PCs were classified during the initial spontaneous sharp wave rhythm, the categorization was maintained for the consecutive gamma frequency oscillations. However, the ability to fire bursts of APs was verified after the initiation of the active gamma field. Based on their firing behavior during spontaneous sharp wave and gamma frequency oscillations, the subicular PCs were identified as active or not active (silent). The activity was evaluated for each network oscillation separately so that a cell could change activity mode throughout the duration of the experiment. Cells were considered silent if they did not fire any APs at RMP in a 60 s recording period. Cells that did fire APs were considered active. If a neuron fired APs within the first 10 min after impalement but ceased firing after recovery, this cell was classified as not active, with the firing being attributed to the depolarization of membrane potential following impalement.

2.9 Biocytin Staining

2% biocytin was added to the intracellular solution for staining. During the time of the electrophysiological recordings, biocytin diffused into the impaled soma and spread throughout the cell. The depolarizing current injection used for identifying the electrophysiological properties enhanced the distribution of the staining agent. After the recordings, the slices were removed from the recording chamber. In order to extract the lens cleaning paper on which the slices rested throughout the experiment, they were dissolved within ACSF. The ACSF was then drained and replaced by a fixative solution containing 4% paraformaldehyde, in which the slices were immersed for at least 24 hours before being prepared for the staining process. Slices were processed as described in previous publications (Dugladze et al. 2012). The slices were washed three times in 0.1 M phosphate buffer (PB). The avidin–biocytin complex reaction (Vectastain, ABC kit, Vector Laboratories Inc., CA, USA) was allowed to occur overnight at 4°C in the presence of 0.3 % Triton X-100 (Sigma-Aldrich Co. LLC, USA). Afterwards the sections were rinsed several times before development with 0.02 % diaminobenzidine (DAB, Sigma-Aldrich Co. LLC, USA) in 0.1 M PB. The reaction product was intensified with 0.5% osmium tetroxide (OsO_4) (Sigma-Aldrich Co. LLC, USA) and sections were mounted and coverslipped. The cell's morphology was then examined using a Camera Lucida device (MicroBrightField, Inc, VT, USA). Photomicrographs were taken from the stained cells with a Neurolucida Zeiss Axioskop (Carl Zeiss Microscopy GmbH, Göttingen, Germany) and further processed in Photoshop (Adobe Systems Inc., CA, USA). In order to achieve a depth-field view of the microscopic images, stack processing of consecutive focal planes was performed with the combineZP software (version 2, http://www.hadley-web.pwp.blueyonder.co.uk/; Alan Hadley, GNU public license).

3. Results

3.1 LFP within the Subiculum

Two major network states, SWR and gamma frequency oscillations, were recorded within the subiculum *in vitro* (Table 1 and Figure 5). Sharp waves occurred spontaneously and without electrical or pharmacological stimulation with a mean frequency of 2.2 Hz (n = 42) and a mean amplitude of 2.0 mV (n = 42; Table 1). Throughout the experiments, two different groups of sharp waves were detected distinguished by polarities: one displaying a positive maximum (n = 31), the other a negative one (n = 11; Figure 5). The orientation of sharp waves altered between slices but was stable during one recording. The high frequency ripple oscillations superimposing the sharp waves were found for both sharp wave polarities (Figure 5). However, the ripple event within a single recording displayed variable frequencies and not every sharp wave displayed a prominent ripple component so that the fast ripple oscillations were not investigated further. Following kainate application (400 nM), the sharp wave rhythm was gradually reduced in amplitude and frequency. After a brief transitory state with no clear network pattern, oscillations in the gamma frequency range appeared to increase progressively in power before reaching a steady state. Gamma oscillations displayed a mean frequency of 43.7 ± 0.3 Hz (n = 22) and a mean power of $3.2 \times 10^{-4} \pm 1.3 \times 10^{-5}$ mV^2/Hz (n = 22; Table 1). There were no significant differences in amplitude or frequency of network oscillations between the recordings of IB and RS cells (Table 2).

	sharp waves	gamma frequency oscillations
amplitude	0.20 mV (42)	$3.2 \times 10^{-4} \pm 1.3 \times 10^{-5}$ mV^2/Hz (22)
frequency	2.2 Hz (42)	43.7 ± 0.3 Hz (22)

Table 1. Properties of sharp waves and gamma frequency oscillation within the subiculum.

	IB	RS	*p*
sharp wave frequency [Hz]	2.2 (24)	2.3 (18)	0.816
sharp wave amplitude [mV]	0.19 (24)	0.21 (18)	0.439
gamma frequency [Hz]	44.2 ± 0.4 (11)	43.3 ± 0.6 (11)	0.728
gamma power [mV^2/Hz]	$3.8 \times 10^{-4} \pm 2.9 \times 10^{-5}$(11)	$2.6 \times 10^{-4} \pm 2.3 \times 10^{-5}$ (11)	0.375

Table 2. Properties of LFP during recordings of subicular IB and RS PCs.

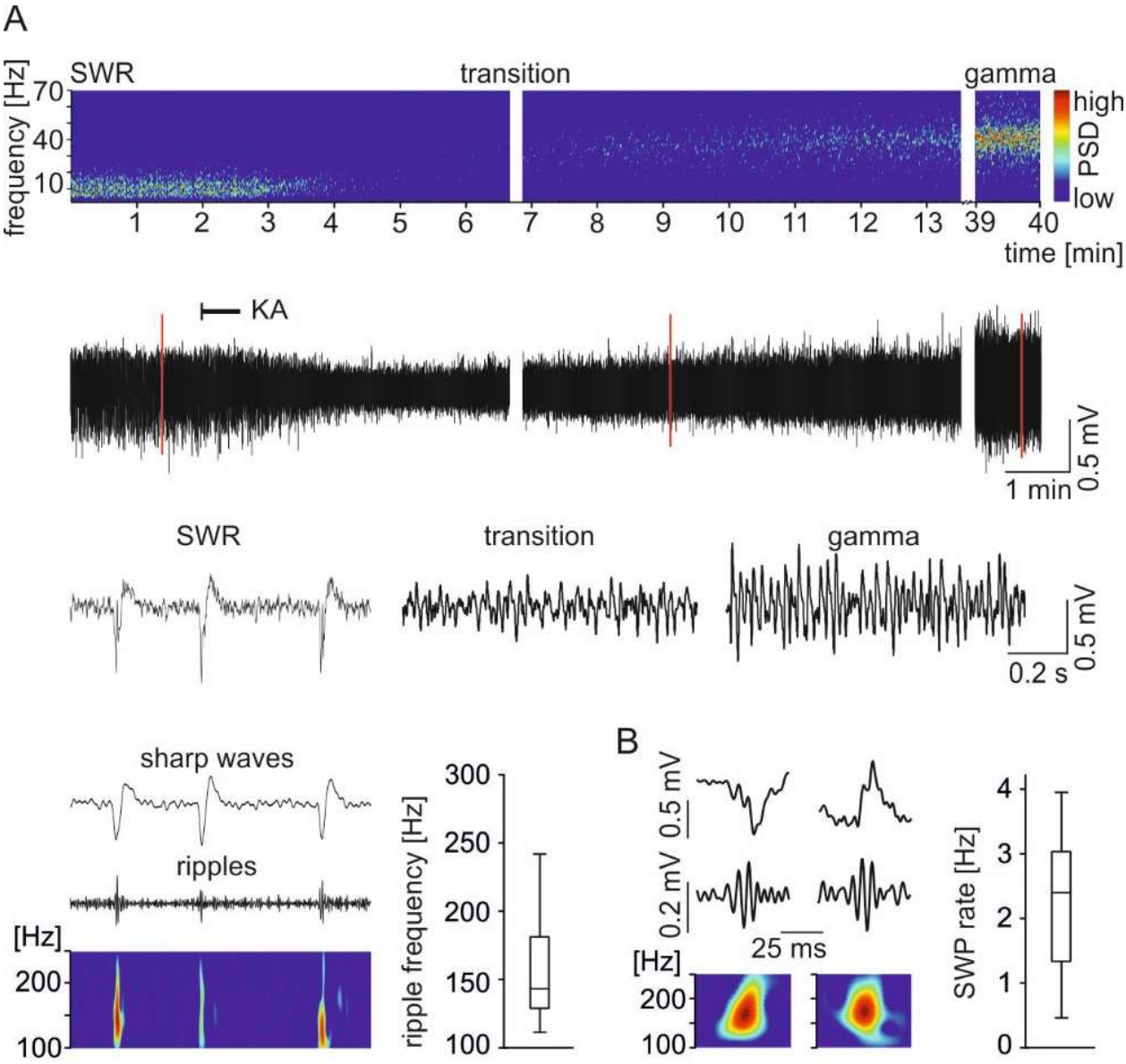

Figure 5. Network oscillatory activity within the subiculum.

(A) The spectrogram (top row) with color-coded power spectral density (PSD) exemplifies the transition from spontaneously occurring SWR to gamma frequency oscillations within the subiculum. The corresponding LFP recordings are displayed below. The application of kainic acid (KA, onset marked by an arrow) abolishes the SWR rhythm and induced, after a brief transitory period, stable gamma frequency oscillations. The recording interruptions of the top spectrograms and the underlying LFP traces are 12 s (middle) and 25 min (right). The red lines mark three examples that are illustrated below with higher temporal resolution (SWR, transition, and gamma). (A, bottom left) The SWR activity (filtered 2-300 Hz), the corresponding sharp waves (filtered 2-50 Hz), and the ripple components (filtered 100-300 Hz) supplemented by the color-coded power spectral density wavelet transform. (A, bottom right) The boxplot depicts the distribution of the

wavelet peak power spectral frequencies of 100 analyzed consecutive ripple events of the upper example trace. (B) Sharp waves of both polarities are exemplified on the left with each SWR trace (filtered 2-300 Hz, top), the ripple trace (filtered 100-300 Hz, middle) and the corresponding wavelet transform as color-coded power spectral density plot (bottom). The boxplot (right) illustrates the distribution of the mean sharp wave rates of all slices investigated (n=42).

3.2 Electrophysiological Properties of Subicular PCs

3.2.1 Electrophysiological Characterization of Subicular PCs

A total of 48 subicular PCs were recorded within the subiculum, 42 of which showed stable electrophysiological conditions and were included into further investigations. 24/42 cells (57%) were classified as IB neurons. Following a depolarizing current injection, these cells responded with a burst of APs (Figure 6 and Figure 7). The ISI between the first and second AP within the burst was 5.0 ± 0.1 ms (n = 24), which is consistent with previous publications (Mattia et al. 1997b; Staff et al. 2000; Wu et al. 2006). When the depolarization was maintained, a train of single APs followed the initial burst. 18/42 cells (43%) were identified as RS cells due to their lack of burst firing. In these cells, bursting could not be induced by depolarizing current injection. RS neurons respond to a depolarizing current injection with a train of single APs (Figure 6 and Figure 7). There was no significant difference in AP half-width, amplitude, or firing threshold between IB and RS cells (Table 3). However, the shape of AP differed between subicular PC classes (Figure 6). RS cells displayed a prominent AHP, whereas IB cells showed an AHP only very infrequently and to a lesser degree ($p = 0.0006$; Figure 7 and Table 3). An ADP was observed regularly in IB neurons but only in one single RS cell ($p = 0.0002$; Figure 7 and Table 3). Following a depolarizing current injection, the ADP in IB cells was reduced in amplitude. The results suggest that subicular IB and RS neurons constitute a homogenous group concerning the intrinsic properties, including RMP, R_{in}, and τ (RMP: $p = 0.263$; R_{in}: $p = 0.306$; τ: $p = 0.586$; Table 3).

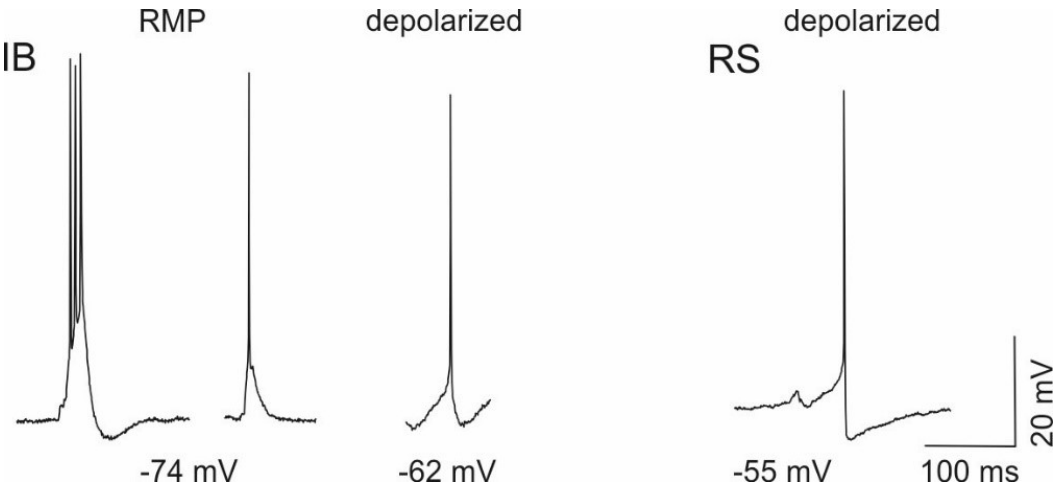

Figure 6. AP shapes of subicular IB and RS cells.

The distinct shapes of AP are displayed for subicular IB (left) and RS (right) cells. The APs are displayed at RMP ('RMP') for the IB cell example and after positive current injection ('depolarized') for both subicular PC classes. At RMP IB cells fire bursts of APs (left) or single APs with prominent ADPs (right). The burst is characterized by the underlying depolarized wave and the distinct hyperpolarizing afterpotential. The ADP vanishes when the IB cell is depolarized. The majority of RS PCs are silent at RMP. They display APs with prominent AHPs when depolarized above threshold.

3.2.2 Sag Potential

A prominent difference that distinguishes the two classes of subicular PCs was the reaction to a hyperpolarizing current injection. In response to a negative current pulse, IB cells displayed a prominent hyperpolarization-activated sag potential. This was observed in accordance to previous studies (Greene and Mason 1996; Greene and Totterdell 1997; Kim and Spruston 2012; Mason 1993; Stewart and Wong 1993; Taube 1993; van Welie et al. 2006). In RS cells, on the other hand, the sag potential was not constantly observed and was significantly lower. There is a highly significant difference between subicular IB and RS neurons with regard to the sag potential at −300 pA ($p = 0.0045$), −200 pA ($p = 0.0001$), and −100 pA ($p = 0.0001$; Figure 7 and Table 3).

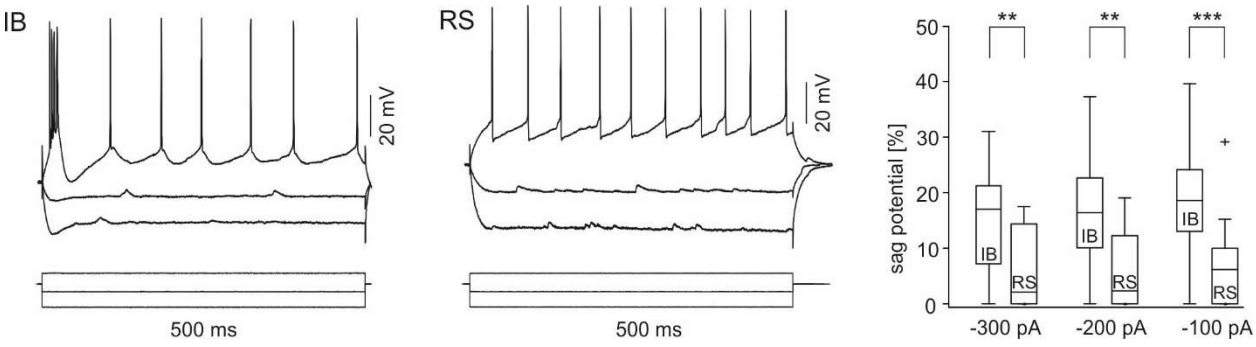

Figure 7. Current-voltage relationship of subicular IB and RS cells.

*The current-voltage relationship of IB (left) and RS (center) cells is displayed with current steps of +140 pA, −100 pA and −300 pA, respectively. IB cells respond to a hyperpolarizing current injection with a sag in membrane potential. A positive current pulse leads to burst firing followed by a train of single APs if the stimulus is maintained. RS cells do not fire bursts and show little or no sag. They answer to a depolarizing current injection with a train of single APs. The population data on the right reveals a significant differences of sag potential in percentage sag at −300 pA (IB: n = 22; RS: n = 18), −200 pA (IB: n = 23; RS: n = 18), and −100 pA (IB: n = 23; RS: n = 18). Asterisks indicate the significance level (** = p ≤ 0.01; *** = p ≤ 0.001).*

3.2.3 Accommodation of AP Firing

The train of single APs that followed the burst after positive current injection in IB cells showed minor adaptation behavior. The accommodation of AP firing in percentage accommodation averaged 69.1 ± 0.7% of control (n = 19). In marked contrast, RS cells displayed an adaptation of AP discharge of 36.7 ± 1.0% of control (n = 16; Table 3). They did not burst at the initiation of a positive current injection. There was a highly significant difference in the accommodation behavior between the two classes of subicular PCs ($p < 0.0001$; Table 3).

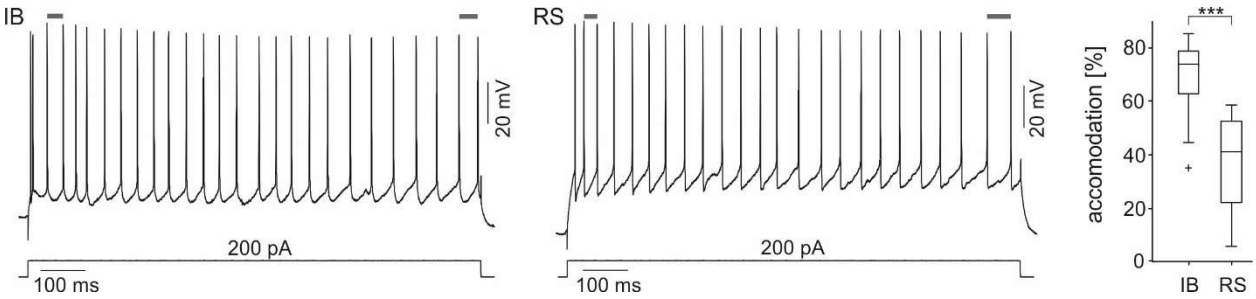

Figure 8. Accommodation behavior of subicular IB and RS cells.

Typical accommodation behavior of IB (left, n = 19) and RS (center, n = 16) subicular PCs following a positive current injection of 200 pA. The analytically relevant ISI is illustrated as a grey bar above the first and last pair of APs. After an initial burst, IB cells show a train of single APs with minor firing adaptation (86.4% of control in the displayed example). RS cells display a prominent accommodation of AP spiking (55.0% of control in the displayed example). The population data on the right reveals a significant difference in accommodation behavior between subicular PC classes indicated by the asterisk (p < 0.0001).

Hence, given the distinct ability to generate bursts of APs, the different AP waveforms, sag potentials, and accommodation behavior, subicular IB and RS cells clearly represent two distinct physiological PC classes.

	IB	RS	*p* value
RMP [mV]	−67.5 ± 0.3 (24)	−70.3 ± 0.5 (18)	0.263
R_{in} [MΩ]	85.6 ± 1.6 (23)	98.2 ± 2.1 (18)	0.306
τ [ms]	6.4 ± 0.2 (23)	7.0 ± 0.2 (18)	0.586
AP amplitude [mV]	67.5 ± 0.4 (24)	68.5 ± 0.5 (18)	0.761
AP half-width [ms]	0.9 ± 0.01 (24)	1.0 ± 0.01 (18)	0.078
AP threshold [mV]	−58.9 ± 0.2 (23)	−56.2 ± 0.5 (17)	0.233
ADP [mV]	4.7 ± 0.2 (23)	0.2 ± 0.0 (18)	0.0002 **
AHP [mV]	−1.3 ± 0.1 (24)	−3.8 ± 0.1 (18)	0.0006 **
sag −300pA [%]	14.3 ± 0.4 (22)	6.2 ± 0.4 (18)	0.0045 **
sag −200pA [%]	16.2 ± 0.4 (23)	6.7 ± 0.4 (18)	0.0021 **
sag −100pA [%]	18.5 ± 0.4 (23)	6.7 ± 0.4 (18)	0.0001 ***
accommodation [%]	69.1 ± 0.7 (19)	36.7 ± 1.0 (16)	<0.0001 ***

Table 3. Electrophysiological properties of subicular PCs.

*Significance level indicated by asterisk (** = $p \leq 0.01$; *** = $p \leq 0.001$).*

3.3 Morphology

20 electrophysiologically identified subicular cells (11 IB and 9 RS) were intracellularly stained with biocytin. All stained neurons displayed the typical shape of pyramidal cells with a pyramidal shaped cell body, long apical dendrites that extended into the molecular layer with some reaching the hippocampal fissure, and short basal dendrites that spread within the deep portions of the str. pyramidale. The axon left from the subiculum via the alveus to travel in the direction of the hippocampal CA1 area and the EC. No prominent morphological variations between the two subicular PC classes could be found by visual inspection (Figure 9). In one case, however, two PCs were equally well stained even though only one cell had been recorded from during the experiment. The electrophysiologically identified neuron was an IB cell. The biocytin staining of the recorded IB cell resulted in the staining of another PC in close vicinity. The phenomenon of dye coupling was exclusively observed in one IB cell (1/11) and not in RS PCs (0/9).

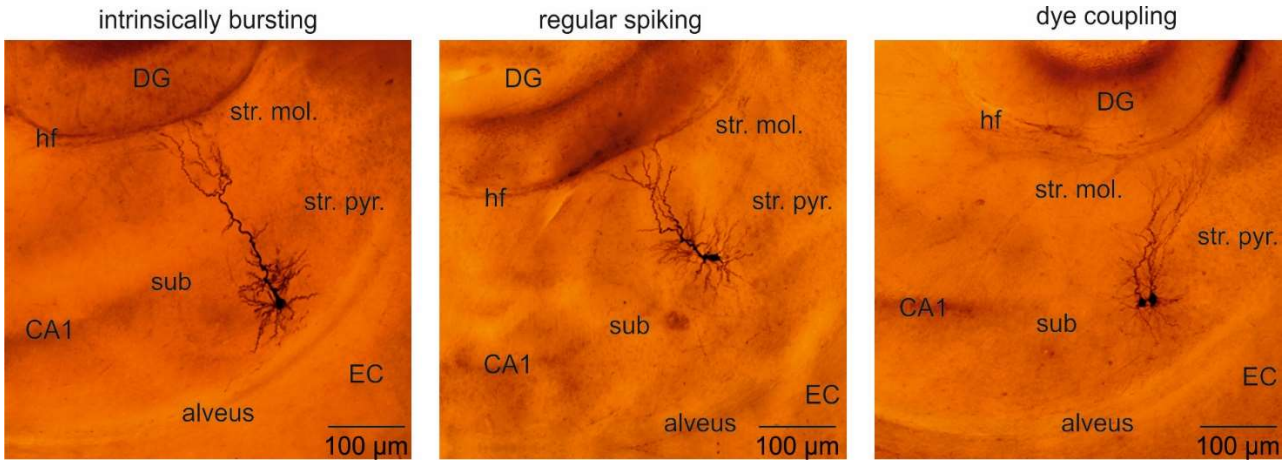

Figure 9. Morphology of subicular IB and RS cells.

The microphotographs of biocytin-stained IB (left) and RS (center) cells show the typical shape of subicular pyramidal cells. The subiculum (sub) is located adjacent to the hippocampal CA1 area and the EC. The apical dendrites of subicular PCs extent into str. molecular (str. mol.), some reaching the hippocampal fissure (hf) beyond which lies the DG. The basal dendrites spread within the pyramidal cell layer (str. pyr.). Dye coupling (right) was observed in one stained IB (1/11) but not in RS (0/9) cells. Both somata are pyramidal cell-like shaped with clear apical and basal dendrites. The dye-coupled cells are equally well stained and no obvious membrane defect can be found.

3.4 Spontaneous Sharp Wave Oscillations

3.4.1 Firing Behavior

During spontaneously occurring sharp waves within the subiculum, the majority of IB cells were active (16/24, 67%) whereas RS cells remained mostly silent (14/18, 78%).

8/24 IB cells (33%) remained silent at RMP and displayed a significantly hyperpolarized RMP compared to the active IB neurons ($p = 0.0085$; Table 4). Furthermore, the R_{in} of the active IB cells was significantly greater than of the silent ones ($p = 0.0345$; Table 4). There was no further difference in intrinsic or active membrane parameters within the IB cell group (Table 4).

	active IB	inactive IB	*p* value
sharp wave amplitude [mV]	0.17 (16)	0.23 (8)	0.144
sharp wave frequency [Hz]	2.2 (16)	2.2 (8)	0.964
RMP [mV]	−64.8 ± 0.4 (16)	−72.9 ± 0.7 (8)	0.0085 **
R_{in} [MΩ]	97.8 ± 2.7 (15)	62.7 ± 1.6 (8)	0.035 *
τ [ms]	7.2 ± 0.3 (16)	4.9 ± 0.2 (8)	0.195
AP amplitude [mV]	67.7 ± 0.7 (16)	66.9 ± 1.1 (8)	0.871
AP half-width [ms]	0.9 ± 0.01 (16)	0.9 ± 0.03 (8)	1.000
ISI burst [ms]	5.3 ± 0.1 (16)	4.5 ± 0.2 (8)	0.090
AP threshold	−69.0 ± 0.5 (16)	62.0 ± 0.9 (8)	0.070
ADP [mV]	5.4 ± 0.3 (15)	3.4 ± 0.4 (8)	0.338
AHP [mV]	−0.9 ± 0.1 (16)	−2.0 ± 0.3 (8)	0.139
sag −300pA [%]	13.4 ± 0.6 (14)	15.9 ± 1.1 (8)	0.555
sag −200pA [%]	15.4 ± 0.6 (15)	17.7 ± 1.6 (8)	0.622
sag −100pA [%]	15.7 ± 0.6 (15)	23.6 ± 1.0 (8)	0.059
accommodation [%]	71.1 ± 1.3 (11)	66.3 ± 1.4 (8)	0.451

Table 4. Electrophysiological properties of active and silent subicular IB PCs.

Significance level indicated by asterisk ($p \leq 0.05$; ** $p \leq 0.01$).*

The large majority of RS cells (14/18, 78%) remained functionally silent during subicular sharp wave activity, displaying a mixed postsynaptic potential (PSP) of excitatory and inhibitory components at RMP (Figure 10). 4/18 RS cells (22%) were active and fired single APs at RMP. In accordance to the observations in the IB PC class, active RS neurons displayed a significantly more depolarized RMP than silent RS cells (p = 0.030; Table 5). Concerning the intrinsic and active properties as well as the shape of AP, there was no difference between the active and inactive RS cell group (Table 5).

	silent RS	active RS	p value
sharp wave amplitude [mV]	0.20 (14)	0.26 (4)	0.378
sharp wave frequency [Hz]	2.1 (14)	2.7 (4)	0.281
RMP [mV]	−72.6 ± 0.5 (14)	−62.3 ± 2.3 (4)	0.030 *
R_{in} [MΩ]	98.2 ± 3.0 (14)	98.1 ± 3.2 (4)	0.997
τ [ms]	6.7 ± 0.2 (14)	8.0 ± 0.6 (4)	0.482
AP amplitude [mV]	67.3 ± 0.7 (14)	72.6 ± 2.3 (4)	0.360
AP half-width [ms]	1.0 ± 0.01 (14)	0.9 ± 0.06 (4)	0.500
AP threshold	−61.3 ± 0.5 (14)	−66.7 ± 2.3 (3)	0.663
ADP [mV]	0.0 (14)	0.7 ± 0.3 (4)	0.059
AHP [mV]	−3.8 ± 0.2 (14)	−3.5 ± 0.3 (4)	0.840
sag −300pA [%]	5.0 ± 0.5 (14)	10.3 ± 1.4 (4)	0.212
sag −200pA [%]	6.0 ± 0.5 (14)	9.0 ± 1.5 (4)	0.486
sag −100pA [%]	6.4 ± 0.5 (14)	7.6 ± 1.4 (4)	0.800
accommodation [%]	35.6 ± 1.5 (12)	40.2 ± 3.1 (4)	0.663

Table 5. Electrophysiological properties of active and silent subicular RS PCs.
Significance level indicated by asterisks (= $p \leq 0.05$).*

3.4.2 Temporal Correlation of AP Generation

In addition to the activity mode, subicular IB and RS PCs differed with regard to the phase correlation of AP generation to the LFP. There was no significant difference between the frequency and amplitude of the local network that could account for the different firing pattern of the subicular PCs (Table 2).

11/16 active IB cells displayed AP generation in strict correlation to the peak of the sharp wave rhythm (Figure 10 and accumulated data in Figure 18). Of these participating active cells, six PC displayed burst firing at RMP. The remaining active IB cells showed single AP firing and voltage-dependent bursting behavior. Most of the silent IB cells also showed a phase-coupled firing pattern when depolarized above threshold (n = 5/8; Figure 11). The phase-coherent active and silent IB cells displayed comparable general phase-locked behavior during the subicular sharp wave rhythm so that the data for analysis was pooled together.

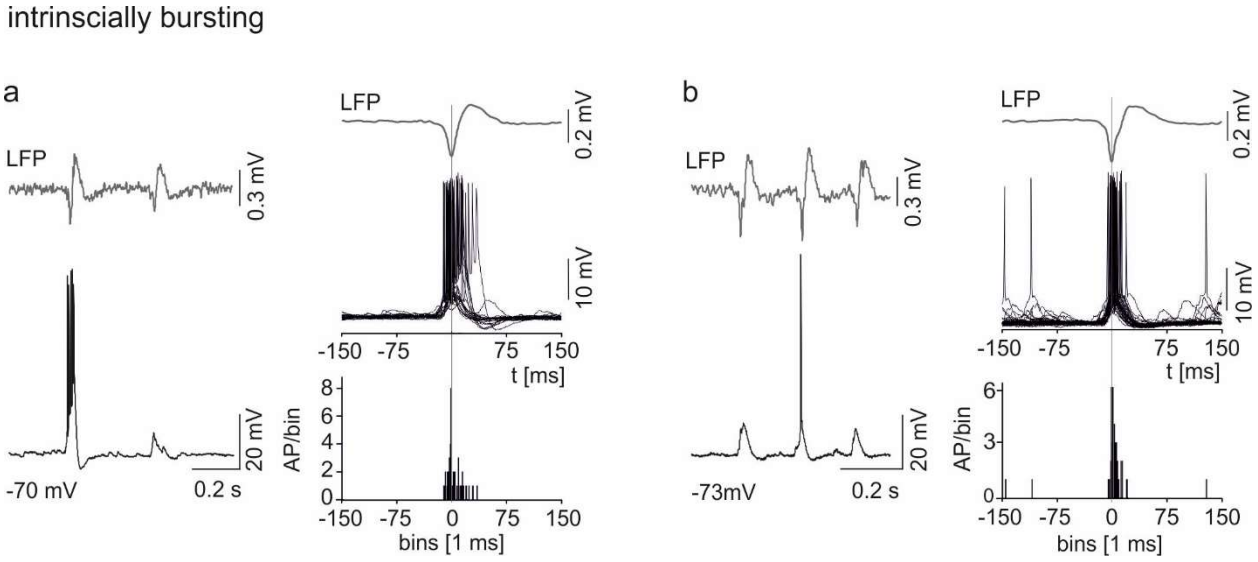

Figure 10. Temporal correlation of AP generation of active IB cells during sharp waves.

Simultaneous LFP (top traces in grey) and intracellular recordings (bottom traces in black) at RMP show examples of traces of phase-correlated discharge behavior of two active subicular IB cells. The intracellular recordings reveal bursts (a) or single APs (b) as well as prominent PSP in strict correlation to the local sharp wave rhythm. On each right, a cumulative spike time analysis and histogram is plotted and the clear peak of AP generation in close vicinity to the sharp wave peak is illustrated. The vertical line indicates the maximum mean sharp wave deflection adopted as time point 0.

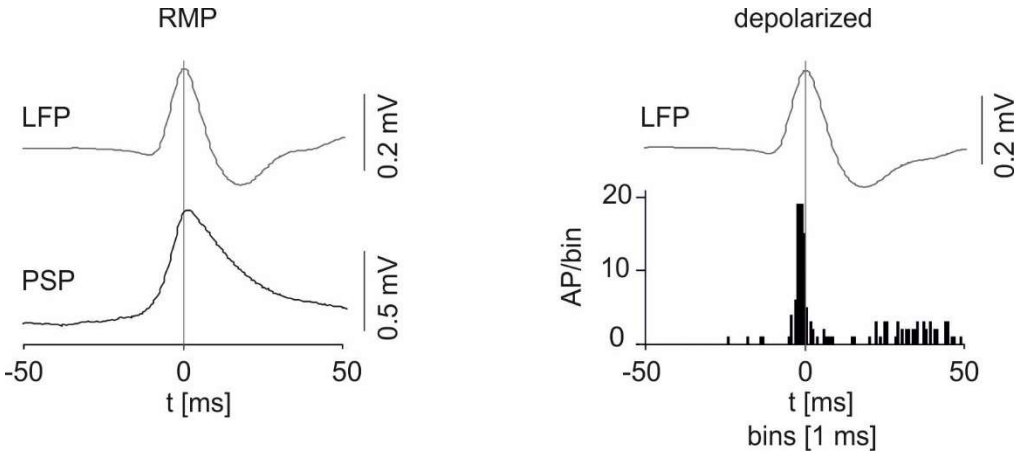

Figure 11. Silent IB cells during sharp waves.

Accumulated population data of silent IB neurons at RMP (n = 8; left) and under condition of depolarizing current injection (n = 5; right) are displayed during spontaneous sharp wave activity. (left column) The intracellular recordings at RMP show an aggregate phase-correlated PSP without AP generation. (right column) When depolarized above threshold, IB cells show AP generation phase-locked to the mean sharp wave as displayed in the spike time histogram. The vertical lines mark the maximum of sharp wave deflection indicated as time point 0. The firing pattern closely resembles the one of active IB cells (Figure 10).

A minority of 4/24 active IB neurons (17%) showed a prominent hyperpolarization at the peak of the sharp wave deflection which resulted in a disruption of AP firing (Figure 12). These IB cells displayed a significantly higher τ of 14.0 ± 0.5 ms (n = 4) compared to the phase-locked IB neurons, 4.8 ± 0.1 ms (n = 16; $p < 0.0001$). They also showed a significantly less prominent sag potential at −100 pA and at −300 pA ($p = 0.0012$ and $p = 0.046$, respectively).

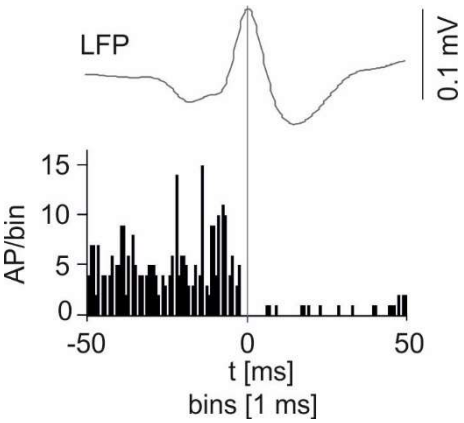

Figure 12. Pause of AP firing in IB cells during sharp waves.

Four IB cells displayed a prominent pause of AP firing right after the peak of mean sharp wave deflection as illustrated by the spike time histogram (n = 4). The vertical line indicates the peak of the mean sharp wave as time 0.

In three silent and one active IB cells the number of triggered APs was not sufficient for analytic purposes and these cells were excluded from further analysis.

During spontaneous sharp waves, the majority of RS remained functionally silent at RMP without AP generation (14/18, 78%). They displayed a mixed subthreshold potential of EPSP and IPSP components (Figure 13 and accumulated data in Figure 18). When depolarized above threshold, however, the silent RS cells revealed AP generation with a prominent pause of AP firing at the peak of the sharp wave deflection (n = 8), in stark contrast to the IB cell firing pattern.

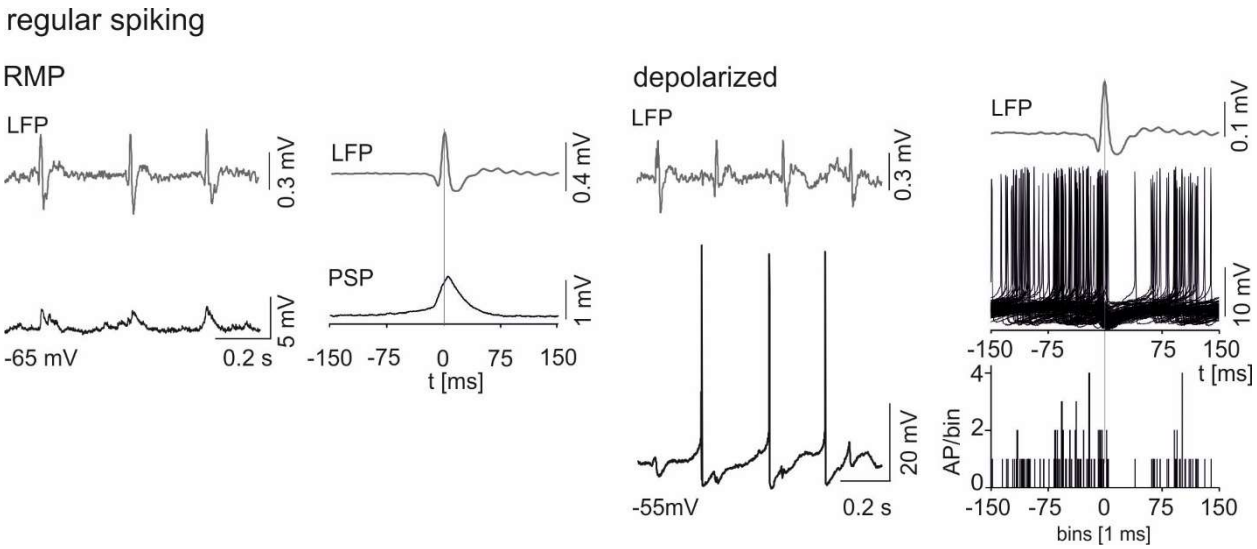

Figure 13. Temporal correlation of AP generation of silent RS PCs during sharp waves.

RS cell example at RMP ('RMP', left) and after depolarizing current injection ('depolarized', right) of the same cell during the spontaneous sharp wave rhythm. Simultaneous LFP (top traces in grey) and intracellular recordings (bottom traces in black) exemplify the phase-correlated behavior of subicular RS cells. (left column) The intracellular recording of a silent RS cell reveals a sharp wave-associated PSP with a prominent membrane excitation without AP generation as plotted in the adjacent spike time analysis. (right column) When depolarized above threshold the RS cell displays AP firing. The plotted spike time analysis and histogram on the right show a prominent pause of AP generation around the peak of the mean sharp wave deflection. The vertical line marks the maximum of LFP indicated as time 0.

Four RS cells were active during sharp wave activity (4/18, 22%). Three of the active cells displayed the same firing pattern, depicting the prominent pause of AP generation around the peak of sharp wave activity (n = 3; Figure 14).

Only one silent subicular RS PC showed phase-correlated firing behavior to the LFP peak (Figure 15) as observed in subicular IB cells.

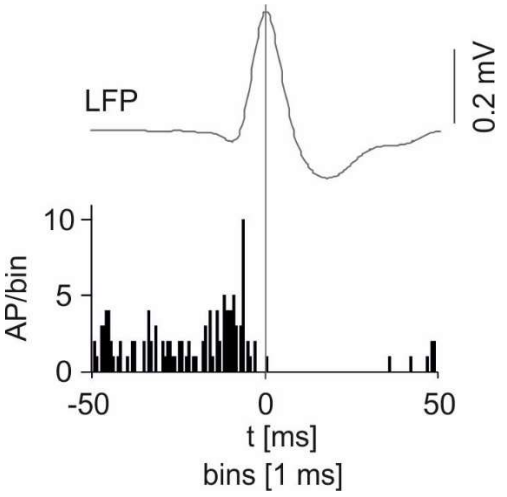

Figure 14. Active RS cells during sharp waves.

Accumulated data of active RS cells at RMP during the spontaneous sharp waves rhythm (n = 3). The firing pattern plotted in the spike time histogram shows a prominent pause of AP firing around the LFP peak resembling the firing pattern of silent RS cells after depolarization (Figure 13). The vertical line indicates the maximum of sharp wave peak indicated as time point 0.

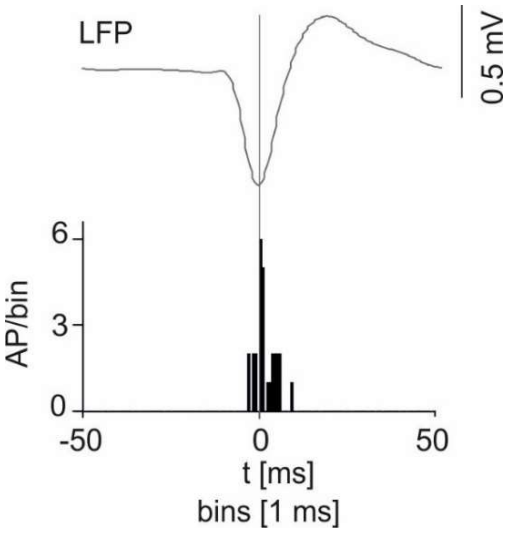

Figure 15. Phase-correlated AP generation in one RS PC during sharp waves.

One subicular RS cell displayed AP generation phase-locked to the maximum peak of mean sharp wave deflection as illustrated in the spike time histogram. The firing pattern resembled the phase-coherent AP generation of subicular IB cells (see Figure 10 and Figure 11).

Five silent and one active RS cell displayed and insufficient amount of AP generation and were excluded from this analysis.

3.4.3 Synaptic Potentials

For the purpose of the analysis of synaptic potentials, only PCs that showed the typical behavior of their subicular PC class at RMP or after depolarizing current injection were further considered. This included the active and silent IB cells that showed phase-locked AP generation (n = 16; Figure 10 and Figure 11) and the active and silent RS cells that displayed a prominent pause of AP firing around the peak of sharp wave deflection (n = 11; Figure 13 and Figure 14).

Both classes of subicular PCs displayed excitatory and inhibitory synaptic potentials that were correlated to the sharp wave field (Figure 16). In IB cells, the amplitude of EPSP was significantly greater than in RS cells (IB: 3.7 ± 0.2 mV, n = 12; RS: 2.3 ± 0.1 mV, n = 13; $p = 0.033$; Figure 17). However, there was no significant difference in the IPSP amplitude between the subicular PC classes (IB: −5.3 ± 0.9 mV, n = 3; RS: −7.6 ± 2.5 mV, n = 4; $p = 0.516$; Figure 17). The EPSP/IPSP ratio was 0.70 and 0.30 for IB and RS cells, respectively.

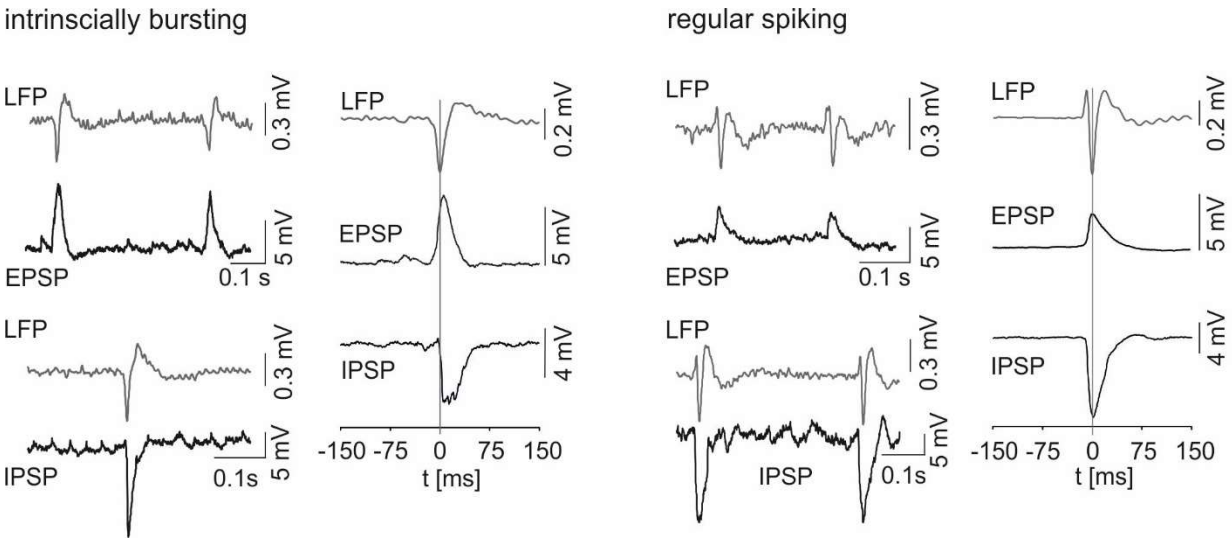

Figure 16. Synaptic potentials of subicular PCs during sharp waves.

Intracellular recordings (bottom traces in grey) of excitatory and inhibitory synaptic potentials of IB (left) and RS (right) cells in correlation to the local sharp wave field (top traces in black) with plotted analysis of mean potential deflection on each right. The vertical lines indicate the peak deflection of the mean sharp wave. Both examples show both EPSP and IPSP that are phase-correlated to the local sharp wave. The IB example displays a greater EPSP amplitude compared to the RS cell, whereas the IPSPs show a comparable amplitude.

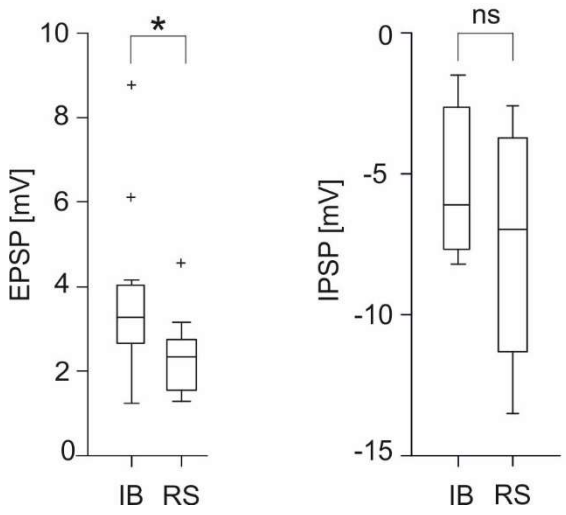

Figure 17. Amplitude of synaptic potentials of subicular PCs during sharp waves.

IB cells receive significantly higher synaptic excitation than RS cells (IB: n = 12; RS: n =13; p = 0.033), whereas the amplitude of IPSP is similar in both subicular PC classes (IB: n = 3; RS: n = 4; p = 0.516). Significance level indicated by asterisk (p ≤ 0.05); ns, not significant.*

The maximum deflection of the mean EPSP amplitude was similar in the two classes of subicular PCs. It was reached 5 ms after the LFP peak in IB (n = 12) and 4 ms after the peak in RS cells (n = 13; Figure 18). However, there was a difference in the exact timing of the inhibitory synaptic input between subicular PC classes. RS neurons (n = 4) received the IPSP 3.5 ms earlier within the sharp wave cycle than the IB PCs (Figure 18).

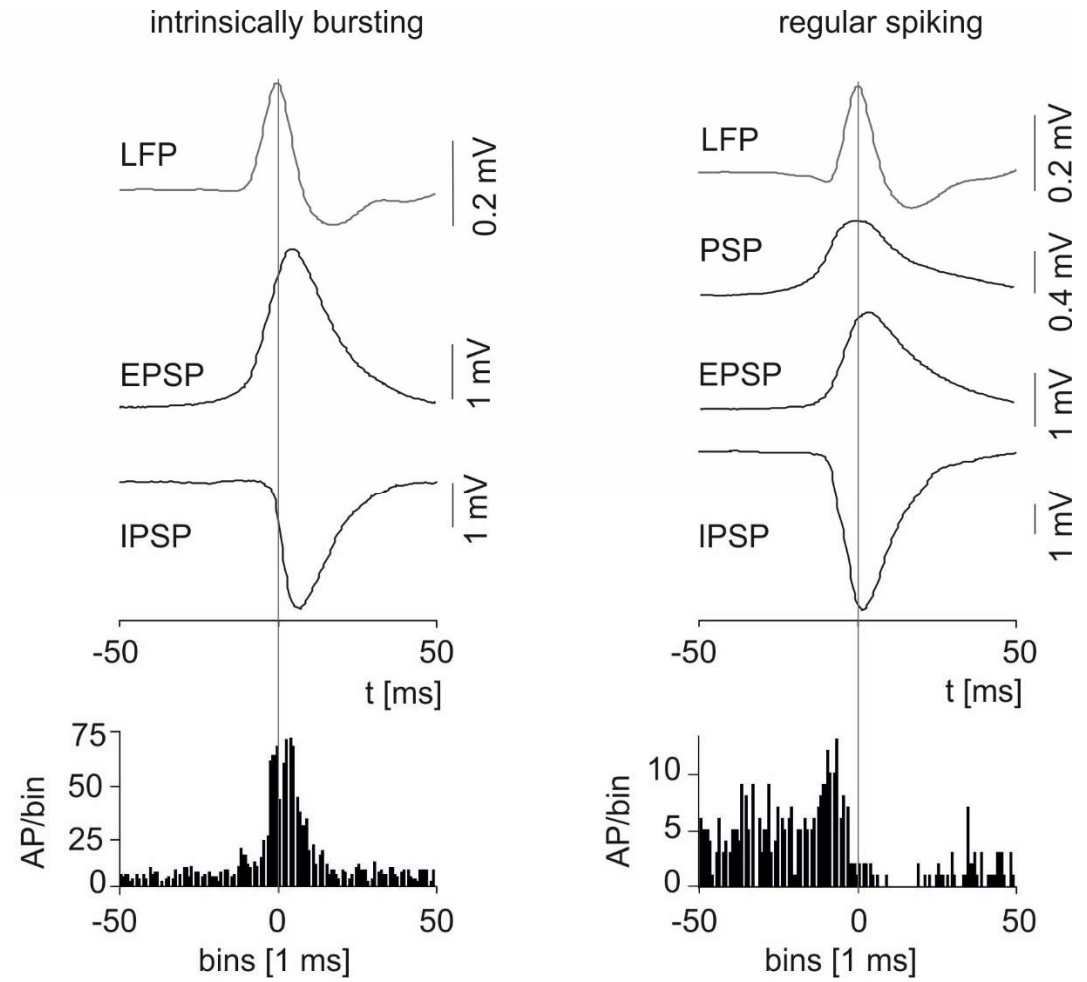

Figure 18. Synaptic potentials and firing behavior of subicular PCs during sharp waves.

Population data of the mean synaptic potentials (EPSP, IPSP, and PSP) and the cumulative analysis of the firing behavior (spike time histogram below) of subicular IB (left) and RS (right) cells in correlation to the sharp wave activity. Only IB cells that showed the typical phase-locked AP generation in correlation to the sharp wave field (n = 16) and RS cells that display a prominent pause of AP firing (n = 11) were considered. The accumulated mean sharp wave deflection is shown at the top and the vertical line marks its maximum which was adopted as time 0. In IB cells, the maximum of grand mean EPSP (n = 12) and IPSP (n = 3) deflection occurs 5 ms after the peak of the sharp wave rhythm. The EPSP (n = 13) of RS cells is situated 4 ms after the LFP maximum. The IPSP peak of RS (n = 4) PCs occurs 3.5 ms earlier than in IB cells. In addition, the population data for the silent RS cells (n = 7) aggregate a phase-locked mixed PSP. The accumulated population data of the firing behavior is plotted as a cumulative spike time histogram below and illustrates the clear peak of AP generation in close vicinity to the sharp wave peak in IB cells (n = 16). In stark contrast, the spike time analysis of spontaneously active and depolarized RS (n = 11) reveals a prominent sharp wave peak-correlated pause of AP firing.

3.5 Gamma Frequency Oscillations

A total of 22 PCs were recorded during spontaneous sharp wave and subsequent gamma frequency oscillations within the subiculum. 11 cells were identified as IB (50%) and 11 as RS cells (50%).

3.5.1 Network-induced Membrane Depolarization

The initiation of gamma frequency oscillations leads to the depolarization of membrane potential in both subicular PC classes. However, there was a significantly higher depolarization in IB cells of 9.2 ± 0.3 mV (n = 11) compared to RS neurons, 6.3 ± 0.3 mV (n = 11; $p = 0.037$; Figure 19 and Table 6). This resulted in a significantly more depolarized membrane potential in IB cells, −59.6 ± 0.4 mV (n = 11) compared to RS cells, −65.6 ± 0.7 mV (n = 11; $p = 0.042$; Table 6). There was no difference in AP threshold between the two subicular PC classes.

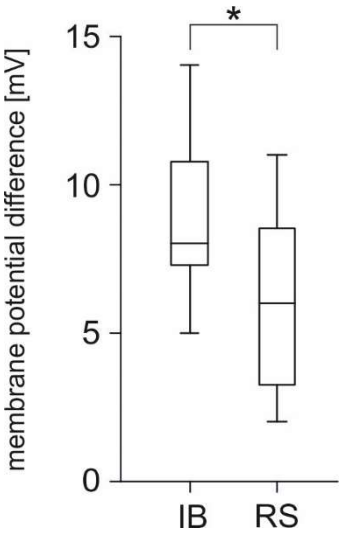

Figure 19. Membrane potential depolarization after the initiations of gamma frequency oscillations.

*IB PCs (n = 11) showed a significantly greater depolarization of membrane potential compared to RS cells (n = 11; p = 0.037). The significance level is indicated by an asterisk (*p ≤ 0.05).*

3.5.2 Electrophysiological Properties of Subicular PCs during Gamma Oscillations

In contrast to the distinct influence of the active gamma network on the membrane potentials of the subicular PC classes, the passive membrane properties including R_{in} and τ remained unchanged (Table 6). The sag potential was present in IB as well as RS cells during gamma frequency oscillations. There was a significant difference of percentage sag between the subicular PC classes at −100 pA ($p = 0.020$) and −200 pA ($p = 0.013$) but not at −300 pA ($p = 0.112$; Table 6). This was mainly caused by a single RS cell that displayed a prominent sag potential which was larger in

amplitude than in the other nonbursting cells. In contrast to the distinct differences in the AP shape during subicular sharp wave activity between PC classes (Table 3), there was no difference between ADP and AHP amplitude during gamma frequency oscillations.

	IB	RS	*p* value
MP [mV]	−59.6 ± 0.4 (11)	−65.6 ± 0.7 (11)	0.042 *
depolarization [mV]	9.2 ± 0.3 (11)	6.3 ± 0.3 (11)	0.037 *
R_{in} [MΩ]	99.7 ± 3.8 (11)	84.1 ± 1.9 (11)	0.303
τ [ms]	6.5 ± 0.3 (11)	6.4 ± 0.3 (11)	0.968
AP amplitude [mV]	66.9 ± 0.7 (11)	66.2 ± 1.1 (10)	0.866
AP half-width [ms]	1.0 ± 0.01 (11)	1.0 ± 0.01 (10)	0.652
AP threshold	−59.4 ± 0.8 (11)	−51.8 ± 1.1 (9)	0.093
ADP [mV]	1.1 ± 0.2 (11)	0.0 (11)	0.083
AHP [mV]	−2.0 ± 0.2 (11)	−2.7 ± 0.2 (11)	0.418
sag −300pA [%]	12.4 ± 0.6 (11)	7.1 ± 0.7 (11)	0.112
sag −200pA [%]	13.6 ± 0.6 (11)	5.1 ± 0.6 (11)	0.013 *
sag −100pA [%]	13.7 ± 0.9 (11)	5.2 ± 0.4 (11)	0.020 *

Table 6. Electrophysiological properties of subicular PCs during the active gamma network.

Significance level indicated by asterisk ($p \leq 0.05$).*

In order to learn how the two subicular PC classes differed during the two major network states, IB and RS cells were compared with each other before and after the activation of the gamma network (Table 7 and Table 8). In this context, considering the length of the experimental protocol, it was examined whether one PC class was more prone to damage-induced cell death, which could have influenced the experimental observations. The stable intrinsic parameters of subicular IB and RS PCs indicate that the conditions remained stable throughout both oscillatory network states, so that the observed differences do indeed represent physiological conditions.

In IB neurons, the membrane potential varied significantly during the network states ($p = 0.0032$; Table 7) corresponding to the observation of the strong membrane depolarization during gamma frequency oscillations. Concerning the active membrane properties, the sag potential was smaller in IB and RS PCs during gamma oscillations than during sharp waves. However, there was no significant difference. The shape of AP in IB cells varied significantly between the two network states. The ADP, which was prominent at RMP, decreased significantly ($p = 0.018$) during gamma oscillations. A hyperpolarizing current injection restoring the RMP did not lead to a recovery of ADP. In order to examine whether this was a network-induced effect, kainate was washed out in one IB cell. In this neuron the membrane potential returned to RMP and the ADP reappeared. There were no further differences in electrophysiological parameters between the sharp wave and gamma oscillations in IB neurons. Within the RS PC class, there was no significant variation in the recorded parameters during the two major network states (Table 8).

IB	sharp waves	gamma oscillations	*p* value
RMP / MP [mV]	−67.5 ± 0.3 (24)	−59.6 ± 0.4 (11)	0.0032 **
R_{in} [MΩ]	85.6 ± 1.6 (23)	99.7 ± 3.8 (11)	0.348
τ [ms]	6.4 ± 0.2 (23)	6.5 ± 0.3 (11)	0.961
AP amplitude [mV]	67.5 ± 0.4 (24)	66.9 ± 0.7 (11)	0.870
AP half-width [ms]	0.9 ± 0.01 (24)	1.0 ± 0.01 (11)	0.073
AP threshold [mV]	−58.9 ± 0.2 (23)	−59.4 ± 0.8 (11)	0.848
ADP [mV]	4.7 ± 0.2 (23)	1.1 ± 0.2 (11)	0.018 *
AHP [mV]	−1.3 ± 0.1 (24)	−2.0 ± 0.2 (11)	0.328
sag −300 pA [%]	14.3 ± 0.4 (22)	12.4 ± 0.6 (11)	0.559
sag −200 pA [%]	16.2 ± 0.4 (23)	13.6 ± 0.6 (11)	0.453
sag −100 pA [%]	18.5 ± 0.4 (23)	13.7 ± 0.9 (11)	0.188

Table 7. Electrophysiological properties of IB cells during sharp wave and gamma frequency oscillations.

*Significance level indicated by asterisk (** $p \leq 0.01$; * $p \leq 0.05$).*

RS	sharp waves	gamma oscillations	*p* value
RMP / MP [mV]	−70.3 ± 0.5 (18)	−65.6 ± 0.7 (11)	0.157
R_{in} [MΩ]	98.2 ± 2.1 (18)	84.1 ± 1.9 (11)	0.276
τ [ms]	7.0 ± 0.2 (18)	6.4 ± 0.3 (11)	0.627
AP amplitude [mV]	68.5 ± 0.5 (18)	66.2 ± 1.1 (10)	0.573
AP half-width [ms]	1.0 ± 0.01 (18)	1.0 ± 0.01 (10)	0.743
AP threshold [mV]	−56.2 ± 0.5 (17)	−51.8 ± 1.1 (9)	0.227
ADP [mV]	0.2 ± 0.0 (18)	0.0 (11)	0.444
AHP [mV]	−3.8 ± 0.1 (18)	−2.7 ± 0.2 (11)	0.276
sag −300 pA [%]	6.2 ± 0.4 (18)	7.1 ± 0.7 (11)	0.761
sag −200 pA [%]	6.7 ± 0.4 (18)	5.1 ± 0.6 (11)	0.599
sag −100 pA [%]	6.7 ± 0.4 (18)	5.2 ± 0.4 (11)	0.552

Table 8. Electrophysiological properties of RS cells during sharp wave and gamma frequency oscillations.

3.5.3 Firing Behavior

During gamma frequency oscillations, the majority of subicular IB PCs were active whereas most of the RS cells remained silent, corresponding to the observation in the sharp wave network state. 10/11 IB PCs (91%) were active during gamma frequency oscillations. Three of these active IB cells had been silent during preceding sharp waves. However, the network-induced depolarization led to a change in firing mode. Only one IB cell remained inactive during the gamma rhythm. This neuron displayed a low membrane potential of −70.0 mV, whereas the active IB cells had a mean membrane potential of −58.6 ± 0.3 mV (n = 10). The silent IB cell also showed a less pronounced depolarization after the initiation of gamma oscillations of 5 mV compared to the active IB neurons with 9.3 ± 0.3 mV (n = 10). There were no further differences. In contrast to the sharp waves, none of the IB cells burst at membrane potential without current injection (n = 10; Figure 20). The IB cell group still showed voltage-dependent burst behavior following current injection. Of the six IB

cells that burst spontaneously and phase-locked to the sharp wave rhythm, four cells were recorded during subsequent gamma oscillations. Hyperpolarizing these cells to the RMP observed during sharp wave activity did not lead to spontaneous burst firing during gamma frequency oscillations.

The majority of the RS neurons (7/11, 64%) remained silent during the gamma rhythm. Two RS cells that were silent during sharp waves changed activity mode and became active. The active RS cells (4/11, 36%) showed a lower threshold for AP initiation of −61.3 ± 2.7 mV (n = 3) compared to the silent RS cells with −47.1 ± 1 mV (n = 6; p = 0.035). There was no further difference in intrinsic properties.

3.5.4 Time Correlation of AP Generation

During gamma frequency oscillations, the firing pattern of the majority of IB cells (8/11, 73%) displayed a bimodal peak of AP discharge with a prominent pause of AP firing around the peak deflection of the gamma wave (Figure 20 and accumulated data in Figure 26). When depolarized above threshold, the single silent IB cell displayed a similar firing pattern and thus the data was pooled together for further analysis. As a rule, an individual IB cell discharged once per gamma cycle, either before or after the peak of maximal LFP deflection. In most IB cells, the discharge probability was slightly higher after the maximum peak of gamma than before it. There was no indication of AP doublet firing or rebound depolarization following inhibitory input from local interneurons (Cobb et al. 1995). IB cells fired with a frequency of 11.4 ± 0.8 Hz (n = 6). 3/11 active IB PCs (27%) showed a diffuse firing pattern with no clear peak of AP generation (Figure 21). There were no differences in electrophysiological properties between these two groups of subicular IB cells that could account for the different firing behavior during gamma frequency oscillations. These three IB cells were excluded from further analysis due to excessively low frequency of AP discharge.

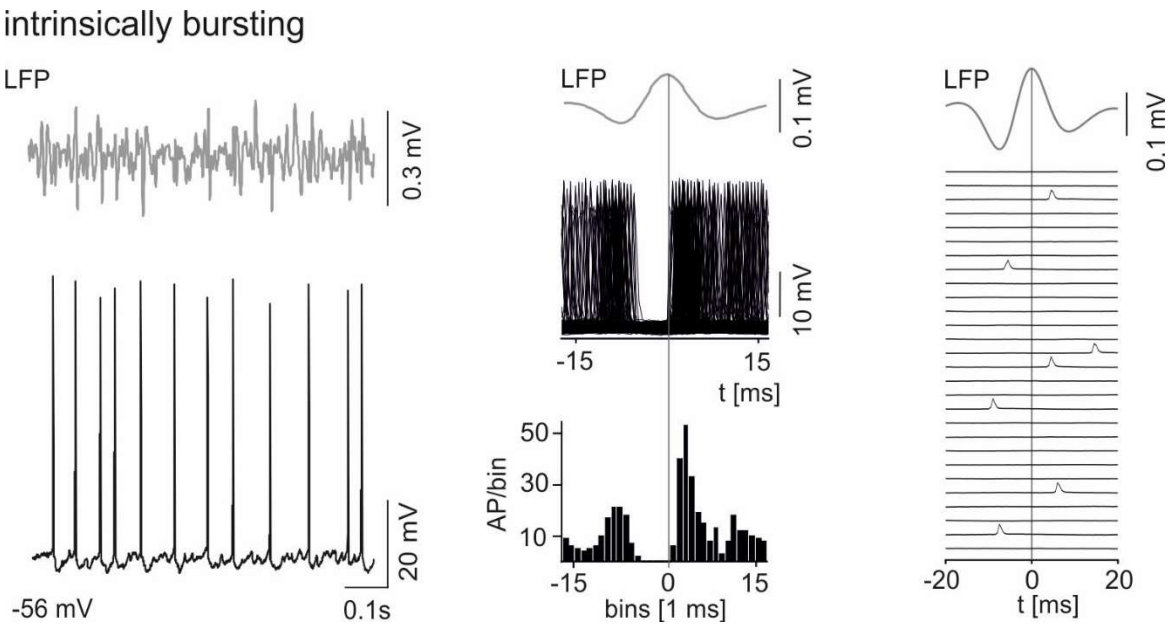

Figure 20. Temporal correlation of the AP generation of active IB PCs during gamma frequency oscillations.

Example of an active IB cell during gamma frequency oscillations demonstrating the temporal correlation of AP generation. (left column) Simultaneous LFP (top trace in grey) and intracellular recordings (bottom trace in black) show phase-correlated discharge behavior. At membrane potential, the IB cell fires single APs in correlation to the gamma field. (center column) cumulative spike time analysis and histogram reveal the two prominent peaks and the pause of AP generation which characterizes the typical firing pattern of subicular IB cells during gamma oscillations. The grey line indicates the maximum deflection of the gamma wave and marks time 0. (right column) Single intracellular recording cutouts (40 ms each) of consecutive triggered LFP gamma cycles illustrate the typical IB cell AP pattern for oscillatory network gamma activity together with the mean LFP trace of these recordings on top.

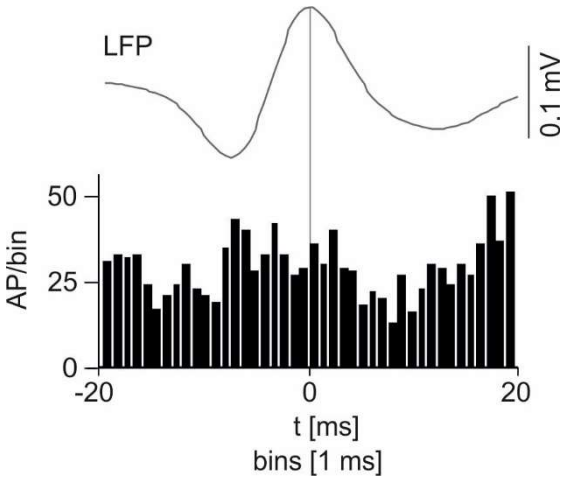

Figure 21. Discharge of three IB PCs during gamma frequency oscillations.

Population data of three subicular IB cells plotted as a spike time histogram with no clear AP generation distribution in relation to the overlying mean gamma wave. The vertical line marks the maximum deflection of the mean gamma wave.

Most of the subicular RS cells (7/11, 64%) were silent during gamma frequency oscillations. The silent RS cells displayed mixed EPSPs/IPSPs with the excitatory component preceding the inhibitory one (n = 7; Figure 22). When depolarized above threshold, the silent RS cells showed AP firing with a firing pattern resembling the one observed in IB cells (n = 5; Figure 22 and accumulated data in Figure 26). The active RS cells (4/11, 36%) displayed the same prominent bimodal discharge distribution as observed in the inactive PCs (Figure 23) and thus the data was pooled together. Similar to IB PCs, RS neurons discharge only once per gamma cycle and there was no indication of rebound depolarization. Two RS PCs did not show a sufficient AP number for analysis and were excluded from further investigations.

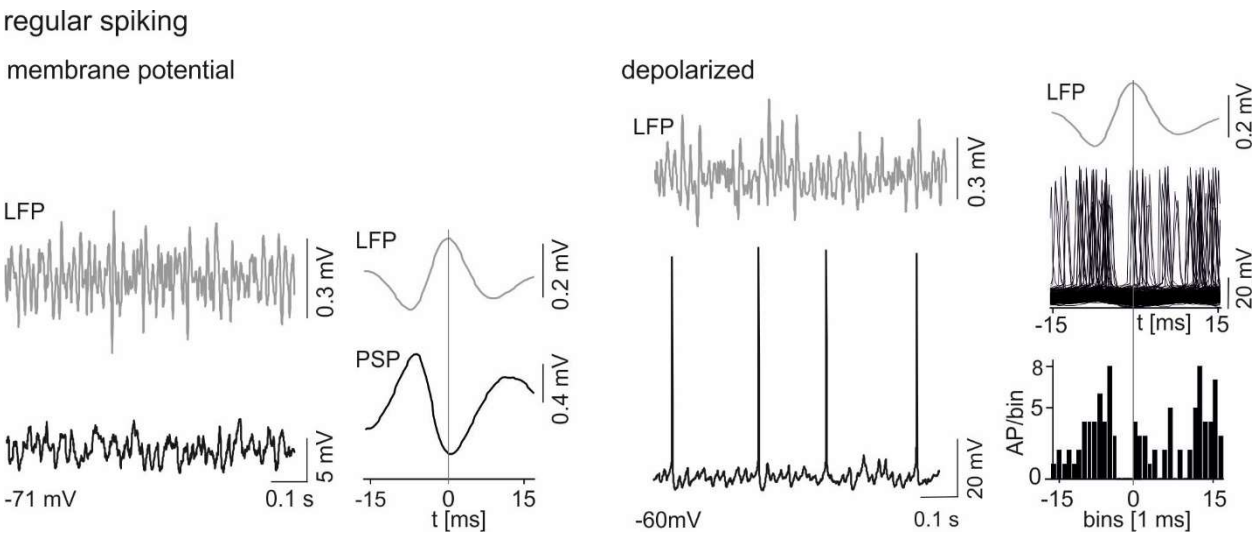

Figure 22. Temporal correlation of the AP generation of silent RS PCs during gamma frequency oscillations.

RS cell example recording at membrane potential (left) and after depolarizing current injection ('depolarized', right) of the same cell during gamma frequency oscillations. Simultaneous LFP (top traces in grey) and intracellular recordings (bottom traces in black) exemplify the typical phase-correlated behavior of subicular RS PCs. (left column) The intracellular recording reveals a LFP-associated PSP with an excitatory component preceding an inhibitory one as plotted in the adjacent potential analysis. (right column) When depolarized above threshold, RS cells display AP firing. The plotted spike time analysis and histogram on the right show a prominent peak of AP generation before the peak of the gamma wave followed by a pause of AP firing. The vertical line marks the maximum of LFP deflection indicated as time 0.

Thus, the majority of IB cells were active during gamma frequency oscillations, whereas the RS cells remained functionally silent. However, when depolarized above threshold, RS cells displayed the same firing patterns as IB neurons. In order to investigate the underlying network mechanism, the synaptic potentials of subicular PCs during gamma oscillations were examined. For the purpose of this analysis, all RS cells (n = 11) and only IB PCs that showed the typical bimodal distribution of AP generation at membrane potential or after depolarization (n = 8) were included.

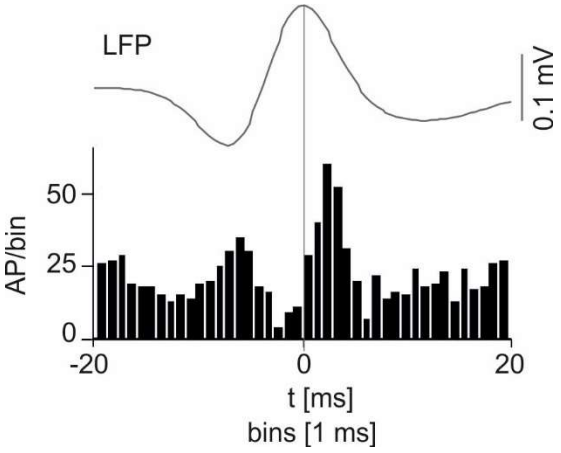

Figure 23. Firing properties of active RS PCs during gamma frequency oscillations.

Accumulated population data of active RS PCs during gamma frequency oscillations (n = 4). The firing pattern plotted as a spike time histogram reveals two prominent peaks of AP discharge before and after the overlying mean gamma wave. The distribution of AP generation resembles the one observed in the majority of IB PCs (Figure 20) and silent RS cells (Figure 22) within the subiculum during the active gamma field.

3.5.5 Synaptic Potentials

Both subicular IB and RS PCs displayed EPSPs and IPSPs that were phase-locked to the underlying gamma wave. In marked contrast to the subicular sharp waves, there was no difference in the EPSP amplitude between subicular IB and RS PCs (IB: 1.79 ± 0.1 mV, n = 8; RS: 1.84 ± 0.1 mV, n = 11; $p = 0.862$; Figure 25). Concerning the IPSP, there was also no significant variation between the two subicular PC classes (IB: −5.36 ± 0.2 mV, n = 5; RS: −4.49 ± 0.5 mV, n = 5; $p = 0.555$; Figure 25). Consistent with this, the EPSP/IPSP ratio was similar for both classes of subicular PCs (IB: 0.33 and RS: 0.41). Furthermore, in contrast to the sharp wave activity, there was no prominent differences in the time to LFP peak of synaptic input between the two subicular PC classes (IB: EPSP: −2.5 ms, IPSP: −1.5 ms; RS: EPSP: −1 ms, IPSP: −0.5 ms; Figure 26).

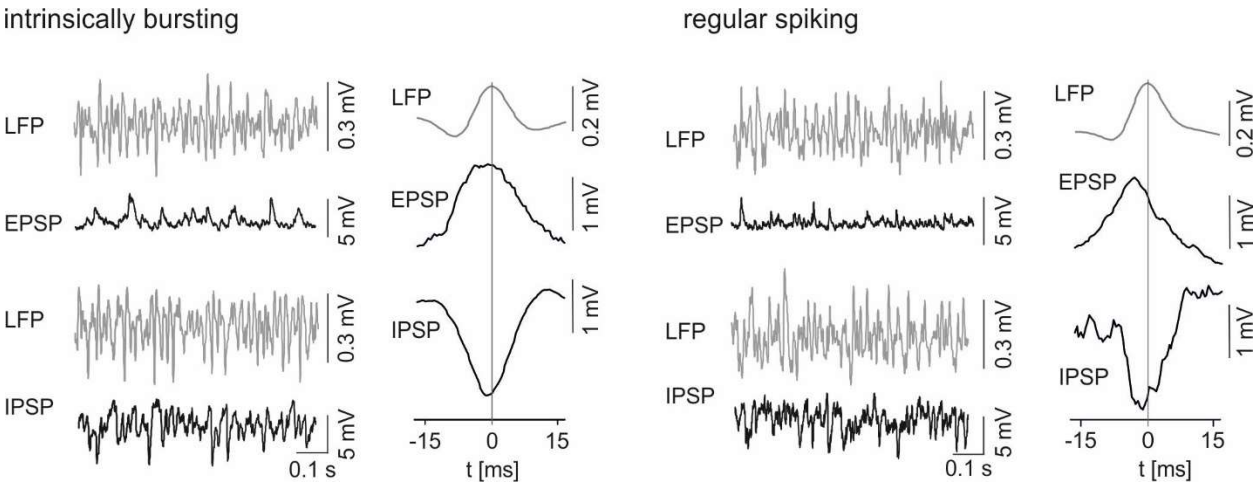

Figure 24. Synaptic potentials of subicular PCs during gamma network oscillations.

Intracellular recordings of excitatory and inhibitory synaptic potentials of IB (left) and RS (right) cells in correlation to the gamma rhythm with plotted analysis of mean potential deflection on each right. The LFP (top traces in grey) was recorded simultaneously with the synaptic potentials (bottom traces in black). The vertical line indicates the peak deflection of the mean gamma wave. The intracellular example traces show that EPSPS and IPSPs are phase-correlated to the gamma frequency oscillation in both subicular IB and RS PCs.

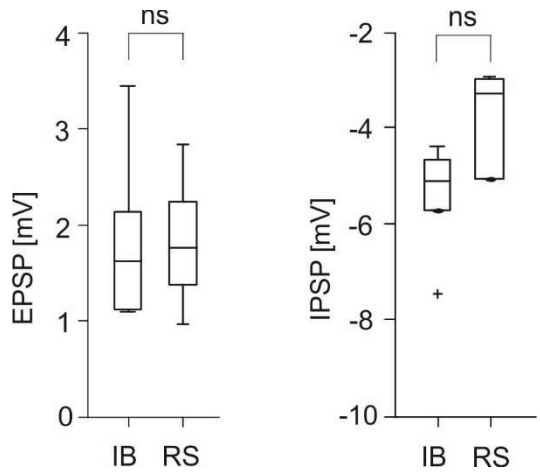

Figure 25. Postsynaptic potentials of subicular PCs during gamma oscillations.

There is no significant difference (ns) between the amplitude of EPSP (IB: n = 8; RS: n = 11; p = 0.862) and IPSP (IB: n = 5; RS: n = 5; p = 0.555) during gamma frequency oscillations.

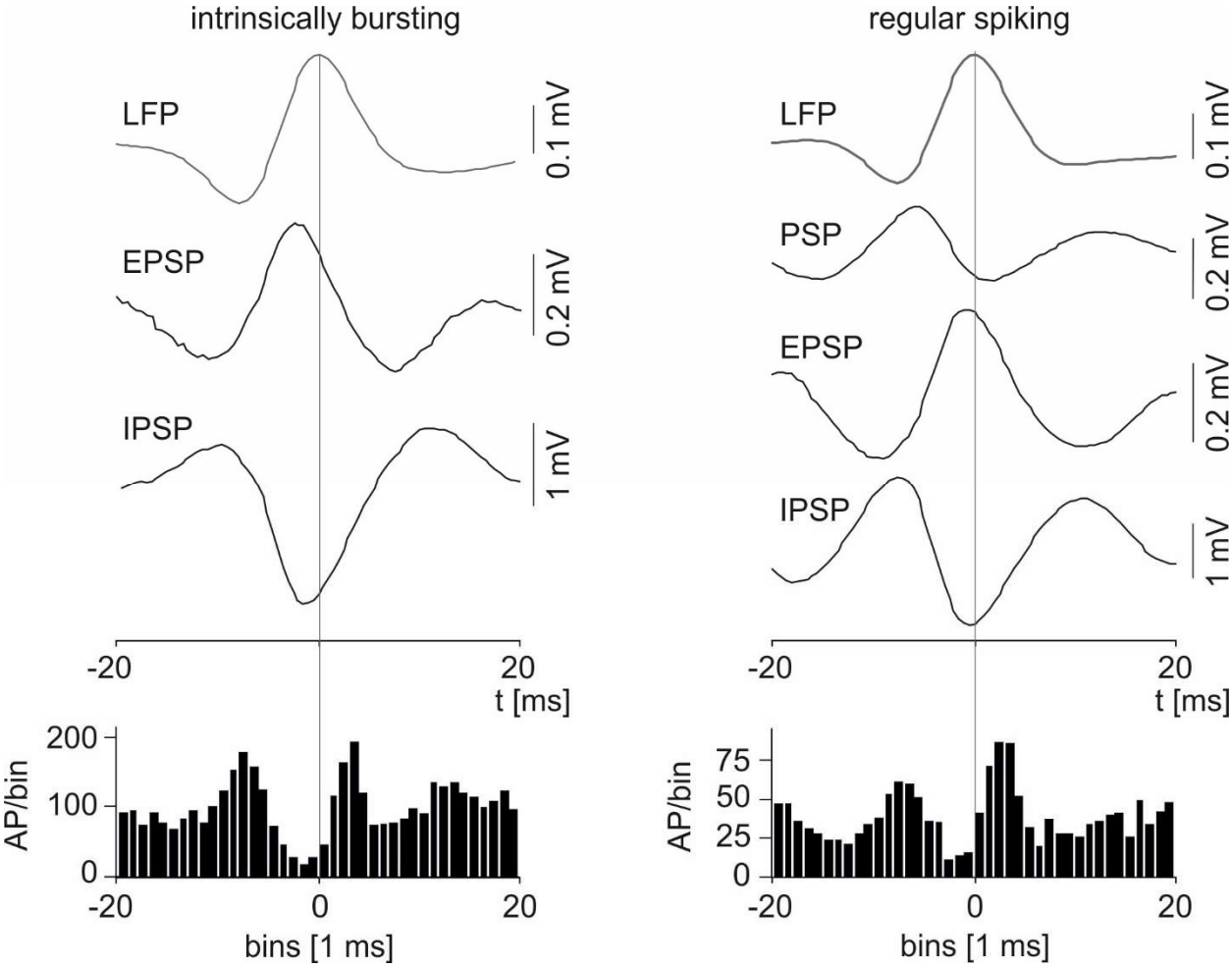

Figure 26. Synaptic potentials and firing behavior of subicular PCs during gamma frequency oscillations.

Population data of the mean of LFP and synaptic potentials (EPSP, IPSP, and PSP) and the cumulative analysis of the firing behavior (spike time histogram below) of subicular IB (left column) and RS (right column) cells. The accumulated mean gamma wave deflection is shown at the top and the vertical line marks its maximum which indicates time 0. In IB cells, the maximum cumulative peak deflection of EPSP (n = 5) and IPSP (n = 5) is reached at −2.5 ms and −1 ms prior to the peak of maximum gamma wave. In RS PCs, the EPSP (n = 11; −1 ms) and IPSP (n = 5; −0.5 ms) occur almost simultaneously within the gamma cycle. In addition, the population data for the silent RS cells (n = 7) aggregate a phase-locked mixed PSP with the excitatory component preceding the inhibitory one. Plotted below is the accumulated population data of the spike time histogram illustrating the bimodal peak of AP generation in both classes of subicular PCs (IB: n = 8; RS: n = 9).

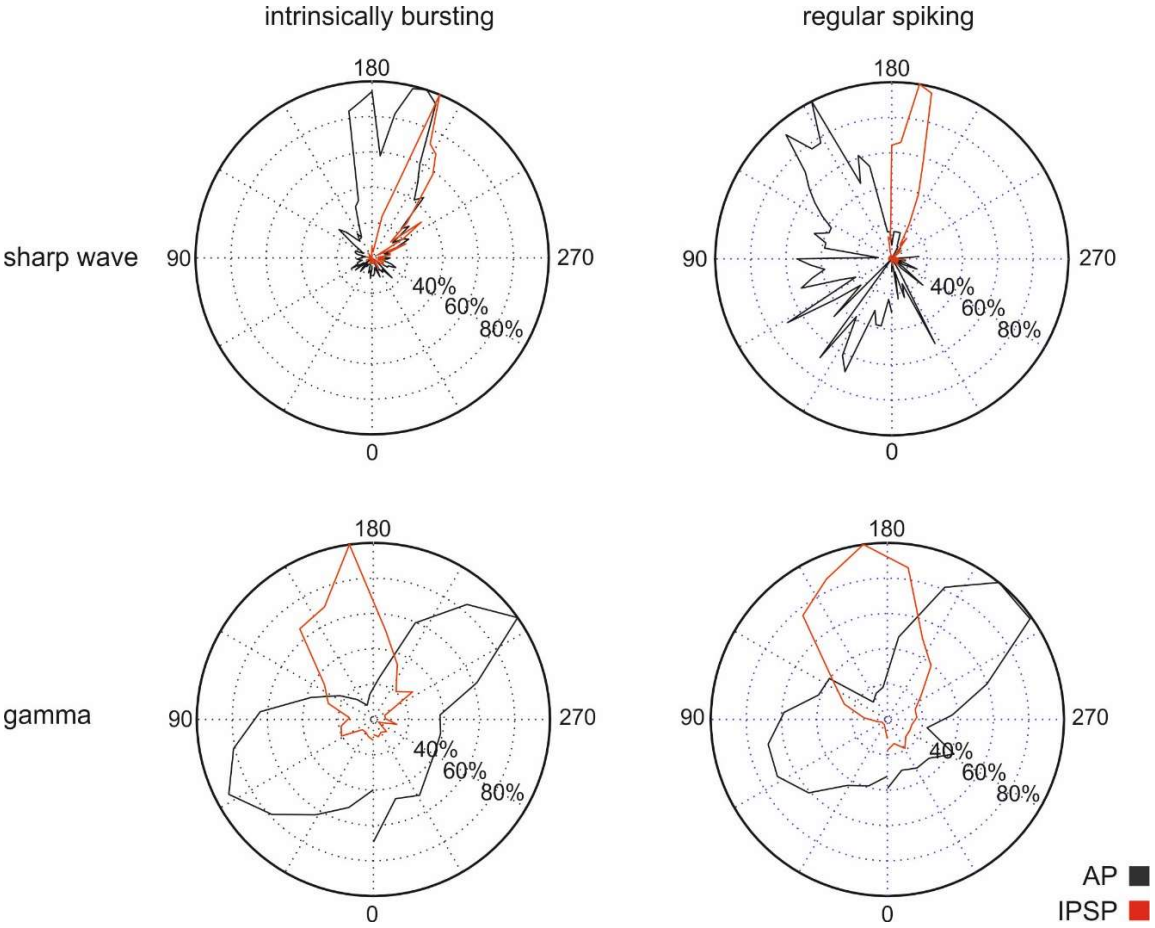

Figure 27. Phase distribution of APs and synaptic inhibition during sharp waves and gamma frequency oscillations.

APs (black) and synaptic inhibition (red) of IB (left) and RS (right) PCs during sharp wave (upper row, 80 ms projected time window) and gamma frequency (lower row, 24 ms projected time window) oscillations projected on a standard phase polar diagram. The oscillatory peak activity is displayed at 180°, the ascending slope encodes the lower and the descending one the higher values. The illustration of the APs is based on the cumulative AP population histograms (Figure 18 and Figure 26). The synaptic inhibition is represented by the distribution of time points for maximal deflection in the cellular cumulative IPSPs analysis (Figure 18 and Figure 26). All values are normalized to the respective maximum activity level and expressed as percentages. During sharp wave activity, the activity of IB and RS subicular cell classes is separated in the time domain illustrated by a distinct phase distribution. RS PCs (active and depolarized) show an early AP discharge pattern (n = 11) as well as an early peak of synaptic inhibition (n = 4) with respect to the IB PCs phase distribution (n =16; n = 3, respectively). In stark contrast to this, during gamma oscillations both classes of subicular PCs reveal a similar activity pattern with two distinct AP peaks (IB: n = 8; RS: n = 9) and an intermediate prominent IPSP (IB: n = 5; RS: n = 5).

4. Discussion

The participation of subicular IB and RS cells was studied in two major oscillatory network rhythms: subicular sharp wave and gamma frequency oscillations. The two types of subicular PCs constitute a homogenous group concerning the intrinsic properties, however, they differ with regard to the active membrane characteristics. In addition to this electrophysiological dichotomy, a functional segregation between the active, participating IB and the mostly silent but potentially participating RS cells was revealed. For the IB cells, a low or moderate network activity, like the one observed in this experimental setting, seems to represent a sufficient excitatory drive during both sharp wave and gamma frequency oscillations. In stark contrast, RS PCs appear to require a high network excitation in order to participate in the generation of network oscillatory activity. Hence, the distinct activation level of the two subicular PC classes suggests a bimodal working model operating under different levels of network excitation. The results of this study suggest that a state-dependent information processing of hippocampal output is represented by the two distinct classes of subicular PCs and therefore support the idea of two parallel processing channels within the subiculum.

4.1 Electrophysiological Properties of Subicular PCs

A total of 42 subicular PCs (57.1 % IB and 43.9 % RS cells) was recorded within the subiculum. Thus, in agreement with previous observations (Behr et al. 1996; Knopp et al. 2005; Mason 1993; Mattia et al. 1993; Mattia et al. 1997a; Stewart and Wong 1993; Taube 1993; Wu et al. 2006), a higher number of IB than RS cells were encountered within the subiculum. The relative numbers of the two classes of subicular PCs show a wide range of variation in the publications (54-100% for IB and 0-41% for RS PCs). A morphological sampling study suggested a sampling bias effect and found IB cell somata to be larger in size, making them easier targets for the blind microelectrode technique (Menendez de la Prida et al. 2002). Furthermore, it is conceivable that the voltage-dependent switch in spiking mode of the IB cells may account for some of the difference in the relative number. The single spiking mode of IB PCs triggered by the depolarization of membrane potential makes the discrimination between RS cells and depolarized IB cells difficult. To prevent an error in categorization in this study, a hyperpolarizing current was applied to all cells so that bursting in IB cells could be unraveled. Additionally, by obtaining intracellular recordings from the entire span of the subiculum, this study aimed at examining and representing the subicular network as a whole and thus preventing region-dependent sample sizing errors. Some authors, however, recorded exclusively from the ventral (Greene et al. 1997; Greene and Mason 1996;

Mason 1993) or dorsal subiculum (Mattia et al. 1997a; b) so that the position of the recording electrode can account for some of the differences in the relative cell number, since the distribution of subicular PCs varies within the subiculum (see 1.2.2). These authors did not provide distinct regional borders even though a reproducible segregation is of great interest, especially because the hippocampus as well as the subiculum have been demonstrated to contain region-dependent separation of functions (Amaral et al. 1991; Fanselow and Dong 2010; Stewart 1997). During gamma frequency oscillations, the same number of IB and RS neurons was recorded in this study.

There was no difference in passive membrane characteristics, suggesting that the two subicular PC classes constitute a homogenous group concerning their intrinsic properties in agreement with previous publications (Knopp et al. 2005; Staff et al. 2000; Stewart 1997; Taube 1993). Thus, as means of discrimination, the RMP, R_{in}, and τ appear to be unreliable factors. This causes considerable discordance amongst authors (see 1.2.1). Active membrane properties such as the sag potential and the district shape of APs, the ADP and AHP, seem to constitute a more dependable parameter which also proved to be consistent across studies (Behr et al. 1996; Greene and Totterdell 1997; Menendez de la Prida et al. 2003; Stewart and Wong 1993; Taube 1993; Wu et al. 2006). Additionally, within the present study, the accommodation of AP firing differs highly significantly between IB and RS subicular PCs, suggesting that there might be a cellular difference with regard to the subtypes of ion channels involved in the generation of AP. However, apart from the fundamental eponymous ability to generate bursts of APs, none of the physiological parameters were exclusive for one subicular cell type and therefore not suited for a distinguishing categorization. This observed lack of unity might result from a further subdivision of IB cells into weak and strong bursting and of RS cells into PC with and without tonic firing adaptation by some authors (Jung et al. 2001; Knopp et al. 2005; Menendez de la Prida 2003; Menendez de la Prida et al. 2003; Staff et al. 2000). However, these observations are exclusively restricted to patch clamp studies. No subdivision within the subicular PC population was observed in this intracellular microelectrode study. This is supported by a cluster analysis performed by Graves et al. (2012) that did not find any subdivision among bursting and non-bursting cells in the subiculum and the hippocampal CA1 area. To explain a fraction of the observed discrepancy in the published data, the different species of experiment animals, including mice, rats, and guinea pigs, as well as the different experimental conditions and techniques, including patch clamp and microelectrode recordings can be taken into account. Furthermore, data from dendritic as well as somatic impalements could have been included in studies, leading to disagreeing data (Greene and Totterdell 1997). This applies especially to the blind recording techniques.

Given the very fine differences in electrophysiological properties and the high degree of uncertainty within publications, the question arises whether bursting and nonbursting subicular cells are indeed distinct cell types. Extensive *in vivo* studies have confirmed their existence in the intact brain (Cohen et al. 2002; Finch et al. 1988; Gigg et al. 2000; Ranck 1973; Sharp and Green 1994). Furthermore, the physiological correlate of the bursting behavior has been attributed to higher and lower Ca^{2+} currents in IB and RS cells, respectively (Jung et al. 2001). The conversion of RS cells into IB cells has been attempted by a blockade of glutamate or GABAergic receptors (Behr et al. 1996; Menendez de la Prida 2006; Panuccio et al. 2012; Staff et al. 2000) and the blockade of the I_h current (van Welie et al. 2006), all of which did not lead to burst firing in RS cells. So far, as means of pharmacological induction, only the application of a blocker of slowly inactivating D-type Na^+ channels converted RS cell into bursting cells (Staff et al. 2000). Electrically, the application of a repeated short current injection resulted in the bursting of subicular and hippocampal RS cells; but still the exact timing of bursting differed between cell types (Graves et al. 2012). However, the same study proved in a detailed cluster analysis that bursting and non-bursting PCs are two independent, stable cell types with distinct morphological and electrophysiological properties. All evidence suggests that the dichotomy of subicular PCs can in fact be attributed to distinct electrophysiological properties leading to a physiological as well as functional dichotomy within the subicular PC class.

4.1.1 Dye Coupling in Subicular PCs

Morphologically, subicular IB and RS cells show the typical form of pyramidal neurons (Graves et al. 2012; Greene and Totterdell 1997; Taube 1993). The present study revealed one case, in which two PCs were equally well stained (see 3.3 and Figure 9). Dye coupling as a consequence of a damaged cell membrane appears unlikely, since the contours were clear and sharp. Furthermore, the electrophysiological recordings were stable so that there is no indication for membrane damage. The R_{in} of the electrophysiologically identified IB cell was consistent with the other subicular PCs, suggesting that there was no difference in the quality of impalement. In line with the hippocampal CA1 area, dye coupling was exclusively observed between IB cells (Baimbridge et al. 1991). It has been suggested that gap junctions may be the anatomical basis of both dye and electrophysiological coupling. Functionally, this suggests an electrically connected subicular IB PC network which could represent a significant feature of network generation in the subiculum.

4.2 Local Field Oscillations within the Subiculum

Within the hippocampus, the two major network states, sharp waves and gamma frequency oscillations, appear to be functionally connected, facilitating memory consolidation and storage (Bartos et al. 2007; Bragin et al. 1995; Buzsáki 1998; Colgin and Moser 2010; Zylla et al. 2013). Never coexisting, they appear to be competitive neuronal rhythms, possibly indicating the involvement of the same cellular network mechanisms in their generation. It has been suggested that the basic cellular connectivity is similar within differently oscillating networks but the alteration of channels and receptors results in the support of either one oscillatory activity or another (Buzsáki et al. 2003).

4.3 Sharp Waves in the Subiculum

Sharp waves were recorded in combined hippocampal-subicular-entorhinal-cortex slices. The sharp wave rhythm appeared spontaneously without chemical or electrical stimulation (Wu et al. 2006). The lack of cortical cholinergic input due to the preparation technique might serve to explain the spontaneous occurrence of sharp waves *in vitro* (Buzsáki et al. 1989; Kubota et al. 2003). However, it had been suggested that in thin (< 500µm) hippocampal slices, sharp waves cannot be consistently recorded due to a lack of interneuronal connections (Wu et al. 2005b). Thus, a thicker preparation method was recommended to preserve the network connectivity. However, in this study, it could be demonstrated that sharp waves are present in thin acute slice preparation (400 µm) within the subiculum. The subicular sharp waves observed were similar in terms of amplitude, frequency, and polarity to the sharp wave activity recorded within the thick murine subicular slices (Wu et al. 2005b; Wu et al. 2006), to the ones in the hippocampal CA1 area (Maier et al. 2003; Wu et al. 2002), and to the ones observed *in vivo* (Buzsáki et al. 1992; Chrobak and Buzsáki 1996; Csicsvari et al. 1999; Maier et al. 2011; Ylinen et al. 1995). Sharp waves with both negative and positive polarities were observed within the subiculum in agreement with previous observations (Wu et al. 2006).

4.3.1 Cellular Participation in the Spontaneous Sharp Wave Rhythm

During the spontaneous sharp wave rhythm, the majority of RS PCs remained functionally silent without AP generation, whereas subicular IB cells fired bursts or single AP in correlation to the extracellular field. There was no significant difference in frequency or power of field sharp waves that could account for the different activity and firing behavior of the two recorded PC classes. IB cells received significantly higher excitatory input compared to RS PCs. RS cells, on the other

hand, received pronounced inhibition, resulting in a pause in AP firing when depolarized above threshold. These differences are reflected in the EPSP/IPSP ratio. There was no significant difference in the membrane potentials between IB and RS PCs. In contrast to this, the membrane potential between active and inactive cells within the IB and RS cell groups varied significantly. The minority of IB cells was silent during subicular sharp waves and displayed a significantly more hyperpolarized membrane potential than the functionally active IB cells. The same applies to the RS PCs, the non-participating silent cells featured a more hyperpolarized membrane potential than the active minority of RS cells. It appears that within the PC classes, the state of excitation is crucial for the participation of the individual cell within the sharp wave network rhythm.

A segregation of participating and non-participating neurons, similar to the one discovered between subicular IB and RS cells, has been observed within the CA1 hippocampal region (Bähner et al. 2011; Maier et al. 2003). Within the CA 1 area, the majority of hippocampal PCs receives inhibitory input, preventing AP firing at the peak of the sharp wave activity while the minority of PCs is active and fires phase-coupled to the field. The strong inhibition acts to synchronize PC firing and in its summation represents the extracellular sharp wave rhythm (Maier et al. 2003). Given the fact that the intrinsic properties of CA1 cells do not differ significantly from subicular PCs and the synaptic components in the CA1 and subicular area rely on the same neuronal receptors, glutamatergic AMPA and inhibitory $GABA_A$ receptors, respectively (Maier et al. 2003; Wu et al. 2006), a similar network mechanism can be hypothesized for the subiculum. In this context, it is interesting to note, that CA1 cells were found more likely to fire bursts of AP during the SWR rhythm than in its absence (Buzsáki et al. 1992). In the present study, bursting firing was phase-locked to the subicular sharp waves, possibly suggesting that bursting represents an essential mechanism for sharp wave generation within the subiculum as well as the hippocampal areas. Furthermore, this might indicate that the cellular dichotomy and distinct activity pattern in the subiculum represent a strategy for information processing.

There were individual neurons that showed a firing pattern different from the majority of their PC class. Within the IB group, the majority of cells fired phase-locked to the sharp wave peak, whereas a minority was inhibited at the peak of sharp wave deflection. These cells also showed a significantly lower sag potential and a higher τ than the majority of the IB cell group. In contrast, the majority of RS cells showed a prominent pause in the vicinity of the sharp wave peak, whereas a minority showed phase-correlated AP generation. As a biological system, the participation of the individual PC classes seems to show some variability. It appears that the electrophysiological affiliation with a PC class does not automatically determine the functional participation in local

network rhythms. Instead, this seems to be dominated by the synaptic connectivity of the cell group within the cellular network. In support of this, atypically located RS cells deep in the subicular cell layer were found to show the same electrophysiological properties as the RS PCs in the typical superficial location (Greene and Mason 1996). However, depending on the position within the cell layer, the axonal distribution of subicular PCs varies, which can affect the synaptic connectivity within the subicular network (see 1.2.2). Consequently, the position of the cell can influence the firing pattern and activity mode of the cell. Furthermore, the participation in a functional system seems to influence, or to be influenced by, the electrophysiological properties of the participating cells as demonstrated by the group of IB cells that showed less pronounced sag potential and R_{in} and exhibited a phase correlation diverging from the majority of subicular IB cells. In this context, it would be interesting to examine whether atypically located RS and IB cells show an atypical firing pattern during sharp wave activity in the subiculum. However, the exact position of the recorded cells within the subicular cell layer was not examined within this experimental study so that this might represent a goal of future studies.

In addition to the morphological observations (Greene and Totterdell 1997; Harris et al. 2001), the different connectivity of subicular IB and RS cells within the subiculum is supported by the distinct synaptic input received during sharp waves. The subicular IB cell group receives significantly higher excitatory input than the RS PCs (Figure 16 and Figure 17). This input was received almost simultaneously within IB and RS cell groups, eliminating the possibility that the active and participating IB cell class activates the silent RS cell group through synaptic excitation. The peak of aggregated IPSPs, on the other hand, occurred earlier in RS cells than in IB cells parallel to the earlier peak in the spike time histogram (Figure 27). This altogether suggests that RS cells receive a different set of synaptic inputs. In conclusion, the distinct activity mode and firing pattern as well as the divergent amplitude of EPSPs and the time delay of IPSP in IB cells suggest the existence of distinct subicular input structures, even though there has been no evidence for this so far (Stewart and Wong 1993; Taube 1993). Considering that SWR oscillations are believed to represent behavioral relevant activation of neuronal assemblies in a time compressed manner (O'Neill et al. 2006), the distinct neuronal activity pattern of subicular IB and RS cells segregated in the time domain of the sharp wave rhythm is an important clue for a task-related differentiation of the two classes of subicular PCs.

4.4 Gamma Frequency Oscillations in the Subiculum

Network oscillations in the gamma frequency range were recorded within the subiculum and intracellular recordings of 11 IB and 11 RS cells were made simultaneously with the local network rhythm. The firing behavior and the phase correlation to the LFP were examined and compared with the observations made during preceding sharp waves.

4.4.1 Gamma Oscillation Induced Changes of Electrophysiological Properties of PCs

After the initiation of gamma frequency oscillations, IB cells depolarized significantly more than RS cells (Figure 19). Both types of subicular PC classes showed stable electrophysiological properties throughout the experimental protocol so that there were no signs of deterioration of recording conditions or higher susceptibility to damage induced cell death of one of the subicular PC classes (see 3.5.2). Thus, the recordings conditions remained stable and valid allowing a comparison between the network states. The depolarization of membrane potential in IB cells caused a change of firing mode, field-correlated burst firing was no longer present. The ceasing of bursting cannot, however, be attributed to the mere depolarization of membrane potential as observed during sharp wave activity, since it was not reversible when hyperpolarizing the membrane potential to values of the RMP. The discontinuation of spontaneous burst firing during the gamma wave might reveal distinct operational mechanisms of information processing during sharp wave and consecutive gamma frequency oscillations within the subiculum. The amplification capability of IB cells appears to be essential for the sharp wave rhythms and presumably for the generation of the ripple component, but it seems not to be crucial for gamma oscillatory activity, at least under *in vitro* experimental conditions. In addition, the prominent ADP in IB cells vanished in the active gamma network and could not be restored by hyperpolarization. This might be attributed to a change in ion channel conductance in subicular IB cells triggered by the activation of the gamma field rhythm, since it was not reversible by hyperpolarization to RMP values. Following the imitation of the gamma rhythm, a reduction of membrane sag potential was observed in both IB and RS subicular PCs. This can be attributed to the application of the same recording protocol during sharp wave and consecutive gamma oscillations. Since the cells were less depolarized at RMP during sharp waves, the influence of the injected current within the IV curve-protocol resulted in a more pronounced sag potential, especially because the input resistance remained unchanged.

The pronounced depolarization of membrane potential in subicular IB PCs during gamma network oscillations results in a higher excitability of IB cells within the active network. This is supported

by the observation that the application of the cholinergic agonist carbachol (30-100 µM) in a concentration sufficient to induce gamma frequency oscillations in the hippocampus (20µM, Fisahn et al. 1998) leads to membrane depolarizations and plateau potentials in IB cells (Kawasaki et al. 1999). Kawasaki and colleagues did not record local field activity but noticed an increase in IB intrinsic cell excitability. Under physiological conditions, acetylcholine functions as a neuromodulator within the mammalian brain. The induced effects were attributed to intrinsic changes within the IB neurons mediated by a Ca^{2+} dependent nonselective cationic conductance and were not influenced by glutamate and GABA receptor antagonists. Furthermore, the activation of the local field network in the theta frequency range triggered by carbachol also resulted in a depolarization of membrane potential in IB cells, while RS cells were not recorded (D'Antuono et al. 2001). The observed effects appear to be triggered by a change in network activity mediated by carbachol or kainate within the intact brain. Within subicular IB cells, intrinsic mechanisms appear to be activated, resulting in an increased cellular excitation expressed by a stronger depolarization, distinguishing IB from RS cells. This indicates that the cellular dichotomy within the subiculum represents an information processing mechanism that aims to modulate input differently. In accordance with these observations, the results of this study indicate that the electrophysiological as well as functional dichotomy arise from distinct cellular mechanisms triggered by a network-dependent process.

To some extent, the effects distinguishing the subicular PC population could result from a cell type-specific variation regarding the number of kainate receptors or a receptor location closer to the soma. However, to date, there exists no indication for such differences (Gigg et al. 2000; Harris et al. 2001; Taube 1993). It is also possible that the glutamate receptor subtype varies within the subicular PC class administering a stronger effect on the IB cell class. It has been shown that the glutamate receptor subunit 6 in the somatodendritic regions of both hippocampal interneurons and pyramidal cells is responsible for the oscillogenic as well as epileptogenic effects of kainate (Fisahn et al. 2004). To date, there are no studies examining the number, density, and subunits of kainate receptors on subicular PCs. The molecular details of cellular differences between the subicular PC classes represents an interesting and challenging target for future studies.

4.4.2 Cellular Participation in the Gamma Network Oscillation

The functional dichotomy of IB and RS PC was retained during subsequent gamma frequency oscillations. There was no significant difference in frequency or power of gamma oscillations during the recordings of IB and RS PCs. The majority of subicular IB PCs displayed a bimodal distribution of firing probability within a gamma cycle, the synaptic inhibition essentially shaping the output pattern (Figure 27). In contrast to the distinct firing pattern during the subicular sharp wave rhythm, the same firing pattern was displayed by RS cells when depolarized above threshold. This suggests that a higher level of network excitation is necessary to activate the subicular RS cells to participate in the network activity. In contrast to the sharp wave rhythm, however, the distinct activity pattern of subicular IB and RS PCs during gamma oscillations cannot be attributed to a different strength of synaptic input (see 3.5.5.). Within a cellular network consisting of PCs and interneurons, the interaction of synaptic input with intrinsic conductance can be sufficient to synchronize cell assemblies into gamma oscillatory frequency (Cobb et al. 1995). This suggests that the influence of interneurons on PCs can be altered depending on the intrinsic properties. In this way, the distinct network-induced alteration of intrinsic mechanisms could result in cellular processes leading to different firing behavior and consequently to a cell-type specific alteration of subicular output.

In stark contrast to sharp wave activity, all but one subicular IB cell was active in the gamma rhythm. The discharge frequency of the active subicular IB cells was slightly higher than described for hippocampal PCs in the CA3-CA1 circuit (Gloveli et al. 2005a; Hájos et al. 2004). This might be attributed to the relatively high depolarization of IB cells during the active gamma field. A minority of subicular IB PCs did not show the prominent bimodal peak of AP generation but diffuse AP generation instead (Figure 21). There were no differences in intrinsic properties between the two IB cell groups. These cells had participated within the subicular sharp wave rhythm exhibiting the typical phase-locked AP generation. It is possible that owing to the orientation of slice preparation, intercellular connections were cut so that the participation of these IB PCs in the gamma rhythm was impaired. Unlike the situation during sharp waves, silent and active RS PCs showed a comparable level of membrane potential, however, the threshold for AP generation was lower in active compared to silent RS PCs. Thus, in addition to the membrane potential, the AP threshold might act as a selection mechanism to identify cells to participate in the network rhythm.

So far, there exists only a very limited number of studies that examine the oscillatory properties of the subicular network and the firing features of subicular PCs during gamma frequency oscillations. The subicular gamma rhythm has been induced tetanically (Colling et al. 1998; Stanford et al. 1998). Following pulsed current injections, IB cells answer with AP doublets whereas RS cells fire rarely (Stanford et al. 1998). There was no indication of doublet or rebound firing in subicular PCs during the present experimental setting. Electrically induced oscillations differ from chemically induced ones with respect to the occurrence of large transient population events and spike doublets within stimulated single neurons which seem to result from an unphysiologically strong tonic depolarization of both PCs and interneurons (Colling et al. 1998; Stanford et al. 1998; Traub et al. 2000; Whittington et al. 1997). The manifestation of spike doublets appears therefore to represent a phenomenon attributed to the experimental protocol and does not necessarily contain physiological or functional implications. In a more recent study, Jackson et al. (2011) recorded spontaneous theta-coupled slow and fast gamma within the subiculum after complete hippocampal preparation. The firing of both subicular RS cells and interneurons was found to be phase-locked to the local field, whereas IB cells were selectively excluded from the study. However, a segregation of subicular IB and RS cells during gamma oscillations might prove difficult since IB cells do not fire bursts but rather single APs during gamma frequency oscillations in the subiculum (see 3.5.3). This study is the first to examine pharmacologically induced gamma frequency oscillations and to investigate the participation of both subicular PC classes.

4.5 Distinct Participation of Subicular PCs in the Oscillating Subicular Network

Cellular assemblies constitute a transiently stable network that generates oscillatory activity, the composition of participating neurons is variable due to dynamic recruitment (Menendez de la Prida and Gal 2004; Zylla et al. 2013). Within the subicular PC group, an electrophysiological and functional dichotomy is apparent during sharp waves and gamma frequency oscillations. The question arises how single subicular cells are selected to participate within an active network and how cells are selectively silenced.

4.5.1 Selection Mechanisms of Cells to Participate in the Network Rhythm

It is generally accepted that neurons with the strongest synaptic connectivity are selected to participate in a network by inhibition through a winner-take-all process on a single cell level (Chrobak and Buzsáki 1996). It has been demonstrated, however, that within a single gamma cycle, only a fraction of cells is dynamically selected for participation (de Almeida et al. 2009). These cells display maximal excitation within their cellular reference group so that cells that are active but

comparably less depolarized do not participate in the network rhythm. During gamma oscillations, the dynamic interaction between PCs and interneurons synchronizes cells through feedback inhibition and selects cells to participate through interaction with excitation (Bartos et al. 2007; de Almeida et al. 2009; Fisahn et al. 1998; Fries et al. 2007; Mann and Paulsen 2007). The degree of excitation can be influenced by intrinsic properties, synaptic connectivity, and receptor distribution, making the selection mechanism a network process rather than a mechanism on a single cell level. During subicular sharp waves, it appears that the different strength of synaptic excitation between subicular IB and RS PCs contributes to the difference in activity mode. The time delay of inhibitory input suggests that subicular PC classes receive distinct synaptic input. This is supported by the different firing pattern of subicular PCs during sharp wave activity. In stark contrast to this, there is no difference in synaptic input during subicular gamma oscillation between the two subicular PC classes. However, the initiation of the gamma rhythm leads to a significantly more pronounced depolarization and thus activation in IB compared to RS PCs possibly by an interaction with intrinsic properties. Both subicular PC classes expressed the same firing pattern, however the RS cells are silent at membrane potential. Consequently, the subiculum seems to operate in two different working modes depending on the level of cellular excitation. Under the influence of low or moderate network excitability, like the one observed in this study, the network oscillations appear to be mainly based on the IB cell class, while RS cells can potentially participate in a specific and independent manner when sufficiently depolarized. This additional excitatory network drive might arise from higher general excitation of the subiculum mediated through excitatory inputs independent of IB cells. In line with this suggestion, the phase-coherent RS cell activity during spontaneous slow and fast gamma activity in the complete hippocampal preparation (Jackson et al. 2011) could be attributed to a higher degree of subicular network excitation in the experimental setting. Furthermore, during the spread of epileptic activity within the subiculum, not only IB but also RS cells were found to be involved in the population activity in an *in vitro* epilepsy model (Menendez de la Prida and Gal 2004). A subset of IB cells were found to recruit other IB cells, RS PCs, and subicular interneurons exhibiting a leader-follower mechanism. The leading IB cell group did not consist of the same cells during each epileptic burst but participating cells were recruited dynamically. As a cell class, however, the dichotomy of subicular PCs was prominent with IB PCs holding the leading position and RS cells representing the follower population (Menendez de la Prida and Gal 2004). In accordance with this, in human epileptic tissue, a

subgroup of subicular PCs acted as pacemaker cells, however, these cells were not further classified (Cohen et al. 2002). Altogether, the specific conditions of cellular recruitment within the subiculum needs further investigation.

It remains unclear which intracellular mechanisms are involved in influencing the interaction between subicular PCs and the modulation of network rhythms. One of the few consistent differences between the subicular PC classes is the I_h current which determines the intrinsic properties and RMP of neurons (Pape 1996). However, the I_h current appears not to be involved in the recruitment for the SWR rhythm (Kranig et al. 2013). Within the hippocampal CA3 area, it has been demonstrated that the selective participation in the SWR rhythm is associated with the distance to the place of initiation (Ellender et al. 2010). This supports the assumption that the strength and temporal correlation of synaptic inputs influence the participation of single subicular PCs in the sharp wave activity. In a computational model of theta and gamma oscillations, on the other hand, the I_h current plays a significant role in tuning these network rhythms within the hippocampus by influencing the excitability of participating neurons (Neymotin et al. 2013). Also, it has been shown to change in line with the preferred oscillatory frequency of interneurons in the epileptic hippocampus (Dugladze et al. 2007). IB PCs express a larger I_h current than RS cells with no difference in I_h properties (van Welie et al. 2006). The hyperpolarization-activated current has been demonstrate to determine a cell's RMP, input conductance, and length constant as well as dendritic integration, thereby regulating the reaction to excitatory and inhibitory synaptic inputs (Pape 1996; Robinson and Siegelbaum 2003). In this way, IB PCs have been demonstrated to be better suited to discriminate input in the gamma frequency range displaying less temporal summation than RS PCs (van Welie et al. 2006). Considering the greater I_h current in IB PCs, it is surprising that there was no difference in RMP between the two types of subicular PCs. This might indicate that there are other voltage gated and leaky conductances or a difference in tonic inhibitory control that differ between subicular cell types (Panuccio et al. 2012; van Welie et al. 2006).

Without network activation, IB PCs have been shown to receive more prominent tonic inhibition compared to RS PCs (Panuccio et al. 2012). The stronger tonic control over IB cells appears paradoxical in the context of their active participation in local network mechanisms. However, the inhibitory control might serve to keep IB cells at the membrane potential necessary for burst initiation rather than tonic AP firing (Panuccio et al. 2012). This results in a potentiation of their firing impact rather than a decrease in excitability. It is possible that the difference in tonic control is mediated by distinct subtypes of $GABA_A$ receptors or different classes of interneurons targeting the two types of subicular PC classes (Panuccio et al. 2012). Recently, it has been shown that

subgroups of parvalbumin-positive basket cells distinguish between CA1 PCs, preferentially targeting cells based on their output connectivity and localization within the cell layer and receiving output- and location-specific excitation in turn (Lee et al. 2014). This results in a heterogeneous interneuron-PC microcircuit. A target specificity of subicular interneurons might explain the distinct network behavior of IB and RS PCs. If IB cells exhibited a stronger excitation of subicular interneurons which in turn preferentially targeted RS cells, this would result in the silencing of RS during network activity. So far, however, very limited information exists concerning subicular interneurons, their connectivity, and physiological properties.

In a network model, it has been demonstrated that bursting cells are able to recruit excitatory and inhibitory neurons into an activity state acting as the initiator for oscillatory activity (Traub et al. 1989). Network activity can then be generated solely based on intrinsically and rhythmically oscillating pacemaker neurons. The I_h current is thought to be involved in the generation of spontaneous pacemaker activity of the hippocampal str. oriens interneurons and in the rhythmogenic thalamocortical network (Pape 1996; Robinson and Siegelbaum 2003). The I_h channel is activated during the repolarization of AP, the rebound depolarization supported by low-voltage-activated Ca^{2+} currents results in the firing of subsequent spikes. In the neocortex, a PC dichotomy of fast rhythmic bursting cells and RS cells is apparent. Fast rhythmic bursting cells have been accorded a critical role in the neocortical rhythmogenesis (Cunningham et al. 2004). In the visual cortex, these cells can generate gamma oscillations based solely on their intrinsic conductance properties, whereas RS cells exhibited sparse firing (Cunningham et al. 2004; Gray and McCormick 1996). The neocortex and the hippocampus share similar neuronal structures, including interneurons, gap junctions, and AMPA and $GABA_A$ receptors necessary for the generation of kainate-induced gamma oscillations. Subicular IB cells share some of the properties of neocortical bursting neurons. They express a strong I_h current and voltage-activated Ca^{2+} conductance which can induce rhythmic pacemaker activity and are also thought to be connected via gap junctions (Harris et al. 2001; Pape 1996; Robinson and Siegelbaum 2003). Furthermore, during epileptic discharges within the subiculum, IB cells resume a pacemaking role (Funahashi et al. 1999; Harris and Stewart 2001a; b; Menendez de la Prida and Gal 2004). However, there are also striking differences between the neocortical and subicular bursting neurons and their participation in network oscillations. Within the neocortex, bursting cells were found to answer a gamma wave either with single or multiple APs, which was observed only after tetanic stimulation within the subiculum (Colling et al. 1998; Stanford et al. 1998). Also, the neocortical gamma rhythm depends on electric coupling between fast rhythmic bursting cells among each other as well as with the axons of cortical RS

neurons. There is no indication of this in the subiculum. For future experiments, a further examination of similarities and differences between cortical and subicular bursting neurons might prove expedient to further investigate the propensity of network generating structures within the brain.

4.6 Subicular Network

It has been demonstrated that the subiculum is capable of generating sharp wave and gamma frequency oscillatory activity in isolation (Eller et al. 2015; Jackson et al. 2011; Wu et al. 2006). So far, there exists very little information about the underlying intrinsic mechanisms.

Anatomically, there are two streams of information flow through the hippocampal formation. The long hippocampal processing loop passes through the EC, DG, CA3, and CA1 area of the hippocampus to terminate in the subiculum. In addition, there exists physiological and anatomical evidence for shorter reciprocal circuits between the PrS and the subiculum (Funahashi et al. 1999; Funahashi and Stewart 1997), the CA1 area and the subiculum (Harris and Stewart 2001a; b), and the EC and the subiculum (Gigg et al. 2000). Interestingly, the reciprocal connection with the LEC has been shown to exclusively involve subicular IB PCs (Gigg et al. 2000). The bursting answer appears to be frequency-dependent in this context. The higher the frequency of excitatory input the less likely the IB cell is to answer with a burst of AP (Cooper et al. 2005), which again suggests state-dependent information processing. Furthermore, there have been indications that in addition to the anatomical there exist two parallel functional streams of hippocampal information flow conducted by the IB and RS cells of the hippocampal CA1 area and the subiculum (Graves et al. 2012). The present study appears to confirm the existence of two information streams within the subiculum involving the two distinct classes of subicular PCs. There seems to exist a functional separation between the active, participating IB and the predominantly silent RS cells dependent on the level of subicular network excitation. The role of the RS cells must not be underestimated. Remote from the AP threshold, subthreshold fluctuation can enhance synchronization through shifts in spiking times influencing synaptic plasticity and information processing (Ermentrout et al. 2008). Within the suggested bimodal working model of the subiculum, RS cells might play a crucial role in sustaining the network activity after its initiation following a sufficiently strong excitation (Menendez de la Prida 2006; Stewart 1997; Stewart and Wong 1993). It has been demonstrated that CA1 bursting cells are most likely connected to subicular RS cells and vice versa (Jarsky et al. 2008). Therefore, the strong afferent input, necessary to active subicular RS cells, might be achieved by a discharge of bursts of APs by hippocampal CA bursting cells. Functionally, the distinct activation of RS PCs might be necessary for separating specific memory traces and spreading

them to different brain regions than those targeted by the subicular IB cell class (Naber and Witter 1998; Stewart 1997). By binding different parts of perception together, the gamma rhythm is involved in memory processing. Each item is encoded on a different gamma subcycle nested within low-frequency oscillation (Lisman and Idiart 1995). The distinct and dynamic combination of active cells on each gamma cycle might therefore represent different items of perception processed for memory storage. The intrinsic ability of IB cells to fire bursts of AP can, in addition, ensure a higher probability of transmitter release at the synapses and a possible long-term potentiation or depression (Lisman 1997). The dichotomy of cellular participation and activation of the subicular IB and RS suggests a state-dependent information processing of hippocampal output within the subiculum.

The afferent fibers that reach the subiculum are not restricted to the pyramidal cell class but they contact local subicular interneurons as well (Finch and Babb 1980; Finch et al. 1988; Gigg et al. 2000). Feedforward inhibition has been suggested to play a role in the subicular network mechanism (Menendez de la Prida 2006; Menendez de la Prida and Gal 2004). GABAergic interneurons were found to give long-range projections from the CA1 area to the molecular layers of the subiculum and perisubicular area (Klausberger and Somogyi 2008). Thus, the afferent subicular connection might target both the PCs and the interneurons. Aiding in the rousing of the active network structures, the feedforward activation of the inhibitory cells could serve to alert and time the cellular network prior to the activation of the excitatory network. In this study, combined entorhinal-hippocampal-subicular slices were prepared so that the external input onto the subicular network cannot be excluded. However, in previous studies it was demonstrated that the subiculum is capable of generating the sharp wave rhythm as well as oscillations in the theta and gamma frequency range in isolation devoid of external input (Eller et al. 2015; Jackson et al. 2011; Wu et al. 2006). This suggests that the entorhinal and hippocampal input onto subicular PCs and interneurons might activate and accelerate the generation of synchronized cellular activity within the subiculum but is not necessary for its generation since the underlying intrinsic structures of the subiculum are capable of generating and maintaining cellular oscillations independently. The different EPSP amplitudes and the time delay in inhibitory synaptic contacts of IB and RS cells during subicular sharp wave activity (see 3.4.3 and Figure 18) as well as the simultaneous synaptic excitation and inhibition during gamma frequency oscillations (see 3.5.5 and Figure 26) indicate that the subicular PCs differ with regard to their synaptic contacts which exhibit significant impact on intracellular mechanisms, resulting in a distinct firing pattern and participation in the oscillatory network.

Interconnected cellular assemblies are capable of producing synchronized activity, intrinsically suggesting that an interconnected network is likely to exist within the subiculum (Miles and Wong 1986; 1987). This has been supported by studies examining the spread of synchronized epileptic activity within the subiculum (Behr and Heinemann 1996; Funahashi et al. 1999; Harris and Stewart 2001a; b; Menendez de la Prida and Gal 2004). Furthermore, there has been morphological and electrophysiological evidence of cellular connections between subicular PCs (Harris and Stewart 2001a; Harris et al. 2001). However, during paired recordings of subicular PCs, Wu et al. (2006) could not confirm any intercellular connections between recorded neurons. This might be due to the small number of intracellular contacts and recorded neuron pairs. Within the subiculum, the inhibitory network appears to have a strong influence on the bursting behavior with the ability of single IPSP to delay, prevent, and reset bursting in IB cells (Menendez de la Prida 2003; Stewart 1997). A network of mutually interconnected interneurons can effectively synchronize PC firing via inhibitory synaptic contacts phase-correlating cell firing and subthreshold oscillations (Bartos et al. 2007; Cobb et al. 1995; de Almeida et al. 2009; Whittington et al. 1995). Antidromic stimulation of the CA1 area results in subicular excitation followed by a prolonged inhibition, suggesting that activated PCs excited interneurons which results in an inhibition of AP firing (Gigg et al. 2000). In the context of the active network, interneuron subgroups serve distinct functions (Buhl et al. 1994; Klausberger and Somogyi 2008). The interaction between perisomatic targeting basket cells and PCs via a feedback mechanism has been linked to the generation of gamma frequency oscillation within the hippocampus (Bartos et al. 2007; Buzsáki and Wang 2012; Fisahn et al. 1998; Fries et al. 2007; Mann and Paulsen 2007). A network of interneurons can be activated through glutamatergic synapses of PCs or electric coupling via gap junctions (Bartos et al. 2007; Traub and Bibbig 2000; Traub et al. 2003). In addition to their synchronizing function, the interneurons were found to assist in selecting PCs that participate in the SWR oscillations (Ellender et al. 2010). The loss of GABAergic inhibition within the subiculum has been associated with temporal lobe epilepsy (Cohen et al. 2002; Knopp et al. 2008).

Electric coupling between interneurons and PCs (Hormuzdi et al. 2001; Schmitz et al. 2001) has been attributed an essential role in the generation of synchronized cellular activity. Gap junctions between the axons of pyramidal cells were found sufficient to induce and maintain high frequency oscillations such as are superimposed on slow potential waves during hippocampal SWR oscillations (Draguhn et al. 1998; Maier et al. 2002; Maier et al. 2003; Schmitz et al. 2001; Traub and Bibbig 2000; Traub et al. 1999). During gamma frequency oscillations, axonally coupled pyramidal neurons can generate sustained network oscillations, whereas the dendritic interneuronal gap

junctions act to tighten and sharpen the synchrony of rhythmic cell firing (Bartos et al. 2007; Traub et al. 2000; Traub et al. 2003). Ectopic APs, generated not in the soma but in the pyramidal cell axons, have been suggested to be essential to triggering glutamatergic excitation in the inhibitory cellular network and thus driving the network oscillations (Traub et al. 2000). It has been shown that these ectopic APs do not propagate back into the soma prevented by axo-axonic cells so that the axonal AP frequency might be greater than the one in the soma (Dugladze et al. 2012). Furthermore, gap junctions might play a role in the recruitment of cells during network activity. In the hippocampal CA1 region, the complex role of inhibition and the generation of ectopic spikes within PCs was found responsible for the activation of participating cell groups during SWR oscillation (Bähner et al. 2011). Mediated by $GABA_A$ receptors, interneurons suppress noisy background activity by intense perisomatic inhibition and thus ensure a sparse firing activity of PCs and at the same time facilitate ectopic ripple-coupled AP generation in distal axonal compartments. Electrical coupling between subicular IB cells might result in the selection for network participation. In support of this, dye coupling as the morphological correlate of gap junctions (Baimbridge et al. 1991) has been observed exclusively between subicular IB PCs. The scarcity of dye coupling encountered in hippocampal pyramidal cells in the present study and in previous publications might be due to the sparse connectivity of less than two synaptic contacts per axon (Traub et al. 1999). More recent studies challenge the involvement of electrical synapses in the generation of the fast ripple component (English et al. 2014; Stark et al. 2014). In the CA1 area of the behaving mouse, they found that the interaction between cellular inhibition and excitation and thus the mechanism of shunting contributes the generation of fast network oscillations arguing against the role of ectopic APs.

4.7 Limitations

As a result of the categorization of subicular PCs into IB and RS cells and then further into active, participating and silent, non-participating neuronal groups, the number of recorded PCs in each group was relatively small. A greater sample size can provide a more general approach to the electrophysiological and functional dichotomy of the subiculum, possibly clarifying the still existing discordance concerning the electrophysiological properties of subicular PCs. Furthermore, exclusively horizontal hippocampal slices were examined in this study. Resulting from the columnar organization of the IB and laminar arrangement of the RS axons, a different slice orientation seems necessary in order to examine the functional involvement of subicular RS cells more closely. In this context, a detailed analysis of the histological and morphological organization of the subiculum can provide a clarifying insight into the cellular connectivity within the individual subicular PC classes and between them and the subicular interneurons. The phenomenon of dye coupling has been observed only once in this study, possibly due to the limited number of morphologically identified cells. For future studies, a further examination of the existence of electrical synapses might be interesting for a more detailed understanding of the subicular microcircuit. The *in vitro* model of kainate-induced gamma oscillations was applied in this setting. As the properties of network oscillations are influenced by the different means of initiation mechanisms, each representing distinct features of the oscillations in the intact brain (Bartos et al. 2007), the pharmacological induction of subicular gamma oscillations by carbachol or the metabotropic glutamate receptor agonist represents an additional experimental tool to examine the cellular mechanisms involved in a detailed fashion.

As a complex physiological structure, the hippocampal formation, including the subiculum, holds many challenges for the electrophysiological experiment. The present study aims at identifying the distinct behavior of subicular IB and RS cells during the two main states of network activity. The results of this study indicate the existence of two distinct information processing streams within the subiculum represented by the two classes of subicular PCs. Further analyses of the underlying intracellular mechanisms are necessary to reveal the operational processes that influence the neuronal participation in the network rhythms. Additionally, the level of network excitation appears to play a crucial role in the recruitment and participation of subicular PCs. In this context, a more detailed examination of the distinct input structures of the subicular PCs has not yet been conducted but appears crucial to understanding the suggested bimodal working model. Altogether the subicular neuronal and functional dichotomy still holds many uncertainties that are subject to further intensive research.

4.8 Conclusion

Based on the distinct target areas, firing behavior, electrophysiological properties, and pharmacological modulation (Greene et al. 1997; Greene and Mason 1996; Jung et al. 2001; Kintscher et al. 2012; van Welie et al. 2006), it has been assumed that subicular IB and RS PCs constitute parallel pathways presumably processing distinct modalities of information. With regard to this, this study is the first to examine the involvement and participation of the two classes of PCs during the successive network states of sharp wave and gamma frequency oscillation within the subiculum. In the light of these network activities, the cellular basis of the subicular microcircuit was investigated and there were functional implications of information processing within the subiculum. The two types of subicular PCs showed fundamentally different activity levels during both network states. The functional dichotomy of participating, active subicular IB and predominantly silent RS PCs appears to result from a bimodal working model dependent on the strength of network excitation. Consequently, as a result of recruitment of different cell types in a task-specific manner, the information processing within the hippocampal output structure appears to be more complex than initially assumed. Therefore, further investigations are needed in order to gain a fine scale typology. In this context, the applied *in vitro* model makes it possible to investigate different network activity on a cellular level and appears to be a valuable tool for such scientific questions.

As a consequence of investigating and examining the complex subicular information processing system, it might be possible to gain an insight into neurological disorders such as epilepsy and schizophrenia that root within the hippocampal formation. Patients might benefit from the development of new target areas for medical treatment as a result of a better understanding of the underlying mechanisms.

References

Amaral DG, Dolorfo C, and Alvarez-Royo P. Organization of CA1 projections to the subiculum: a PHA-L analysis in the rat. *Hippocampus* 1: 415-435, 1991.

Amaral DG, and Witter MP. The three-dimensional organization of the hippocampal formation: a review of anatomical data. *Neuroscience* 31: 571-591, 1989.

Andersen P. *The hippocampus book*. New York: Oxford University Press, 2007, p. 832 S.

Andersen P, Bland BH, and Dudar JD. Organization of the hippocampal output. *Exp Brain Res* 17: 152-168, 1973.

Axmacher N, Elger CE, and Fell J. Ripples in the medial temporal lobe are relevant for human memory consolidation. *Brain* 131: 1806-1817, 2008.

Aylward RL, and Totterdell S. Neurons in the ventral subiculum, amygdala and entorhinal cortex which project to the nucleus accumbens: their input from somatostatin-immunoreactive boutons. *J Chem Neuroanat* 6: 31-42, 1993.

Baimbridge KG, Peet MJ, McLennan H, and Church J. Bursting response to current-evoked depolarization in rat CA1 pyramidal neurons is correlated with lucifer yellow dye coupling but not with the presence of calbindin-D28k. *Synapse* 7: 269-277, 1991.

Bartos M, Vida I, and Jonas P. Synaptic mechanisms of synchronized gamma oscillations in inhibitory interneuron networks. *Nat Rev Neurosci* 8: 45-56, 2007.

Behr J, Empson RM, Schmitz D, Gloveli T, and Heinemann U. Electrophysiological properties of rat subicular neurons in vitro. *Neurosci Lett* 220: 41-44, 1996.

Behr J, Gloveli T, and Heinemann U. The perforant path projection from the medial entorhinal cortex layer III to the subiculum in the rat combined hippocampal-entorhinal cortex slice. *Eur J Neurosci* 10: 1011-1018, 1998.

Behr J, and Heinemann U. Low Mg2+ induced epileptiform activity in the subiculum before and after disconnection from rat hippocampal and entorhinal cortex slices. *Neurosci Lett* 205: 25-28, 1996.

Behrens MI, Koh JY, Muller MC, and Choi DW. NADPH diaphorase-containing striatal or cortical neurons are resistant to apoptosis. *Neurobiol Dis* 3: 72-75, 1996.

Bragin A, Jandó G, Nádasdy Z, Hetke J, Wise K, and Buzsáki G. Gamma (40-100 Hz) oscillation in the hippocampus of the behaving rat. *J Neurosci* 15: 47-60, 1995.

Buhl EH, Halasy K, and Somogyi P. Diverse sources of hippocampal unitary inhibitory postsynaptic potentials and the number of synaptic release sites. *Nature* 368: 823-828, 1994.

Buhl EH, Tamás G, and Fisahn A. Cholinergic activation and tonic excitation induce persistent gamma oscillations in mouse somatosensory cortex in vitro. *J Physiol* 513 (Pt 1): 117-126, 1998.

Buzsáki G. Hippocampal sharp waves: their origin and significance. *Brain Res* 398: 242-252, 1986.

Buzsáki G. Memory consolidation during sleep: a neurophysiological perspective. *J Sleep Res* 7 Suppl 1: 17-23, 1998.

Buzsáki G. Two-stage model of memory trace formation: a role for "noisy" brain states. *Neuroscience* 31: 551-570, 1989.

Buzsáki G, Buhl DL, Harris KD, Csicsvari J, Czéh B, and Morozov A. Hippocampal network patterns of activity in the mouse. *Neuroscience* 116: 201-211, 2003.

Buzsáki G, and Draguhn A. Neuronal oscillations in cortical networks. *Science* 304: 1926-1929, 2004.

Buzsáki G, Horváth Z, Urioste R, Hetke J, and Wise K. High-frequency network oscillation in the hippocampus. *Science* 256: 1025-1027, 1992.

Buzsáki G, Leung LW, and Vanderwolf CH. Cellular bases of hippocampal EEG in the behaving rat. *Brain Res* 287: 139-171, 1983.

Buzsáki G, Ponomareff GL, Bayardo F, Ruiz R, and Gage FH. Neuronal activity in the subcortically denervated hippocampus: a chronic model for epilepsy. *Neuroscience* 28: 527-538, 1989.

Buzsáki G, and Wang XJ. Mechanisms of gamma oscillations. *Annu Rev Neurosci* 35: 203-225, 2012.

Bähner F, Weiss EK, Birke G, Maier N, Schmitz D, Rudolph U, Frotscher M, Traub RD, Both M, and Draguhn A. Cellular correlate of assembly formation in oscillating hippocampal networks in vitro. *Proc Natl Acad Sci U S A* 108: E607-616, 2011.

Chrobak JJ, and Buzsáki G. High-frequency oscillations in the output networks of the hippocampal-entorhinal axis of the freely behaving rat. *J Neurosci* 16: 3056-3066, 1996.

Cobb SR, Buhl EH, Halasy K, Paulsen O, and Somogyi P. Synchronization of neuronal activity in hippocampus by individual GABAergic interneurons. *Nature* 378: 75-78, 1995.

Cohen I, Navarro V, Clemenceau S, Baulac M, and Miles R. On the origin of interictal activity in human temporal lobe epilepsy in vitro. *Science* 298: 1418-1421, 2002.

Colgin LL, Kubota D, Jia Y, Rex CS, and Lynch G. Long-term potentiation is impaired in rat hippocampal slices that produce spontaneous sharp waves. *J Physiol* 558: 953-961, 2004.

Colgin LL, and Moser EI. Gamma oscillations in the hippocampus. *Physiology (Bethesda)* 25: 319-329, 2010.

Colling SB, Stanford IM, Traub RD, and Jefferys JG. Limbic gamma rhythms. I. Phase-locked oscillations in hippocampal CA1 and subiculum. *J Neurophysiol* 80: 155-161, 1998.

Cooper DC, Chung S, and Spruston N. Output-mode transitions are controlled by prolonged inactivation of sodium channels in pyramidal neurons of subiculum. *PLoS Biol* 3: e175, 2005.

Csicsvari J, Hirase H, Czurkó A, Mamiya A, and Buzsáki G. Oscillatory coupling of hippocampal pyramidal cells and interneurons in the behaving Rat. *J Neurosci* 19: 274-287, 1999.

Csicsvari J, Jamieson B, Wise KD, and Buzsáki G. Mechanisms of gamma oscillations in the hippocampus of the behaving rat. *Neuron* 37: 311-322, 2003.

Cunningham MO, Whittington MA, Bibbig A, Roopun A, LeBeau FE, Vogt A, Monyer H, Buhl EH, and Traub RD. A role for fast rhythmic bursting neurons in cortical gamma oscillations in vitro. *Proc Natl Acad Sci U S A* 101: 7152-7157, 2004.

D'Antuono M, Kawasaki H, Palmieri C, and Avoli M. Network and intrinsic contributions to carbachol-induced oscillations in the rat subiculum. *J Neurophysiol* 86: 1164-1178, 2001.

de Almeida L, Idiart M, and Lisman JE. A second function of gamma frequency oscillations: an E%-max winner-take-all mechanism selects which cells fire. *J Neurosci* 29: 7497-7503, 2009.

Draguhn A, Traub RD, Schmitz D, and Jefferys JG. Electrical coupling underlies high-frequency oscillations in the hippocampus in vitro. *Nature* 394: 189-192, 1998.

Dugladze T, Heinemann U, and Gloveli T. Entorhinal cortex projection cells to the hippocampal formation in vitro. *Brain Res* 905: 224-231, 2001.

Dugladze T, Schmitz D, Whittington MA, Vida I, and Gloveli T. Segregation of axonal and somatic activity during fast network oscillations. *Science* 336: 1458-1461, 2012.

Dugladze T, Vida I, Tort AB, Gross A, Otahal J, Heinemann U, Kopell NJ, and Gloveli T. Impaired hippocampal rhythmogenesis in a mouse model of mesial temporal lobe epilepsy. *Proc Natl Acad Sci U S A* 104: 17530-17535, 2007.

Ellender TJ, Nissen W, Colgin LL, Mann EO, and Paulsen O. Priming of hippocampal population bursts by individual perisomatic-targeting interneurons. *J Neurosci* 30: 5979-5991, 2010.

Eller J, Zarnadze S, Bäuerle P, Dugladze T, and Gloveli T. Cell Type-Specific Separation of Subicular Principal Neurons during Network Activities. *PLoS One* 10: e0123636, 2015.

English DF, Peyrache A, Stark E, Roux L, Vallentin D, Long MA, and Buzsáki G. Excitation and inhibition compete to control spiking during hippocampal ripples: intracellular study in behaving mice. *J Neurosci* 34: 16509-16517, 2014.

Ermentrout GB, Galán RF, and Urban NN. Reliability, synchrony and noise. *Trends Neurosci* 31: 428-434, 2008.

Fanselow MS, and Dong HW. Are the dorsal and ventral hippocampus functionally distinct structures? *Neuron* 65: 7-19, 2010.

Fidzinski P, Wawra M, Dugladze T, Gloveli T, Heinemann U, and Behr J. Low-frequency stimulation of the temporoammonic pathway induces heterosynaptic disinhibition in the subiculum. *Hippocampus* 21: 733-743, 2011.

Finch DM, and Babb TL. Neurophysiology of the caudally directed hippocampal efferent system in the rat: projections to the subicular complex. *Brain Res* 197: 11-26, 1980.

Finch DM, Nowlin NL, and Babb TL. Demonstration of axonal projections of neurons in the rat hippocampus and subiculum by intracellular injection of HRP. *Brain Res* 271: 201-216, 1983.

Finch DM, Tan AM, and Isokawa-Akesson M. Feedforward inhibition of the rat entorhinal cortex and subicular complex. *J Neurosci* 8: 2213-2226, 1988.

Fisahn A. Kainate receptors and rhythmic activity in neuronal networks: hippocampal gamma oscillations as a tool. *J Physiol* 562: 65-72, 2005.

Fisahn A, Contractor A, Traub RD, Buhl EH, Heinemann SF, and McBain CJ. Distinct roles for the kainate receptor subunits GluR5 and GluR6 in kainate-induced hippocampal gamma oscillations. *J Neurosci* 24: 9658-9668, 2004.

Fisahn A, Pike FG, Buhl EH, and Paulsen O. Cholinergic induction of network oscillations at 40 Hz in the hippocampus in vitro. *Nature* 394: 186-189, 1998.

Fries P, Nikolić D, and Singer W. The gamma cycle. *Trends Neurosci* 30: 309-316, 2007.

Funahashi M, Harris E, and Stewart M. Re-entrant activity in a presubiculum-subiculum circuit generates epileptiform activity in vitro. *Brain Res* 849: 139-146, 1999.

Funahashi M, and Stewart M. Presubicular and parasubicular cortical neurons of the rat: functional separation of deep and superficial neurons in vitro. *J Physiol* 501 (Pt 2): 387-403, 1997.

Funahashi M, and Stewart M. Properties of gamma-frequency oscillations initiated by propagating population bursts in retrohippocampal regions of rat brain slices. *J Physiol* 510 (Pt 1): 191-208, 1998.

Garthwaite J, Charles SL, and Chess-Williams R. Endothelium-derived relaxing factor release on activation of NMDA receptors suggests role as intercellular messenger in the brain. *Nature* 336: 385-388, 1988.

Gigg J, Finch DM, and O'Mara SM. Responses of rat subicular neurons to convergent stimulation of lateral entorhinal cortex and CA1 in vivo. *Brain Res* 884: 35-50, 2000.

Gloveli T, Dugladze T, Rotstein HG, Traub RD, Monyer H, Heinemann U, Whittington MA, and Kopell NJ. Orthogonal arrangement of rhythm-generating microcircuits in the hippocampus. *Proc Natl Acad Sci U S A* 102: 13295-13300, 2005a.

Gloveli T, Dugladze T, Saha S, Monyer H, Heinemann U, Traub RD, Whittington MA, and Buhl EH. Differential involvement of oriens/pyramidale interneurones in hippocampal network oscillations in vitro. *J Physiol* 562: 131-147, 2005b.

Graves AR, Moore SJ, Bloss EB, Mensh BD, Kath WL, and Spruston N. Hippocampal pyramidal neurons comprise two distinct cell types that are countermodulated by metabotropic receptors. *Neuron* 76: 776-789, 2012.

Gray CM, and McCormick DA. Chattering cells: superficial pyramidal neurons contributing to the generation of synchronous oscillations in the visual cortex. *Science* 274: 109-113, 1996.

Gray JA, Feldon J, Rawlins JNP, Hemsley DR, and Smith AD. The neuropsychology of schizophrenia. *Behav Brain Sci* 14: 1-20, 1991.

Greene JR, Lin H, Mason AJ, Johnson LR, and Totterdell S. Differential expression of NADPH-diaphorase between electrophysiologically-defined classes of pyramidal neurons in rat ventral subiculum, in vitro. *Neuroscience* 80: 95-104, 1997.

Greene JR, and Mason A. Neuronal diversity in the subiculum: correlations with the effects of somatostatin on intrinsic properties and on GABA-mediated IPSPs in vitro. *J Neurophysiol* 76: 1657-1666, 1996.

Greene JR, and Totterdell S. Morphology and distribution of electrophysiologically defined classes of pyramidal and nonpyramidal neurons in rat ventral subiculum in vitro. *J Comp Neurol* 380: 395-408, 1997.

Hablitz JJ, and Johnston D. Endogenous nature of spontaneous bursting in hippocampal pyramidal neurons. *Cell Mol Neurobiol* 1: 325-334, 1981.

Harris E, and Stewart M. Intrinsic connectivity of the rat subiculum: II. Properties of synchronous spontaneous activity and a demonstration of multiple generator regions. *J Comp Neurol* 435: 506-518, 2001a.

Harris E, and Stewart M. Propagation of synchronous epileptiform events from subiculum backward into area CA1 of rat brain slices. *Brain Res* 895: 41-49, 2001b.

Harris E, Witter MP, Weinstein G, and Stewart M. Intrinsic connectivity of the rat subiculum: I. Dendritic morphology and patterns of axonal arborization by pyramidal neurons. *J Comp Neurol* 435: 490-505, 2001.

Hormuzdi SG, Pais I, LeBeau FE, Towers SK, Rozov A, Buhl EH, Whittington MA, and Monyer H. Impaired electrical signaling disrupts gamma frequency oscillations in connexin 36-deficient mice. *Neuron* 31: 487-495, 2001.

Hájos N, and Mody I. Synaptic communication among hippocampal interneurons: properties of spontaneous IPSCs in morphologically identified cells. *J Neurosci* 17: 8427-8442, 1997.

Hájos N, Pálhalmi J, Mann EO, Németh B, Paulsen O, and Freund TF. Spike timing of distinct types of GABAergic interneuron during hippocampal gamma oscillations in vitro. *J Neurosci* 24: 9127-9137, 2004.

Ishizuka N. Laminar organization of the pyramidal cell layer of the subiculum in the rat. *J Comp Neurol* 435: 89-110, 2001.

Jackson J, Goutagny R, and Williams S. Fast and slow γ rhythms are intrinsically and independently generated in the subiculum. *J Neurosci* 31: 12104-12117, 2011.

Jarsky T, Mady R, Kennedy B, and Spruston N. Distribution of bursting neurons in the CA1 region and the subiculum of the rat hippocampus. *J Comp Neurol* 506: 535-547, 2008.

Jung HY, Staff NP, and Spruston N. Action potential bursting in subicular pyramidal neurons is driven by a calcium tail current. *J Neurosci* 21: 3312-3321, 2001.

Kawasaki H, Palmieri C, and Avoli M. Muscarinic receptor activation induces depolarizing plateau potentials in bursting neurons of the rat subiculum. *J Neurophysiol* 82: 2590-2601, 1999.

Kehrer C, Dugladze T, Maziashvili N, Wójtowicz A, Schmitz D, Heinemann U, and Gloveli T. Increased inhibitory input to CA1 pyramidal cells alters hippocampal gamma frequency oscillations in the MK-801 model of acute psychosis. *Neurobiol Dis* 25: 545-552, 2007.

Kim Y, and Spruston N. Target-specific output patterns are predicted by the distribution of regular-spiking and bursting pyramidal neurons in the subiculum. *Hippocampus* 22: 693-706, 2012.

Kintscher M, Breustedt J, Miceli S, Schmitz D, and Wozny C. Group II metabotropic glutamate receptors depress synaptic transmission onto subicular burst firing neurons. *PLoS One* 7: e45039, 2012.

Klausberger T, Magill PJ, Márton LF, Roberts JD, Cobden PM, Buzsáki G, and Somogyi P. Brain-state- and cell-type-specific firing of hippocampal interneurons in vivo. *Nature* 421: 844-848, 2003.

Klausberger T, and Somogyi P. Neuronal diversity and temporal dynamics: the unity of hippocampal circuit operations. *Science* 321: 53-57, 2008.

Knopp A, Frahm C, Fidzinski P, Witte OW, and Behr J. Loss of GABAergic neurons in the subiculum and its functional implications in temporal lobe epilepsy. *Brain* 131: 1516-1527, 2008.

Knopp A, Kivi A, Wozny C, Heinemann U, and Behr J. Cellular and network properties of the subiculum in the pilocarpine model of temporal lobe epilepsy. *J Comp Neurol* 483: 476-488, 2005.

Kranig SA, Duhme N, Waldeck C, Draguhn A, Reichinnek S, and Both M. Different functions of hyperpolarization-activated cation channels for hippocampal sharp waves and ripples in vitro. *Neuroscience* 228: 325-333, 2013.

Kubota D, Colgin LL, Casale M, Brucher FA, and Lynch G. Endogenous waves in hippocampal slices. *J Neurophysiol* 89: 81-89, 2003.

Köhler C. Intrinsic projections of the retrohippocampal region in the rat brain. I. The subicular complex. *J Comp Neurol* 236: 504-522, 1985.

Lee SH, Marchionni I, Bezaire M, Varga C, Danielson N, Lovett-Barron M, Losonczy A, and Soltesz I. Parvalbumin-Positive Basket Cells Differentiate among Hippocampal Pyramidal Cells. *Neuron* 82: 1129-1144, 2014.

Lisman JE. Bursts as a unit of neural information: making unreliable synapses reliable. *Trends Neurosci* 20: 38-43, 1997.

Lisman JE, and Idiart MA. Storage of 7 +/- 2 short-term memories in oscillatory subcycles. *Science* 267: 1512-1515, 1995.

Lynch G, and Schubert P. The use of in vitro brain slices for multidisciplinary studies of synaptic function. *Annu Rev Neurosci* 3: 1-22, 1980.

Maier N, Güldenagel M, Söhl G, Siegmund H, Willecke K, and Draguhn A. Reduction of high-frequency network oscillations (ripples) and pathological network discharges in hippocampal slices from connexin 36-deficient mice. *J Physiol* 541: 521-528, 2002.

Maier N, Nimmrich V, and Draguhn A. Cellular and network mechanisms underlying spontaneous sharp wave-ripple complexes in mouse hippocampal slices. *J Physiol* 550: 873-887, 2003.

Maier N, Tejero-Cantero A, Dorrn AL, Winterer J, Beed PS, Morris G, Kempter R, Poulet JF, Leibold C, and Schmitz D. Coherent phasic excitation during hippocampal ripples. *Neuron* 72: 137-152, 2011.

Mann EO, and Paulsen O. Role of GABAergic inhibition in hippocampal network oscillations. *Trends Neurosci* 30: 343-349, 2007.

Mason A. Electrophysiology and burst-firing of rat subicular pyramidal neurons in vitro: a comparison with area CA1. *Brain Res* 600: 174-178, 1993.

Mattia D, Hwa GG, and Avoli M. Membrane properties of rat subicular neurons in vitro. *J Neurophysiol* 70: 1244-1248, 1993.

Mattia D, Kawasaki H, and Avoli M. In vitro electrophysiology of rat subicular bursting neurons. *Hippocampus* 7: 48-57, 1997a.

Mattia D, Kawasaki H, and Avoli M. Repetitive firing and oscillatory activity of pyramidal-like bursting neurons in the rat subiculum. *Exp Brain Res* 114: 507-517, 1997b.

Menendez de la Prida L. Control of bursting by local inhibition in the rat subiculum in vitro. *J Physiol* 549: 219-230, 2003.

Menendez de la Prida L. Functional features of the rat subicular microcircuits studied in vitro. *Behav Brain Res* 174: 198-205, 2006.

Menendez de la Prida L, and Gal B. Synaptic contributions to focal and widespread spatiotemporal dynamics in the isolated rat subiculum in vitro. *J Neurosci* 24: 5525-5536, 2004.

Menendez de la Prida L, Suarez F, and Pozo MA. Electrophysiological and morphological diversity of neurons from the rat subicular complex in vitro. *Hippocampus* 13: 728-744, 2003.

Menendez de la Prida L, Suarez F, and Pozo MA. The effect of different morphological sampling criteria on the fraction of bursting cells recorded in the rat subiculum in vitro. *Neurosci Lett* 322: 49-52, 2002.

Miles R, and Wong RK. Excitatory synaptic interactions between CA3 neurones in the guinea-pig hippocampus. *J Physiol* 373: 397-418, 1986.

Miles R, and Wong RK. Inhibitory control of local excitatory circuits in the guinea-pig hippocampus. *J Physiol* 388: 611-629, 1987.

Naber PA, and Witter MP. Subicular efferents are organized mostly as parallel projections: a double-labeling, retrograde-tracing study in the rat. *J Comp Neurol* 393: 284-297, 1998.

Naber PA, Witter MP, and Lopes Silva FH. Networks of the hippocampal memory system of the rat. The pivotal role of the subiculum. *Ann N Y Acad Sci* 911: 392-403, 2000.

Neymotin SA, Hilscher MM, Moulin TC, Skolnick Y, Lazarewicz MT, and Lytton WW. Ih tunes theta/gamma oscillations and cross-frequency coupling in an in silico CA3 model. *PLoS One* 8: e76285, 2013.

Norimoto H, Matsumoto N, Miyawaki T, Matsuki N, and Ikegaya Y. Subicular activation preceding hippocampal ripples in vitro. *Sci Rep* 3: 2696, 2013.

O'Keefe J, and Recce ML. Phase relationship between hippocampal place units and the EEG theta rhythm. *Hippocampus* 3: 317-330, 1993.

O'Mara SM, Commins S, Anderson M, and Gigg J. The subiculum: a review of form, physiology and function. *Prog Neurobiol* 64: 129-155, 2001.

O'Neill J, Senior T, and Csicsvari J. Place-selective firing of CA1 pyramidal cells during sharp wave/ripple network patterns in exploratory behavior. *Neuron* 49: 143-155, 2006.

O'Reilly KC, Gulden Dahl A, Ulsaker Kruge I, and Witter MP. Subicular-parahippocampal projections revisited: development of a complex topography in the rat. *J Comp Neurol* 521: 4284-4299, 2013.

Panuccio G, Vicini S, and Avoli M. Cell type-specific properties of subicular GABAergic currents shape hippocampal output firing mode. *PLoS One* 7: e50241, 2012.

Pape HC. Queer current and pacemaker: the hyperpolarization-activated cation current in neurons. *Annu Rev Physiol* 58: 299-327, 1996.

Ranck JB. Studies on single neurons in dorsal hippocampal formation and septum in unrestrained rats. I. Behavioral correlates and firing repertoires. *Exp Neurol* 41: 461-531, 1973.

Robinson RB, and Siegelbaum SA. Hyperpolarization-activated cation currents: from molecules to physiological function. *Annu Rev Physiol* 65: 453-480, 2003.

Sadowski JH, Jones MW, and Mellor JR. Ripples make waves: binding structured activity and plasticity in hippocampal networks. *Neural Plast* 2011: 960389, 2011.

Schlingloff D, Káli S, Freund TF, Hájos N, and Gulyás AI. Mechanisms of sharp wave initiation and ripple generation. *J Neurosci* 34: 11385-11398, 2014.

Schmitz D, Schuchmann S, Fisahn A, Draguhn A, Buhl EH, Petrasch-Parwez E, Dermietzel R, Heinemann U, and Traub RD. Axo-axonal coupling. a novel mechanism for ultrafast neuronal communication. *Neuron* 31: 831-840, 2001.

Scoville WB, and Milner B. Loss of recent memory after bilateral hippocampal lesions. *J Neurol Neurosurg Psychiatry* 20: 11-21, 1957.

Sharp PE, and Green C. Spatial correlates of firing patterns of single cells in the subiculum of the freely moving rat. *J Neurosci* 14: 2339-2356, 1994.

Singer W. Synchronization of cortical activity and its putative role in information processing and learning. *Annu Rev Physiol* 55: 349-374, 1993.

Soriano E, Martinez A, Fariñas I, and Frotscher M. Chandelier cells in the hippocampal formation of the rat: the entorhinal area and subicular complex. *J Comp Neurol* 337: 151-167, 1993.

Staff NP, Jung HY, Thiagarajan T, Yao M, and Spruston N. Resting and active properties of pyramidal neurons in subiculum and CA1 of rat hippocampus. *J Neurophysiol* 84: 2398-2408, 2000.

Stanford IM, Traub RD, and Jefferys JG. Limbic gamma rhythms. II. Synaptic and intrinsic mechanisms underlying spike doublets in oscillating subicular neurons. *J Neurophysiol* 80: 162-171, 1998.

Stark E, Roux L, Eichler R, Senzai Y, Royer S, and Buzsáki G. Pyramidal cell-interneuron interactions underlie hippocampal ripple oscillations. *Neuron* 83: 467-480, 2014.

Steward O, and Scoville SA. Cells of origin of entorhinal cortical afferents to the hippocampus and fascia dentata of the rat. *J Comp Neurol* 169: 347-370, 1976.

Stewart M. Antidromic and orthodromic responses by subicular neurons in rat brain slices. *Brain Res* 769: 71-85, 1997.

Stewart M, and Wong RK. Intrinsic properties and evoked responses of guinea pig subicular neurons in vitro. *J Neurophysiol* 70: 232-245, 1993.

Swanson LW, and Cowan WM. An autoradiographic study of the organization of the efferent connections of the hippocampal formation in the rat. *J Comp Neurol* 172: 49-84, 1977.

Swanson LW, and Cowan WM. Hippocampo-hypothalamic connections: origin in subicular cortex, not ammon's horn. *Science* 189: 303-304, 1975.

Swanson LW, Wyss JM, and Cowan WM. An autoradiographic study of the organization of intrahippocampal association pathways in the rat. *J Comp Neurol* 181: 681-715, 1978.

Tamamaki N, Abe K, and Nojyo Y. Columnar organization in the subiculum formed by axon branches originating from single CA1 pyramidal neurons in the rat hippocampus. *Brain Res* 412: 156-160, 1987.

Tamamaki N, and Nojyo Y. Disposition of the slab-like modules formed by axon branches originating from single CA1 pyramidal neurons in the rat hippocampus. *J Comp Neurol* 291: 509-519, 1990.

Taube JS. Electrophysiological properties of neurons in the rat subiculum in vitro. *Exp Brain Res* 96: 304-318, 1993.

Traub RD, and Bibbig A. A model of high-frequency ripples in the hippocampus based on synaptic coupling plus axon-axon gap junctions between pyramidal neurons. *J Neurosci* 20: 2086-2093, 2000.

Traub RD, Bibbig A, Fisahn A, LeBeau FE, Whittington MA, and Buhl EH. A model of gamma-frequency network oscillations induced in the rat CA3 region by carbachol in vitro. *Eur J Neurosci* 12: 4093-4106, 2000.

Traub RD, Miles R, and Wong RK. Model of the origin of rhythmic population oscillations in the hippocampal slice. *Science* 243: 1319-1325, 1989.

Traub RD, Pais I, Bibbig A, LeBeau FE, Buhl EH, Hormuzdi SG, Monyer H, and Whittington MA. Contrasting roles of axonal (pyramidal cell) and dendritic (interneuron) electrical coupling in the generation of neuronal network oscillations. *Proc Natl Acad Sci U S A* 100: 1370-1374, 2003.

Traub RD, Schmitz D, Jefferys JG, and Draguhn A. High-frequency population oscillations are predicted to occur in hippocampal pyramidal neuronal networks interconnected by axoaxonal gap junctions. *Neuroscience* 92: 407-426, 1999.

Traub RD, Whittington MA, Colling SB, Buzsáki G, and Jefferys JG. Analysis of gamma rhythms in the rat hippocampus in vitro and in vivo. *J Physiol* 493 (Pt 2): 471-484, 1996.

van Welie I, Remme MW, van Hooft JA, and Wadman WJ. Different levels of Ih determine distinct temporal integration in bursting and regular-spiking neurons in rat subiculum. *J Physiol* 576: 203-214, 2006.

Whittington MA, Stanford IM, Colling SB, Jefferys JG, and Traub RD. Spatiotemporal patterns of gamma frequency oscillations tetanically induced in the rat hippocampal slice. *J Physiol* 502 (Pt 3): 591-607, 1997.

Whittington MA, Traub RD, and Jefferys JG. Synchronized oscillations in interneuron networks driven by metabotropic glutamate receptor activation. *Nature* 373: 612-615, 1995.

Winkelmann A, Maggio N, Eller J, Caliskan G, Semtner M, Häussler U, Jüttner R, Dugladze T, Smolinsky B, Kowalczyk S, Chronowska E, Schwarz G, Rathjen FG, Rechavi G, Haas CA, Kulik A, Gloveli T, Heinemann U, and Meier JC. Changes in neural network homeostasis trigger neuropsychiatric symptoms. *J Clin Invest* 124: 696-711, 2014.

Witter MP, and Amaral DG. Entorhinal cortex of the monkey: V. Projections to the dentate gyrus, hippocampus, and subicular complex. *J Comp Neurol* 307: 437-459, 1991.

Witter MP, Groenewegen HJ, Lopes da Silva FH, and Lohman AH. Functional organization of the extrinsic and intrinsic circuitry of the parahippocampal region. *Prog Neurobiol* 33: 161-253, 1989.

Witter MP, Naber PA, van Haeften T, Machielsen WC, Rombouts SA, Barkhof F, Scheltens P, and Lopes da Silva FH. Cortico-hippocampal communication by way of parallel parahippocampal-subicular pathways. *Hippocampus* 10: 398-410, 2000.

Wu C, Asl MN, Gillis J, Skinner FK, and Zhang L. An in vitro model of hippocampal sharp waves: regional initiation and intracellular correlates. *J Neurophysiol* 94: 741-753, 2005a.

Wu C, Luk WP, Gillis J, Skinner F, and Zhang L. Size does matter: generation of intrinsic network rhythms in thick mouse hippocampal slices. *J Neurophysiol* 93: 2302-2317, 2005b.

Wu C, Shen H, Luk WP, and Zhang L. A fundamental oscillatory state of isolated rodent hippocampus. *J Physiol* 540: 509-527, 2002.

Wu CP, Huang HL, Asl MN, He JW, Gillis J, Skinner FK, and Zhang L. Spontaneous rhythmic field potentials of isolated mouse hippocampal-subicular-entorhinal cortices in vitro. *J Physiol* 576: 457-476, 2006.

Ylinen A, Bragin A, Nádasdy Z, Jandó G, Szabó I, Sik A, and Buzsáki G. Sharp wave-associated high-frequency oscillation (200 Hz) in the intact hippocampus: network and intracellular mechanisms. *J Neurosci* 15: 30-46, 1995.

Zylla MM, Zhang X, Reichinnek S, Draguhn A, and Both M. Cholinergic plasticity of oscillating neuronal assemblies in mouse hippocampal slices. *PLoS One* 8: e80718, 2013.

Affidavit

I, Joanna Eller certify under penalty of perjury by my own signature that I have submitted the thesis on the topic “Dichotomy of Subicular Principal Cells in the involvement in Sharp Waves and Gamma Frequency Oscillations” I wrote this thesis independently and without assistance from third parties, I used no other aids than the listed sources and resources.

All points based literally or in spirit on publications or presentations of other authors are, as such, in proper citations (see "uniform requirements for manuscripts (URM)" the ICMJE www.ic-mje.org) indicated. The sections on methodology (in particular practical work, laboratory requirements, statistical processing) and results (in particular images, graphics and tables) correspond to the URM (s.o) and are answered by me. My contributions in the selected publications for this dissertation correspond to those that are specified in the following joint declaration with the responsible person and supervisor. All publications resulting from this thesis and which I am author of correspond to the URM (see above) and I am solely responsible.

The importance of this affidavit and the criminal consequences of a false affidavit (section 156,161 of the Criminal Code) are known to me and I understand the rights and responsibilities stated therein.

Date Signature

Declaration of publications

The main results of this thesis have been published:

Eller J, Zarnadze S, Bäuerle P, Dugladze T, and Gloveli T. Cell type-specific separation of subicular principal neurons during network activities. *PLoS One* 10: e0123636, 2015.

Contribution in detail: The simultaneous intracellular and extracellular recordings of the subicular IB and RS PCs during SWR and consecutive gamma frequency oscillations were prepared and performed by Joanna Eller. The data analysis of the extracellular microslice recordings as well as the analysis and interpretation of the intracellular recordings were also performed by her. The data was then prepared and functional implications were drawn for further discussion with the members of the group.

Additionally, Joanna Eller had the following share in the following publication:

Winkelmann A, Maggio N, Eller J, Caliskan G, Semtner M, Häussler U, Jüttner R, Dugladze T, Smolinsky B, Kowalczyk S, Chronowska E, Schwarz G, Rathjen FG, Rechavi G, Haas CA, Kulik A, Gloveli T, Heinemann U, and Meier JC. Changes in neuronal network homeostasis trigger neuropsychiatric symptoms. *J Clin Invest* 124: 696-711, 2014.

Contribution in detail: Joanna Eller has prepared and performed the synchronous extracellular electrophysiological experiments with the knock-out and wild type mice. The data analysis was conducted and the results were then interpreted and prepared by her for discussion with the members of the group.

Signature, date and stamp of the supervising University teacher

_____

Signature of the doctoral candidate

_____

Curriculum Vitae

Mein Lebenslauf wird aus datenschutzrechtlichen Gründen in der elektronischen Version meiner Arbeit nicht veröffentlicht.

List of Publications

Poster presentations

1. Berlin Neuroscience Forum 2012 in Liebenwalde with the title "Involvement of subicular principal cells in the generation of network gamma frequency oscillations"
   Awarded with the poster price

2. ESC Students' Conference 2012 in Berlin with the title "Involvement of principal cells in the generation of fast network oscillations in the rodent subiculum"

Presentation

Austrian Surgical Conference 2013 in Vienna with the title "Prasoticarivadabiapixfondaxaban? Perioperative management of the new antiplatelet drugs and oral anticoagulants for elective surgical interventions"

Publication

Eller J, Zarnadze S, Bäuerle P, Dugladze T, and Gloveli T. Cell type-specific separation of subicular principal neurons during network activities. *PLoS One* 10: e0123636, 2015.

Winkelmann A, Maggio N, Eller J, Caliskan G, Semtner M, Häussler U, Jüttner R, Dugladze T, Smolinsky B, Kowalczyk S, Chronowska E, Schwarz G, Rathjen FG, Rechavi G, Haas CA, Kulik A, Gloveli T, Heinemann U, and Meier JC. Changes in neuronal network homeostasis trigger neuropsychiatric symptoms. *J Clin Invest* 124: 696-711, 2014.

Acknowledgment

First of all, I would like to express my special thanks to my advisor Prof. Dr. Tengis Gloveli. As my former university teacher you have inspired me and awoken my interest in the field of neurophysiology. You have encouraged me in pursing this thesis and supported me in its completion with providing aid and motivation to never stop questioning the results and challenging the conclusions. I appreciate your help as my mentor but also value your friendship during this time. I would also like to thank the current and former members of the research group: Dr. Peter Bäuerle, Dr. Tamara Dugladze, Shalva Gurgenidze, Katrin Luther, Dr. Nino Mazishvili, and Shota Zarnadze. You have provided help, motivation, support, and countless memorable moments as well as many delicious dinners. I would like to address a special thanks to Dr. Peter Bäuerle who never tired in explaining computational theories and statistic processes and who has supported me with competent help, constructive discussions as well as unwinding moments.

A very special thanks to my family, especially my parents, Helena and Zygmunt Fedun. Words cannot express how grateful I am for your constant, endless support and for all of the sacrifices that you've made on my behalf. You have always supported my decisions and I am deeply grateful for that. I am especially thankful for the inspiring example my grandmother Maria Soltysiewicz has provided me with. You have encouraged me to pursue my goals and you are never tired of indulging me with your admiration.

I would also like to thank my friends, especially Catarina Kunze, Matthias Albrecht, and Laura Schmitt, who have supported me and incented me to strive towards my goal never losing faith in me. I appreciate your friendship for all these years.

Finally, I would like to express my very special appreciation to my husband, Jan Eller, who has never failed to believe in me and my success and who has supported me through challenging times. You never tired of reminding me to reach for my goals. Your belief in me and the success of my work and has sustained me thus far. Thank you so much for your time, your patience, and your help!